

**INDOOR LOS MU-MIMO: EFFICIENT BANDWIDTH USAGE OF A
GEOGRAPHICAL AREA**

by

Satinder Singh Gill

M.Sc.E., Saint Cloud State University, 2009
B.Tech., Punjab Technical University, 2006

A Dissertation Submitted in Partial Fulfillment
of the Requirements for the Degree of

Doctor of Philosophy

in the Graduate Academic Unit of Electrical and Computer Engineering

Supervisor: Brent R. Petersen, Ph.D., Electrical and Computer Engineering

Examining Board: Bruce G. Colpitts, Ph.D., Electrical and Computer Engineering
Sal Saleh, Ph.D., Electrical and Computer Engineering
Andrew J. McAllister, Ph.D., Faculty of Computer Science

External Examiner: Salman Durrani, Ph.D., Australian National University

This dissertation is accepted by the
Dean of Graduate Studies

THE UNIVERSITY OF NEW BRUNSWICK
February, 2015

© Satinder Singh Gill, 2015

ABSTRACT

Multuser multi-input multi-output (MU-MIMO) systems are well known to provide performance improvements as compared with single-antenna systems. This thesis investigates the performance of a line-of-sight (LOS) MU-MIMO system present in an office environment. The main focus of this thesis is to demonstrate the effect of allocated user baseband bandwidth on the performance of a bandlimited MU-MIMO system. The condition number of a received channel matrix is used as a performance criterion for a MU-MIMO system. In addition, the effect of geographical dimensions of an office environment on the system's analog-to-digital converters (ADCs) dynamic-range requirements is investigated. The average MU-MIMO bandwidth requirements of an office environment are investigated. The relationship among the physical dimensions of an office environment, average MU-MIMO bandwidth and ADC's dynamic-range requirements is developed. The new term 90-50 MU-MIMO Bandwidth (90-50 MMB) is coined to indicate the MU-MIMO bandwidth of an office environment which results in the existence of an efficient MU-MIMO system over 90% of the portable user locations within an office environment with at least 50% usage of the dynamic range of the system's ADCs. The hypothesis is proposed to estimate the 90-50 MMB of an office environment based on the physical dimensions of an office environment.

A 2 x 2 prototype MU-MIMO system was developed using Hittite HMC497LP4 radio frequency wideband modulators, Hittite HMC597LP4 wideband demodulators, monopole transmit and receive antennas, an Altera[®] Stratix[®] II field programmable gate array (FPGA) development board and the computer software. The indoor LOS

measurements were carried out in 1.24 GHz to 1.30 GHz amateur radio frequency band. It is observed from the measurement results that an office environment with particular dimensions has an average user bandwidth and ADC dynamic range requirements which are required for satisfactory performance of system for the majority of the portable user locations. System performance along with bandwidth utilization and ADC dynamic range utilization is improved by allocating user baseband bandwidth and ADC dynamic range in accordance with the 90-50 MMB.

DEDICATION

To my parents, S. Avtar Singh Gill and Harinder Kaur Gill

ACKNOWLEDGEMENTS

There are many people who have supported me directly and indirectly throughout my doctorate of philosophy research work. I would like to thank all of these people.

First, I would like to express my sincere gratitude to my supervisor, Dr. Brent R. Petersen for his guidance; consistent support and encouragement of my ideas which made this work a possibility. It has been great experience working with him.

Secondly, I would like to thank my thesis examining board members, for taking time to review and improve my thesis with their advice and suggestions.

This research was supported by the University of New Brunswick.

Next, my sincere thanks to the ECE administrative staff Shelley Cormier, Denise Burke and Karen Annett for their kindness and helping me with my queries. I would like to thank ECE technical staff for their support.

I would also like to thank my fellow Ph.D. candidates Brandon C. Brown, Arash Mansouri and Chris D. Rouse. Discussions with them always helped me during the course of my research work.

Last but not least, thanks to my parents and friends for their love and encouragement through my studies.

Table of Contents

ABSTRACT.....	ii
DEDICATION.....	iv
ACKNOWLEDGEMENTS.....	v
Table of Contents.....	vi
List of Tables.....	ix
List of Figures.....	x
List of Abbreviations.....	xiii
List of Nomenclature.....	xv
Chapter 1: Introduction.....	1
1.1 Background.....	1
1.2 Problem Statement.....	2
1.3 Literature Review.....	3
1.4 Thesis Objective.....	6
1.5 Thesis Contributions.....	6
1.6 Thesis Layout.....	7
Chapter 2: Multiuser Multi-Input Multi-Output System.....	9
2.1 Introduction to MU-MIMO System.....	9
2.2 MU-MIMO System Model.....	10
2.3 MU-MIMO Channel Model.....	11
2.4 MU-MIMO System Performance Criterion.....	13
Chapter 3: MU-MIMO Baseband Channel Analysis.....	17
3.1 Discrete-time Baseband MU-MIMO Channel Model.....	17

3.2 The Channel Matrix \mathbf{H}_P Analysis.....	20
3.3 The Channel Matrix \mathbf{H}_M Analysis	32
3.4 90-50 MMB of an Office Environment	39
Chapter 4: MU-MIMO Prototype System Design and Implementation.....	43
4.1 Prototype System Design and Hardware Architecture	44
4.1.1 Portable User.....	44
4.1.2 Receiver	48
4.1.3 Baseband Processing and Control Hub.....	51
4.2 System Implementation	55
4.2.1 Baseband Soft-Data Generation.....	57
4.2.1 Received Baseband Data Processing	60
4.2.1 RS-232 GUI Control	62
Chapter 5: Simulation Results	64
5.1 Required Baseband Bandwidth Trend	68
5.2 ADCs Dynamic Range Requirements	73
5.3 MU-MIMO System Performance Results	79
Chapter 6: Measurement Results	86
6.1 Anechoic Chamber Results.....	86
6.2 Office Environment Results.....	90
Chapter 7: Summary and Future Work.....	105
7.1 Summary.....	105
7.2 Future Work	106

Bibliography	110
Appendix A: Alignment Angle for Spatial Signatures of a 2×2 MU-MIMO System	
119	
Appendix B: MATLAB Source Code	120
B.1 Office Environment Bandwidth Requirement and Allocated User Bandwidth	
Effect on System Performance.....	120
B.2 RS-232 Control for 2×2 MU-MIMO System Measurements.....	127
B.3 Impulse Response and Condition Number Calculation	139
Appendix C: Quartus II Soft-data Generation VHDL Code.....	142
Appendix D: Received Signal Power Level Ratios	145
Vitae	

List of Tables

Table 4.1: Primitive Polynomials	60
Table 5.1: Allocated User Bandwidth Effect on System Performance.....	80
Table 5.2: Office Environment Physical Dimension Effect on ADC Dynamic Range Requirements	82
Table 6.1: Allocated User Bandwidth Effect on System Performance inside Anechoic Chamber for oe_case1	88
Table 6.2: Allocated User Bandwidth Effect on System Performance inside Anechoic Chamber for oe_case4	89
Table 6.3: Allocated User Bandwidth Effect on System Performance inside GWD119 for oe_case1	91
Table 6.4: Allocated User Bandwidth Effect on System Performance inside GWD119 for oe_case4	92
Table 6.5: ADC Dynamic Range Requirements for oe_case1 and oe_case4	101
Table 6.6: Percentage of Portable User Locations for oe_case1 and oe_case4	103

List of Figures

Figure 2.1: MU-MIMO System Model.....	10
Figure 2.2: Parallel Decomposed MU-MIMO System Model.....	15
Figure 3.1: MU-MISO System	21
Figure 3.2: Spatial Signature Combination for Small Allocated User Bandwidth.....	22
Figure 3.3: Spatial Signature Combination for Large Allocated User Bandwidth.....	22
Figure 3.4: Phase Offset for Different Baseband Frequency Range.....	25
Figure 3.5: Phase Offset Slope Difference for Different Baseband Frequency Range	26
Figure 3.5: Phase Offset Slope Difference for Different Baseband Frequency Range	27
Figure 3.6: $ \cos(\phi) $ vs. Small Allocated User Baseband Bandwidth.....	30
Figure 3.7: $ \cos(\phi) $ vs. Large Allocated User Baseband Bandwidth.....	30
Figure 3.8: $ \cos(\phi) $ vs. Allocated User Baseband Bandwidth.....	31
Figure 3.9: Gaussian signal with Zero Mean and Variance One	33
Figure 4.1: Block Diagram of a Prototype MU-MIMO System.....	43
Figure 4.2: Portable-User Module	46
Figure 4.3: Setup Diagram for Portable-User Module.....	46
Figure 4.4: Hittite HMC497LP4 Wideband Modulator Evaluation PCB.....	47
Figure 4.5: Hittite HMC497LP4 Wideband Modulator Schematic	48
Figure 4.6: Receiver Module	50
Figure 4.7: Setup Diagram for Receiver Module.....	50
Figure 4.8: Hittite HMC597LP4 Wideband Demodulator Evaluation PCB.....	51
Figure 4.9: Hittite HMC597LP4 Wideband Demodulator Schematic.....	52
Figure 4.10: Baseband Processing and Control Hub Module.....	53

Figure 4.11: Setup Diagram for Baseband Processing and Control Hub Module	54
Figure 4.12: System Implementation for Prototype MU-MIMO.....	55
Figure 4.13: Received Signal Baseband Processing.....	61
Figure 4.14: RS-232 GUI Control	63
Figure 5.1: Office Environment under Analysis.....	64
Figure 5.2: Grid of Portable User Locations.....	67
Figure 5.2: Bandwidth Requirement for Office Environment with No Room Scaling	69
Figure 5.3: Bandwidth Requirement for oe_case2	70
Figure 5.4: Bandwidth Requirement for oe_case3	71
Figure 5.5: Bandwidth Requirement for oe_case4	71
Figure 5.6: Comparison of Bandwidth Requirement Results	72
Figure 5.7: Power ratio for oe_case1	74
Figure 5.8: Power ratio for oe_case2	74
Figure 5.9: Power ratio for oe_case3	75
Figure 5.10: Power ratio for oe_case4	75
Figure 5.11: ADC Dynamic Range Requirements for oe_case1	76
Figure 5.12: ADC Dynamic Range Requirements for oe_case2	77
Figure 5.13: ADC Dynamic Range Requirements for oe_case3	77
Figure 5.14: ADC Dynamic Range Requirements for oe_case4	78
Figure 5.15: Effect of Allocated User Bandwidth for oe_case1	80
Figure 5.16: Effect of Allocated User Bandwidth for oe_case4.....	81
Figure 5.17: ADC Dynamic Range Requirements for oe_case1 with Multipath Effects.	83
Figure 5.17: ADC Dynamic Range Requirements for oe_case4 with Multipath Effects.	84

Figure 6.1: Prototype MU-MIMO System Setup inside Anechoic Chamber	87
Figure 6.2: Condition Number vs. Allocated User Bandwidths for Anechoic Chamber for oe_case1	88
Figure 6.3: Condition Number vs. Allocated User Bandwidths for Anechoic Chamber for oe_case4	89
Figure 6.4: Prototype MU-MIMO System Setup inside Office Environment GWD119 .	90
Figure 6.5: Condition Number vs. Allocated User Bandwidths for GWD119 for oe_case1	91
Figure 6.6: Condition Number vs. Allocated User Bandwidths inside GWD119 for oe_case4	92
Figure 6.7: Maximum Condition Number for 90% Portable User Locations for oe_case1	93
Figure 6.8: Maximum Condition Number for 90% Portable User Locations for oe_case4	94
Figure 6.9: Maximum Condition Number for different Percentages of Portable User Locations for oe_case1	97
Figure 6.10: Maximum Condition Number for different Percentages of Portable User Locations for oe_case4	97
Figure 6.11: Received Power Ratio vs. Normalized Distance Ratio for oe_case1	99
Figure 6.12: Received Power Ratio vs. Normalized Distance Ratio for oe_case4.....	100
Figure 6.13: ADC Dynamic Range Requirements for oe_case1	101
Figure 6.14: ADC Dynamic Range Requirements for oe_case4	102

List of Abbreviations

ADC	Analog-to-Digital Convertor
ASP	Antenna Separation Product
DR	Dynamic Range
FPGA	Field Programmable Gate Array
GPIO	General Purpose Input Output
GUI	Graphical User Interface
Hz	Hertz
i.i.d.	Independent and Identically Distributed
ITU	International Telecommunication Union
PA	Power Amplifier
LO	Local Oscillator
LOS	Line-of-Sight
LVTTL	Low-Voltage Transistor-Transistor Logic
m	Metre
MHz	Mega Hertz
MIMO	Multi-Input Multi-Output
MU-MIMO	Multiuser Multi-Input Multi-Output
MU-MISO	Multiuser Multi-Input Single-Output
NLOS	Non-Line-of-Sight
ns	Nano Seconds
mW	Milli Watts
PCB	Printed Circuit Board

PN	Pseudorandom Noise
s	Seconds
ps	Pico Second
QAM	Quadrature Amplitude Modulation
RF	Radio Frequency
RMS	Root Mean Square
SISO	Single-Input Single-Output
SRAM	Static Random Access Memory
SU-MIMO	Singleuser Multi-Input Multi-Output
SVD	Singular Value Decomposition
SNR	Signal-to-Noise Ratio
SQNR	Signal-to-Quantization-Noise Ratio
ULAs	Uniform Linear Arrays
USAs	Uniform Square Arrays
USB	Universal Serial Bus
V	Volts
90-50 MMB	90-50 MU-MIMO Bandwidth

List of Nomenclature

\mathbf{H}	Channel Transfer Function Matrix
\mathbf{H}_{LOS}	LOS Component of Channel Transfer Function Matrix
\mathbf{H}_{NLOS}	NLOS Component of Channel Transfer Function Matrix
K	Ratio of Powers between the LOS and NLOS Components of Channel Transfer Function Matrix
N	Number of Receive Antennas
M	Number of Portable Users
T_x	Transmit Antenna
R_x	Receive Antenna
\mathbf{Y}	MU-MIMO N -dimensional Received Signal Vector
\mathbf{X}	MU-MIMO M -dimensional Transmitted Signal Vector
\mathbf{n}	MU-MIMO M -dimensional i.i.d. Zero Mean Complex Gaussian Noise Vector
$h(\tau)$	Time-invariant Channel Impulse Response
a_i	Overall Attenuation between Transmit Antenna and Receive Antenna on the given Path
τ_i	Propagation Delay between Transmit Antenna and Receive Antenna on the given Path
H	Fourier Transform of Time-invariant Channel Impulse Response
$\mathbf{h}(\tau)$	Time-invariant Channel Impulse Response Matrix
f	Frequency of Operation

C	MU-MIMO Capacity in bits/sec/Hz
ρ	Received Signal-to-Noise Ratio
U	Unitary Matrix
V	Unitary Matrix
Σ	Diagonal Matrix
λ_i	Channel Power Gain on the given Path
σ_i	Channel Amplitude Gain on the given Path
W	Baseband Bandwidth in Hz
$\delta(\tau)$	Dirac Delta Impulse Function
T_s	Sampling Period
ϕ	Alignment Angle between Spatial Signatures of MU-MIMO Portable Users
τ_{diff}	Relation between Propagation Delays for a 2×2 MU-MIMO System
A_{max}	Input Signal Maximum Swing
$B_{90-50\text{MMB}}$	90-50 Multiuser MIMO Bandwidth
τ_{max}	Longest Multipath Propagation Delay Component
τ_m	Maximum Possible Propagation Delay between Portable User and Receive Antenna
$x(t)$	Transmitted PN Sequence
$y(t)$	Input to Matched Filter Correlator
$d(t)$	Matched Filter Correlator Output

$h_1(t)$	Matched Filter Impulse Response
T_{PN}	PN Sequence Period
L	PN Sequence Number of Chips
n	PN Sequence Degree
T_c	PN Sequence Bit Period
R_c	PN Sequence Chip Rate
$*$	Time-Domain Convolution
τ_c	Coherence Time of a Channel
f_m	Doppler Spread of a Channel
v_{user}	Velocity of a Portable User
c	Speed of a Light in Vacuum

Chapter 1: Introduction

In this chapter, the background information pertaining to multi-input multi-output (MIMO) systems along with the problem addressed in this thesis is presented. The literature review is presented to discuss the research carried out in the past to address the problem at hand. Thereafter, the thesis objectives and contributions are presented followed by the thesis layout section.

1.1 Background

Ever since the invention of telecommunication devices like the telephone and telegraph peoples' response towards usage of these types of equipment was generally positive. The pioneer telecommunication systems being wired systems, it was mainly the work of Maxwell and Hertz, who laid the foundation of wireless transmission using electromagnetic waves. Soon after their pioneering work the first ever demonstration of transmission of information through wireless communication is acknowledged to Tesla [1]. Thereafter great inventions, advancements and advantages like mobility offered by wireless communication devices resulted in a landmark increase in the number of wireless users [2]. As an example, according to the International Telecommunication Union (ITU) statistics, the rate of increase in the number of wireless subscribers is more than four times that of wireline subscribers. The increase in the number of wireless users results in increased demand for data, which can be easily achieved by allocating more spectrum to a wireless system. Unfortunately, wireless spectrum is pricey and a limited resource and should be used efficiently [3]. A solution to this problem lies in utilizing the available spectrum much more efficiently over space, therefore meeting the demand

of high data rates without using additional spectrum. The cellular concept which calls for replacing a single high power transmitter with many low power transmitters results in an efficient utilization of a wireless spectrum through repeated use of a wireless spectrum at spatially separated locations. The cellular concept has been credited to have provided great capacity improvements over last twenty years. Another way of achieving efficient utilization of the wireless spectrum is through better signal processing. Systems that make use of multiple transmit and receive antennas, referred to as MIMO systems, fall under this category. MIMO systems can be used either to achieve improved signal-to-noise ratio (SNR) through coherent combining of diversity signals or to achieve higher data rates through multiplexing [2]. In addition, depending upon the number of individual users MIMO systems can be classified as single-user MIMO (SU-MIMO) or multiuser MIMO (MU-MIMO). In this thesis we consider MU-MIMO, exploiting multiplexing gain, to achieve higher data rates. Therefore, from this point onwards in this thesis MU-MIMO system performance refers to an achievable data rate through the use of a MU-MIMO system.

1.2 Problem Statement

As discussed in the previous section the MU-MIMO systems can be used to provide enhanced performance as compared with single-antenna systems. However, the achievable system performance enhancement through the use of a MU-MIMO system is highly dependent on the MU-MIMO channel characteristics [4]. These characteristics mainly include the MU-MIMO channel scattering richness, richness relative to the signalling rate, transmit and receive array inter-antenna separation, as well as the distance between transmit and receive antenna arrays. Theoretically, the achievable performance

enhancement through the use of MU-MIMO systems is proportional to the minimum of the number of transmit and receive antennas [5]. Normally in a typical outdoor urban environment the transmit signal reaches the receive antenna through multiple paths due to phenomena such as reflection, diffraction and scattering. Due to the presence of multipath the correlation between different signals at receive antennas is reduced therefore leading to improved system performance. However, in a typical rural outdoor and urban indoor office environment the transmit signal reaches the receive antenna mainly through a line-of-sight (LOS) path. For small transmit and receive inter-antenna separations the correlation between signals at the receive antennas being high leads to degraded system performance. Therefore, the system performance improvement in an LOS environment is one of the major problems of MU-MIMO systems.

1.3 Literature Review

In general much research has been presented to maximize the performance of the MIMO systems (i.e. SU-MIMO and MU-MIMO systems). In most of the presented research the system performance is shown to be dependent on transmit antenna array separation, receive antenna array separation, communication system signalling rates, transmit and receive antenna orientation, angle of incidence, angle of departure and antenna polarization [3, 5, 6, 7, 8, 9, 10, 11]. Some of the important research work includes the following.

Bohagen et al. presented a technique based on optimization of an antenna placement in uniform linear arrays (ULAs) [3]. Here a new geometrical model is used for ULAs which does not require transmit and receive ULAs to be in parallel. Their antenna separation product (ASP) which is a function of sender and receiver separation

distance, wavelength and spherical angles in the local coordinate systems at the transmitter and receiver, has been used as an optimization criterion for the system performance improvement. It has been shown that the optimized LOS MIMO system outperforms the traditional independent and identically distributed (i.i.d.) Rayleigh fading channel MIMO system in terms of Shannon capacity.

Sarris and Nix presented a technique based on antenna element positioning for ULAs to maximize system performance [5]. The optimization criterion was derived and is a function of transmit and receive array separation, as well as orientation and spacing. A significant performance improvement over a conventional MIMO systems is shown to be achieved through use of dual-polarized uniform linear arrays of transmit and receive antennas.

As opposed to ULAs, Liu et al. [7] proposed use of uniform square arrays (USAs) for system performance improvement. The design constraint as a function of a carrier frequency, inter-element spacing and transmission distance is derived for an antenna arrangement structure. Use of antenna polarization is also suggested to relax the derived design constraint. The presented results suggest the use of a high carrier frequency and narrow beam antennas for microwave relay transmission in an LOS MIMO system. In addition to this multi-polarization of antennas, it is shown to be an effective method for relaxing other design constraints.

Use of uniform circular arrays (UCAs) for central access points for MU-MIMO LOS scenarios in rural outdoor environments is proposed by Suzuki et al. [70]. The performance is analyzed by investigating the performance of zero-forcing precoding based MU-MIMO downlink as a function of UCAs inter element spacing, number of user

terminals and number of antenna elements in UCA. It has been shown that the system performance can be improved by employing number of antenna elements in UCA such that it exceeds the number of user terminals by ratio of two for different inter element spacing's.

Use of a reflectarray for performance improvement in a 2×2 LOS MIMO is proposed by Shen et al. [6]. Here the reflectarrays in the form of a cross dipole or meta-material structure were introduced in an LOS channel. Since reflectarrays can control the direction of the reflected waves, therefore their positioning can be optimized to alter the amplitude and phase distribution of the received signals resulting in a performance improvement. A remarkable improvement in the performance of a 2×2 LOS MIMO systems has been shown to be achieved through the use of reflectarrays.

Zhu et al. [11] proposed a new receiver antenna separation distance for performance improvement of an LOS MU-MIMO systems. They consider antenna separation on the scale of symbol wavelength named signalling wavelength to improve channel matrix invertibility of a space time receiver for an LOS MU-MIMO environment. Their work reveals that for LOS environments antenna separation on the scale of a signalling wavelength can lead to improved performance as compared to separation on the scale of carrier wavelength.

In addition to the aforementioned work, much research has been presented for LOS MIMO system performance improvement. As per the literature review, most of the presented research focuses on system performance improvement through optimization of an antenna array structure, inter-element separation and antenna polarization. The downside of the results presented in the literature is their slow adaptability to changes in

the propagation properties of the channel. For example if an optimized system is moved to a different location, with different propagation properties, or if the propagation properties in the same location change with time, then the optimization criterion needs to be changed accordingly. This would require modifications that are time consuming and expensive. Another downside of the presented research is the presumption that application of MU-MIMO systems itself results in an efficient usage of wireless spectrum. No doubt it is true that the application of MU-MIMO systems results in increased efficiency of the usage of a wireless spectrum. However, in this thesis the author is questioning an inefficient usage of wireless spectrum resulting from unnecessary allocation of user bandwidths for MU-MIMO systems. The results presented by Zhu et al. [11] hints at the dependence of the LOS MU-MIMO system performance on the allocated user bandwidth. However the literature review conducted by this author to this date, reveals that no research and constructed systems have been focused to investigate the effect of allocated user bandwidth on the MU-MIMO system performance.

1.4 Thesis Objective

The major objective of this thesis is to estimate the average required MU-MIMO bandwidth and ADC dynamic range requirements of an office environment and use them as criteria for the existence of an efficient MU-MIMO system in an office environment. The second major objective is to demonstrate the effect of allocated user bandwidth on the performance of a bandlimited MU-MIMO system in an LOS office environment.

1.5 Thesis Contributions

The contributions of this thesis are listed below:

- A prototype MU-MIMO system consisting of two portable users each having a single transmit antenna and a base station with two receive antennas have been implemented with the help of an Altera® Stratix® II field programmable gate array (FPGA) development board, computer's software and Hittite radio frequency (RF) modulators and demodulators.
- A hypothesis has been presented to estimate the required user baseband bandwidth and analog-to-digital converters (ADCs) dynamic range requirements of an office environment. This bandwidth is named the 90-50 MU-MIMO bandwidth (90-50 MMB) which indicates a bandwidth that results in existence of an efficient MU-MIMO system over 90% of an area of the office environment with at least 50% usage of the dynamic range of the ADCs.
- A theoretical analysis has been presented to show the dependence of the MU-MIMO system performance on an allocated user baseband bandwidth.
- A MATLAB® simulation and real time measurement results have been presented to attest the theoretical predictions.
- RS-232 control has been developed using the MATLAB graphical user interface (GUI) feature to automate the control of local oscillator power, carrier frequency and receive data collection for baseband analysis.

1.6 Thesis Layout

The remainder of the thesis is divided into six different chapters. Chapter 2 gives a brief explanation of the MU-MIMO system model and channel model. In chapter 3 the theoretical bandwidth analysis and ADC dynamic range analysis of the MU-MIMO

system is presented. Chapter 4 describes the system architecture along with the methods of data generation, signal transmission, signal reception and baseband data processing. In chapter 5, the simulation results are presented which are followed by MU-MIMO measurement results in chapter 6. Chapter 7 summarizes the thesis findings and possible future work.

Chapter 2: Multiuser Multi-Input Multi-Output System

This chapter provides comprehensive information about a MU-MIMO system and is divided into four subsections. In the first subsection the introduction to the MU-MIMO system has been presented which is followed by the MU-MIMO system model subsection. The MU-MIMO channel model subsection describes the channel model used for MU-MIMO system analysis in this thesis. In the last subsection, the system performance criterion used as an indicator of the MU-MIMO system performance has been presented.

2.1 Introduction to MU-MIMO System

It has been known historically that having multiple antennas at the receiver can allow enhanced received SNR through coherent combining. The pioneering work of Winters [12] resulted in an initial excitement about MIMO systems by predicting improved spectral efficiencies as compared with single-input single-output (SISO) systems. Later in 1998 Foschini and Gans [13] used an information theory perspective to demonstrate remarkable capacity improvements attainable through the use of MIMO systems. The geographical separation of antennas in an environment results in different spatial signatures assigned to signals from individual transmit antennas to geographically separated receive antennas. Due to different spatial signatures the multiple antennas at the receiver allow spatial separation of signals from different transmit antennas. Under the constraint that channel has rich multipath scattering the ergodic capacities for MIMO systems can far exceed those of SISO systems by a factor of the minimum of the number of transmit and receive antennas. The MU-MIMO system consists of multiple users each having single or multiple transmit antennas and a receiver equipped with multiple receive

antennas. The MU-MIMO systems being subset of MIMO systems; therefore above presented theory applies equally to MU-MIMO systems.

2.2 MU-MIMO System Model

In this thesis, a LOS MU-MIMO system which consists of M portable users each equipped with a single transmit antenna and a space time receiver equipped with N receive antennas is considered. Such a generalized $N \times M$ system model is depicted in Figure 2.1.

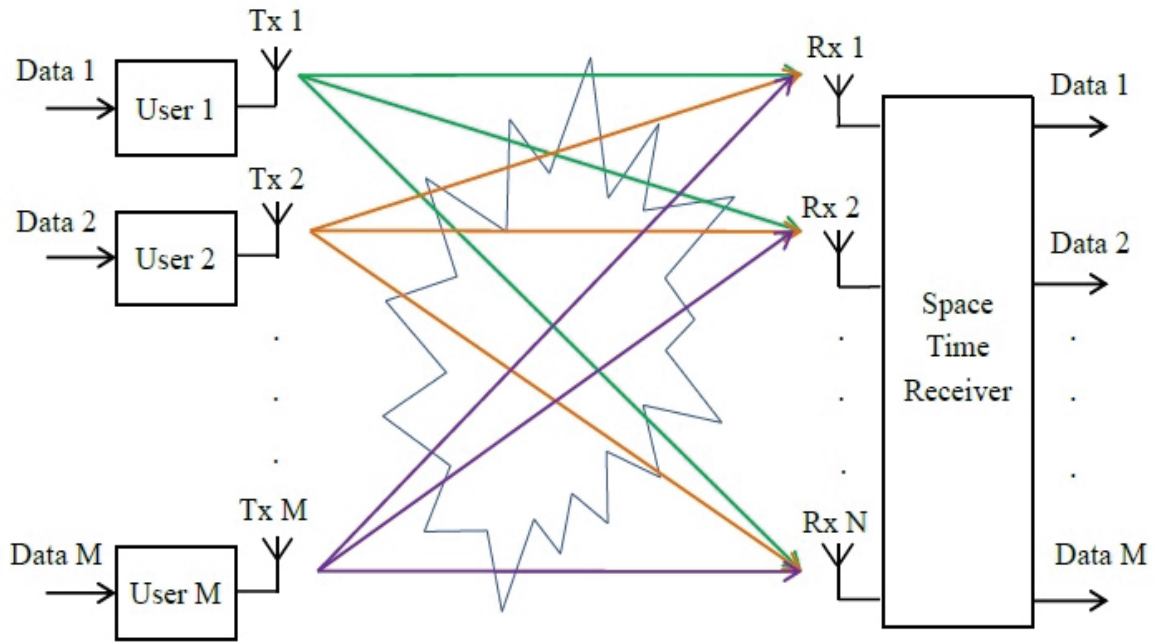


Figure 2.1: MU-MIMO System Model

In Figure 2.1, each portable user RF modulates the individual data stream onto a carrier signal using quadrature amplitude modulation (QAM) which is transmitted with the help of a transmit antenna into the wireless propagation channel. The wireless propagation channel mixes up individual RF modulated data streams in such a manner that each receive antenna obtains a linear combination of different RF modulated data

streams. Therefore, the space time receiver obtains N different copies of linearly modified RF modulated data streams with the help of N receive antennas. At the space time receiver, N copies of the linearly modified RF modulated data streams are RF demodulated and thereafter baseband processing is carried out to separate out individual data streams for different portable users. The resolvability of the individual data streams depend upon the performance of the wireless propagation MU-MIMO channel. If the MU-MIMO channel is well behaved, the N RF demodulated copies represent a linear combination of individual data streams which can be easily separated. The MU-MIMO channel is discussed in more detail in the next section.

2.3 MU-MIMO Channel Model

The wireless propagation channel for the $N \times M$ MU-MIMO system model presented in the previous section can be modelled in the frequency domain using an $N \times M$ channel transfer function matrix \mathbf{H} . Furthermore, the channel transfer function matrix can be decomposed into a deterministic LOS component (rural outdoor or urban indoor environment) and a stochastic non-line-of-sight (NLOS) component (urban outdoor environment). This can be represented as

$$\mathbf{H} = \sqrt{\frac{K}{1+K}} \cdot \mathbf{H}_{LOS} + \sqrt{\frac{1}{1+K}} \cdot \mathbf{H}_{NLOS}, \quad (2.1)$$

where \mathbf{H}_{LOS} denotes deterministic LOS component of channel transfer function matrix, \mathbf{H}_{NLOS} denotes stochastic NLOS component of channel transfer function matrix and K controls the ratio of powers between the LOS and NLOS components of channel transfer function matrix. As K approaches infinity the channel becomes a pure LOS channel and as K approaches zero the channel becomes a pure NLOS channel. In this thesis, a pure

LOS MU-MIMO system is considered; therefore the channel transfer function matrix can be modelled as

$$\mathbf{H} = \mathbf{H}_{LOS}. \quad (2.2)$$

For simplicity it is assumed that the channel is such that it does not change over the interval of a transmission time and also the channel is assumed to be frequency flat over the band of operation. In the frequency domain the input-output relationship for a MU-MIMO system can be modelled as

$$\mathbf{Y} = \mathbf{H}\mathbf{X} + \mathbf{W}, \quad (2.3)$$

$$\begin{pmatrix} Y_1 \\ Y_2 \\ \cdot \\ \cdot \\ Y_N \end{pmatrix} = \begin{pmatrix} H_{11} & H_{12} & \cdot & H_{1M} \\ H_{21} & H_{22} & \cdot & H_{2M} \\ \cdot & \cdot & \cdot & \cdot \\ \cdot & \cdot & \cdot & \cdot \\ H_{N1} & H_{N2} & \cdot & H_{NM} \end{pmatrix} \begin{pmatrix} X_1 \\ X_2 \\ \cdot \\ \cdot \\ X_M \end{pmatrix} + \begin{pmatrix} W_1 \\ W_2 \\ \cdot \\ \cdot \\ W_N \end{pmatrix}, \quad (2.4)$$

where \mathbf{Y} denotes the N -dimensional received signal vector, \mathbf{H} denotes the $N \times M$ channel transfer function matrix (i.e. H_{NM} denotes the channel transfer function between M^{th} portable user and N^{th} receive antenna), \mathbf{X} denotes the M -dimensional transmitted signal vector and \mathbf{W} denotes the N -dimensional i.i.d. zero-mean complex Gaussian noise vector. In a pure LOS environment the time-invariant baseband channel impulse response can be modelled as [17]

$$h(\tau) = a_i(e^{-j2\pi f_c \tau_i})\delta(\tau - \tau_i), \quad (2.5)$$

where $h(\tau)$ denotes the time-invariant channel impulse response, a_i denotes overall attenuation between the transmit antenna and the receive antenna on the given path, τ_i denotes propagation delay between two antennas on the given path and f_c denotes carrier frequency. The channel transfer function H which is obtained by taking the Fourier transform of the channel impulse response can be modelled as

$$H = \int_{-\infty}^{\infty} h(\tau) e^{-j2\pi f\tau} d\tau, \quad (2.6)$$

$$H = a_i e^{-j2\pi f_c \tau_i} e^{-j2\pi f \tau_i}, \quad (2.7)$$

where f denotes the baseband frequency of operation. Therefore the channel impulse response and channel transfer function matrix for a pure LOS MU-MIMO system can be modelled as

$$\mathbf{h}(\tau) = \begin{bmatrix} a_{11}(e^{-j2\pi f_c \tau_{11}})\delta(\tau - \tau_{11}) & \cdot & a_{1M}(e^{-j2\pi f_c \tau_{1M}})\delta(\tau - \tau_{1M}) \\ a_{N1}(e^{-j2\pi f_c \tau_{N1}})\delta(\tau - \tau_{N1}) & \cdot & a_{NM}(e^{-j2\pi f_c \tau_{NM}})\delta(\tau - \tau_{NM}) \end{bmatrix}, \quad (2.8)$$

$$\mathbf{H} = \begin{bmatrix} a_{11}(e^{-j2\pi f_c \tau_{11}})e^{-j2\pi f \tau_{11}} & \cdot & a_{1M}(e^{-j2\pi f_c \tau_{1M}})e^{-j2\pi f \tau_{1M}} \\ a_{N1}(e^{-j2\pi f_c \tau_{N1}})e^{-j2\pi f \tau_{N1}} & \cdot & a_{NM}(e^{-j2\pi f_c \tau_{NM}})e^{-j2\pi f \tau_{NM}} \end{bmatrix}, \quad (2.9)$$

where a_{NM} denotes the overall attenuation between portable user M and receive antenna N , τ_{NM} denotes propagation delay between portable user M and receive antenna N .

2.4 MU-MIMO System Performance Criterion

As stated in chapter 1, the MU-MIMO system performance in this thesis refers to the achievable data rate; therefore the system performance criterion needs to be selected such that it reflects the achievable data rate of the MU-MIMO system. The author began by investigating the commonly used Shannon capacity formula for MU-MIMO systems [13]

$$C = \log_2 \left[\det \left(\mathbf{I}_N + \frac{\rho}{M} \cdot \mathbf{Q} \right) \right], \quad (2.10)$$

where C denotes the MU-MIMO capacity in bits/s/Hz, ρ denotes the SNR and \mathbf{Q} is the Wishart matrix, which is defined as [18]

$$\mathbf{Q} = \begin{cases} \mathbf{H}\mathbf{H}^{HT}, & N < M \\ \mathbf{H}^{HT}\mathbf{H}, & N \geq M \end{cases}, \quad (2.11)$$

where the operator $(.)^{HT}$ denotes the Hermitian transpose. Next, using the singular value decomposition (SVD) theorem the channel transfer function matrix can be decomposed as [18]

$$\mathbf{H} = \mathbf{U}\mathbf{D}\mathbf{V}^{HT}, \quad (2.12)$$

where the $N \times N$ matrix \mathbf{U} and $M \times M$ matrix \mathbf{V} are unitary matrices and the $N \times M$ diagonal matrix \mathbf{D} contains the singular values (σ_i) of matrix \mathbf{H} . Using equation (2.12) in equation (2.11) the Wishart matrix \mathbf{Q} can be rewritten as

$$\mathbf{Q} = \begin{bmatrix} \lambda_1 & 0 & 0 & 0 \\ 0 & \lambda_2 & 0 & 0 \\ \vdots & \vdots & \vdots & \vdots \\ 0 & 0 & 0 & \lambda_r \end{bmatrix}, \quad (2.13)$$

where λ_r denotes the r^{th} eigenvalue of the matrix \mathbf{Q} . Therefore, the MU-MIMO capacity formula presented in equation (2.10) can be rewritten as [18]

$$C = \sum_{r=1}^{\min(M,N)} \log_2 \left(1 + \frac{\rho \lambda_r}{M} \right). \quad (2.14)$$

Equation (2.14) indicates that a MU-MIMO system can be viewed as an equivalent SISO system with $\min(M, N)$ uncoupled parallel sub-channels with each sub-channel having a power gain of λ_i or sub-channel amplitude gain of σ_i [3, 18]. The parallel decomposed system model for MU-MIMO system model presented in Figure 2.1 can be represented as depicted in Figure 2.2. As can be seen in Figure 2.2, a particular user can now be viewed as to have a channel amplitude gain of $\sqrt{\lambda_r}$ to a particular receive antenna while its gain to any other receive antennas is zero. This indicates that the performance criterion needs to be selected such that it reflects the variation of sub-channel amplitude gains.

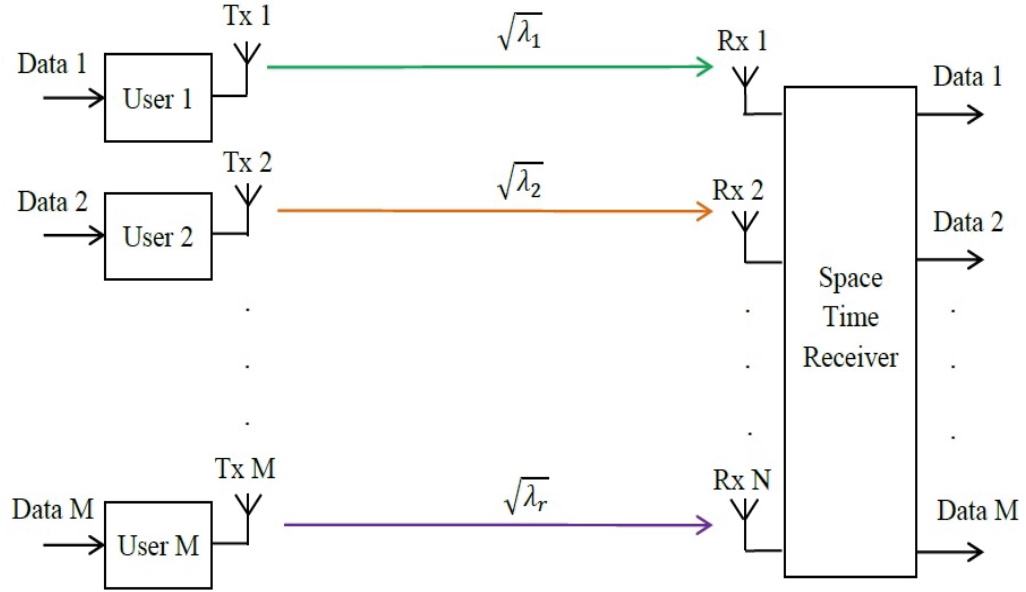


Figure 2.2: Parallel Decomposed MU-MIMO System Model

The condition number of the MU-MIMO channel matrix \mathbf{H} is a criterion that can be used as an indicator of system performance. It is defined as the ratio of the maximum and minimum singular values of the MU-MIMO channel matrix

$$\text{cond}(\mathbf{H}) = \frac{\sigma_{\max}(\mathbf{H})}{\sigma_{\min}(\mathbf{H})}, \quad (2.15)$$

the closer the condition number gets to unity better the MU-MIMO system performance is achieved [7]. A condition number close to unity indicates that all the parallel channel gains in equation (13) are the same, resulting in higher throughput. The absolute value of the determinant of channel matrix \mathbf{H} is proved to be a slightly better criterion for MIMO systems having large number of transmit and receive antennas [16]. However, the problem with the use of the determinant of the channel matrix \mathbf{H} as a performance criterion is that determinant can be obtained only for square matrices which means it can only be used for MIMO systems with equal numbers of transmit and receive antennas.

Normally in the case of MU-MIMO systems the number of portable users and number of receive antennas are different resulting in non-square channel matrices. Therefore, the use of determinant as a performance criterion for MU-MIMO systems has limited feasibility. In this thesis, the condition number of the channel matrix is used as a performance criterion.

Chapter 3: MU-MIMO Baseband Channel Analysis

In this chapter, the theoretical bandwidth analysis of a bandlimited LOS MU-MIMO system is presented. This chapter is basically divided into four sections: in the first section the discrete-time baseband MU-MIMO channel is presented and fragmented into two different parts, in the second section the dependence of the multiuser spatial signature combination on allocated user bandwidth is revealed and the 2×2 LOS MU-MIMO channel matrix \mathbf{H}_P is investigated to derive the relationship between the allocated user bandwidth and the MU-MIMO performance, and in the third section the channel matrix \mathbf{H}_M is investigated to derive the relationship between ADC resolution and location of portable users. Lastly, the relationship is developed between the physical size of an office environment and the 90-50 MU-MIMO bandwidth (90-50 MMB).

3.1 Discrete-time Baseband MU-MIMO Channel Model

Equation (2.5) presented a continuous-time time-invariant baseband channel impulse response for LOS environments. With present day systems being discrete-time, therefore it is useful to convert the continuous-time time-invariant baseband channel impulse response into a discrete-time time-invariant baseband channel impulse response. Let us get started by considering a complex baseband input signal $x_b(t)$, which is strictly bandlimited to a one-sided complex baseband bandwidth of B Hz and is sampled at a Nyquist rate (i.e. sampling period $T_s = 1/2B$ seconds). Making use of an interpolation formula, the continuous-time baseband input signal can be modelled in terms of sample values of an input signal as [44]

$$x_b(t) = \sum_{n=-\infty}^{+\infty} x_b\left(\frac{n}{2B}\right) \text{sinc}(2Bt - n), \quad (3.1)$$

where $x_b(n/2B)$ represents sample values of an input signal $x_b(t)$ taken at intervals of $1/2B$ seconds, n represents sample number and $\text{sinc}(\cdot)$ is the normalized mathematical sinc function. Using the time-domain input-output relation, the system baseband output can be modelled as

$$y_b(t) = x_b(t) * h_b(t) + w_b(t), \quad (3.2)$$

where $*$ denotes time-invariant convolution. Making use of equation (2.5) and equation (3.1) in equation (3.2), the system baseband output can be modelled as

$$y_b(t) = \sum_n x_b\left(\frac{n}{2B}\right) a_i e^{-j2\pi f_c \tau_i} \text{sinc}(2Bt - 2B\tau_i - n) + w_b(t). \quad (3.3)$$

Next, sampling the continuous-time baseband output at the Nyquist rate, the discrete time system output can be modelled as

$$y_b\left(\frac{m}{2B}\right) = \sum_n x_b\left(\frac{n}{2B}\right) a_i e^{-j2\pi f_c \tau_i} \text{sinc}(m - n - 2B\tau_i) + w_b\left(\frac{m}{2B}\right), \quad (3.4)$$

letting $l = m - n$, equation (3.4) can be rewritten as

$$y_b\left(\frac{m}{2B}\right) = \sum_l x_b\left(\frac{m-l}{2B}\right) a_i e^{-j2\pi f_c \tau_i} \text{sinc}(l - 2B\tau_i) + w_b\left(\frac{m}{2B}\right), \quad (3.5)$$

therefore the discrete-time baseband channel impulse response can be modelled as

$$h_b\left(\frac{l}{2B}\right) = a_i e^{-j2\pi f_c \tau_i} \text{sinc}(l - 2B\tau_i). \quad (3.6)$$

Taking the discrete time Fourier transform of equation (3.6), the baseband channel transfer function can be modelled as

$$H = \text{rect}\left(\frac{f}{2B}\right) a_i e^{-j2\pi f_c \tau_i} e^{-j2\pi f \tau_i}. \quad (3.7)$$

The discrete-time baseband channel impulse response matrix for a $N \times M$ MU-MIMO can be modelled as

$$\mathbf{h}(l) = \begin{bmatrix} a_{11} e^{-j2\pi f_c \tau_{11}} \text{sinc}(l - 2B\tau_{11}) & \cdot & a_{1M} e^{-j2\pi f_c \tau_{1M}} \text{sinc}(l - 2B\tau_{1M}) \\ \vdots & & \vdots \\ a_{N1} e^{-j2\pi f_c \tau_{N1}} \text{sinc}(l - 2B\tau_{N1}) & \cdot & a_{NM} e^{-j2\pi f_c \tau_{NM}} \text{sinc}(l - 2B\tau_{NM}) \end{bmatrix}, \quad (3.8)$$

therefore the channel transfer function matrix for a $N \times M$ MU-MIMO system can be modelled as

$$\mathbf{H} = \begin{bmatrix} \text{rect}\left(\frac{f}{2B}\right) a_{11} e^{-j2\pi f_c \tau_{11}} e^{-j2\pi f \tau_{11}} & \cdot & \text{rect}\left(\frac{f}{2B}\right) a_{1M} e^{-j2\pi f_c \tau_{1M}} e^{-j2\pi f \tau_{1M}} \\ \vdots & & \vdots \\ \text{rect}\left(\frac{f}{2B}\right) a_{N1} e^{-j2\pi f_c \tau_{N1}} e^{-j2\pi f \tau_{N1}} & \cdot & \text{rect}\left(\frac{f}{2B}\right) a_{NM} e^{-j2\pi f_c \tau_{NM}} e^{-j2\pi f \tau_{NM}} \end{bmatrix}. \quad (3.9)$$

The MU-MIMO channel transfer function matrix presented in equation (3.9) consists of a mixture of channel magnitude and channel phase response components. The literature review undertaken by author to this date reveals that the LOS MIMO channel transfer function matrix is modelled in either of following two ways:

- Channel transfer function matrix that consists purely of the phase response components. The provided reasoning is that in pure LOS environments the relative differences in free space path-losses are negligible. Due to this small loss the channel magnitude response components can be ignored to obtain the normalized channel transfer function matrix.
- Channel transfer function matrix that is composed of mixture of the channel magnitude and phase response components. This channel matrix does not differentiate between the effect of path loss and path delay on the performance of a MIMO system.

An objective of this thesis is to investigate the effect of physical dimensions of an office environment on ADC resolution requirements and system performance for allocated user baseband bandwidth. For the purpose of analysis the MU-MIMO channel

transfer function matrix presented in equation (3.9) is fragmented into two parts \mathbf{H}_P and \mathbf{H}_M :

$$\mathbf{H}_P = \begin{bmatrix} e^{-j2\pi f \tau_{11}} & \cdot & e^{-j2\pi f \tau_{1M}} \\ \cdot & \cdot & \cdot \\ e^{-j2\pi f \tau_{N1}} & \cdot & e^{-j2\pi f \tau_{NM}} \end{bmatrix}, \quad (3.10)$$

$$\mathbf{H}_M = \begin{bmatrix} \text{rect}\left(\frac{f}{2B}\right) a_{11} e^{-j2\pi f_c \tau_{11}} & \cdot & \text{rect}\left(\frac{f}{2B}\right) a_{1M} e^{-j2\pi f_c \tau_{1M}} \\ \cdot & \cdot & \cdot \\ \text{rect}\left(\frac{f}{2B}\right) a_{N1} e^{-j2\pi f_c \tau_{N1}} & \cdot & \text{rect}\left(\frac{f}{2B}\right) a_{NM} e^{-j2\pi f_c \tau_{NM}} \end{bmatrix}, \quad (3.11)$$

where \mathbf{H}_P represents the channel matrix composed purely of channel phase components and \mathbf{H}_M represents the channel matrix composed of channel magnitude components and free space phase shift components. As can be seen the matrix \mathbf{H}_P is dependent on the baseband frequency range of operation and path delay components whereas the matrix \mathbf{H}_M is dependent on the path loss factors, carrier frequency of operation and path delay components. The carrier frequency of operation in this thesis is not varied; therefore in the analysis to follow it will be considered as a fixed parameter.

3.2 The Channel Matrix \mathbf{H}_P Analysis

The channel matrix \mathbf{H}_P consists purely of the channel phase coefficients which are complex valued entries with magnitude value of one. The ADC resolution requirements are guided solely by the received signal amplitude changes; therefore the channel matrix \mathbf{H}_P does not contain any information that guides the ADC resolution requirements of the system. In this section the effect of channel phase coefficients of channel matrix \mathbf{H}_P on the performance of a MU-MIMO system is analyzed.

The analysis begins by considering a bandlimited multiuser multi-input single-output (MU-MISO) system present in a pure-delay LOS office environment. The

MU-MISO system scenario is depicted in Figure 3.1 which shows two pure-delay LOS wireless propagation paths from two different portable users to the same receive antenna.

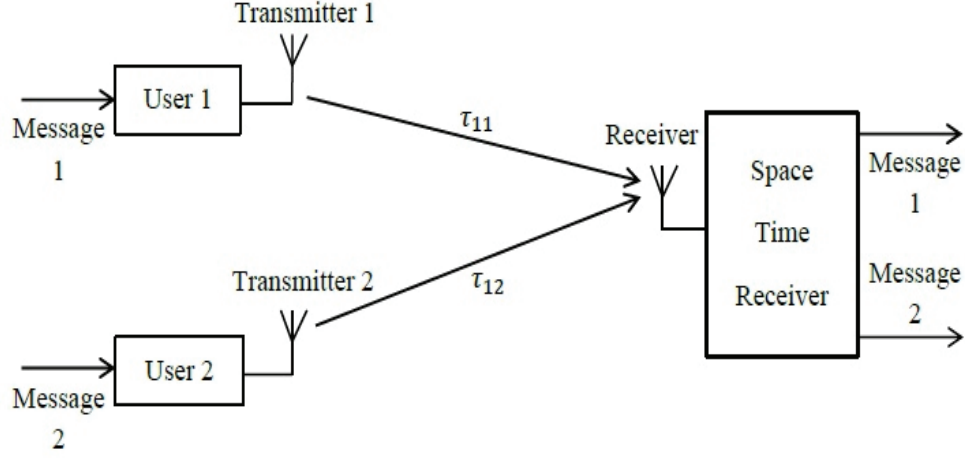


Figure 3.1: MU-MISO System

Considering the aforementioned pure delay LOS scenario and using the discrete-time baseband channel impulse response model presented in equation 3.6, the time-domain spatial signature combination of user 1 and user 2 at the bandlimited receiver can be modelled as

$$h(l) = \text{sinc}(l - 2B\tau_{11}) + \text{sinc}(l - 2B\tau_{12}). \quad (3.12)$$

Equation (3.12) indicates that the spatial signature combination at the receiver is dependent both on individual propagation delays of portable users and the allocated portable user baseband bandwidth. This suggests that for a particular value of propagation delay the spatial signature combination can be changed with change in the allocated user baseband bandwidth. The effect of the allocated user baseband bandwidth on the spatial signature combination for particular value of propagation delays is depicted in Figures 3.2 and 3.3.

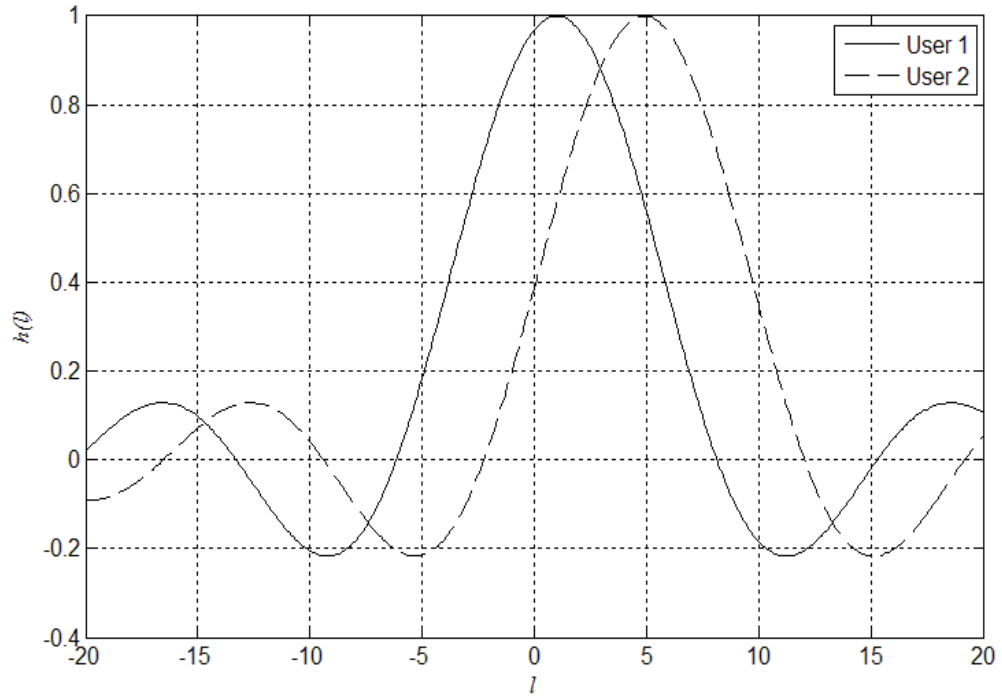


Figure 3.2: Spatial Signature Combination for Small Allocated User Bandwidth

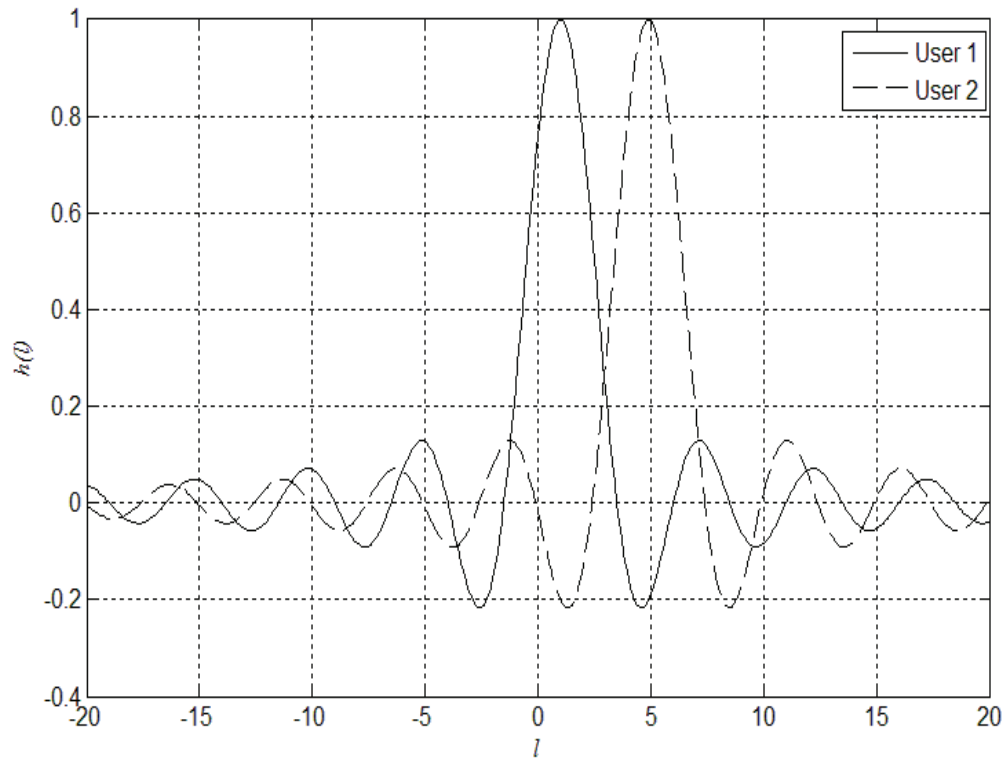


Figure 3.3: Spatial Signature Combination for Large Allocated User Bandwidth

Figures 3.2 and 3.3 show the time-domain user spatial signature combination for fixed propagation delays and different allocated portable user baseband bandwidths. As can be seen, for fixed propagation delays the change in allocated portable user baseband bandwidth results in a change of time domain overlap of the individual spatial signatures. This hints at the dependence of portable user spatial signature combination on the allocated user baseband bandwidth for fixed propagation delays. The performance of a MU-MIMO system is indicated by the ability of the receiver to separate out multiple user signals at the receiver. The separability of the multiple users is dependent upon the alignment of the frequency domain spatial signatures of individual users at the same receive antenna [17]. The less aligned are the spatial signatures, the better are the user separability and vice versa. To investigate the user spatial signature separability based on alignment angle a 2×2 MU-MIMO example is considered.

Using Hadamard's maximal determinant definition [20], the optimal channel matrix having a condition number equal to one for a 2×2 MU-MIMO system has a form

$$\mathbf{H}_{\text{Opt}} = \begin{bmatrix} 1 & 1 \\ 1 & -1 \end{bmatrix}. \quad (3.13)$$

Equation (3.13) indicates that one way of achieving an optimal channel matrix for a 2×2 MU-MIMO system is to have a phase offset of 0 and 180 degrees between the spatial signatures of individual users on respective antennas. This requirement being very stringent, a unitary transformation can be used to transform an optimal channel matrix to a new form still having a condition number equal to one

$$\mathbf{H}'_{\text{Opt}} = \begin{bmatrix} e^{+j\frac{\pi}{2}} & 0 \\ 0 & 1 \end{bmatrix} \begin{bmatrix} 1 & 1 \\ 1 & -1 \end{bmatrix} \begin{bmatrix} 1 & 0 \\ 0 & e^{-j\frac{\pi}{2}} \end{bmatrix}, \quad (3.14)$$

$$\mathbf{H}'_{\text{Opt}} = \begin{bmatrix} e^{+j\frac{\pi}{2}} & e^{+j0} \\ e^{+j0} & e^{+j\frac{\pi}{2}} \end{bmatrix}. \quad (3.15)$$

A closer examination of equation (3.15) reveals that the modified optimal channel matrix having less stringent phase change requirements satisfies the following two requirements:

- The phase offset between the spatial signatures of individual users on a particular receive antenna is 90 degrees.
- The phase offset slopes of individual users on respective receive antennas are opposite.

These two requirements are ideal conditions and result in an optimal channel matrix having a condition number of one. Due to movement of portable users an optimal channel matrix requirements change with the location of the users. The generalized requirements resulting in a suboptimal channel matrix are developed using the frequency-domain baseband channel model presented in equation (3.10). The channel transfer function matrix \mathbf{H}_P for a 2×2 MU-MIMO system is modelled as

$$\mathbf{H}_P = \begin{bmatrix} e^{-j2\pi f\tau_{11}} & e^{-j2\pi f\tau_{12}} \\ e^{-j2\pi f\tau_{21}} & e^{-j2\pi f\tau_{22}} \end{bmatrix}. \quad (3.16)$$

The phase offset between the spatial signatures of individual users on first receive antenna can be modelled as

$$\theta_1(f) = 2\pi f(\tau_{11} - \tau_{12}), \quad (3.17)$$

similarly, the phase offset for second receive antenna can be modelled as

$$\theta_2(f) = 2\pi f(\tau_{21} - \tau_{22}). \quad (3.18)$$

In equations (3.17) and (3.18) the phase offsets are modelled as functions of path delay difference and baseband frequency of operation f . The range of phase offsets is guided by the maximum value of the complex baseband frequency of operation depending upon the location of the portable users. Therefore, for a small value of allocated user baseband bandwidth, the range of baseband frequency of operation f being small, the expected range of phase offsets would be small and vice-versa. This is depicted in Figure 3.4, which shows the phase offset between the spatial signatures of two individual portable users on same receive antenna for fixed value of propagation delays. As can be seen when the baseband frequency range is limited to a small value the range of phase offsets is small whereas for a larger baseband frequency range the phase offsets are distributed over larger range of values.

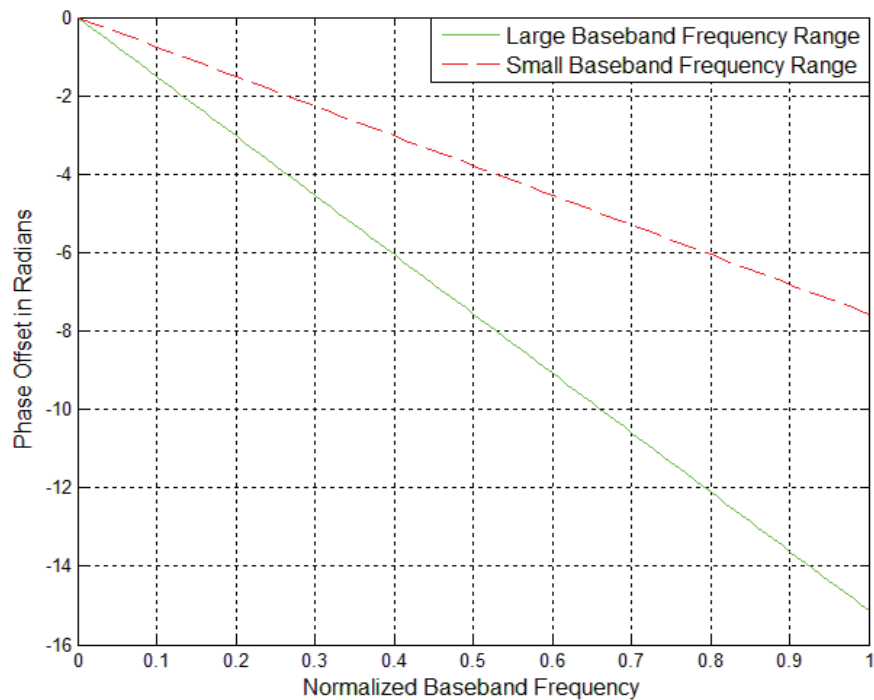


Figure 3.4: Phase Offset for Different Baseband Frequency Range

In addition to this, the phase offset slopes on separate receive antennas affects the separability of the multiple user signals. If the slopes of phase offsets on separate receive antennas are identical this is equivalent to placing two receive antennas at same point in space and hence received signal combination on separate antennas will be identical. This would mean that no multiplexing gain can be achieved. For the given separation of receive antennas in space, the difference between the phase offset slopes is a linear function of baseband frequency of operation. Therefore, for larger value of baseband frequency of operation the phase offset slopes on different receive antennas differ by larger scale and vice versa. This is depicted in Figure 3.5, where it can be seen that the greater baseband frequency range results in phase offset slope difference that supersedes the phase offset slope difference for small baseband frequency range.

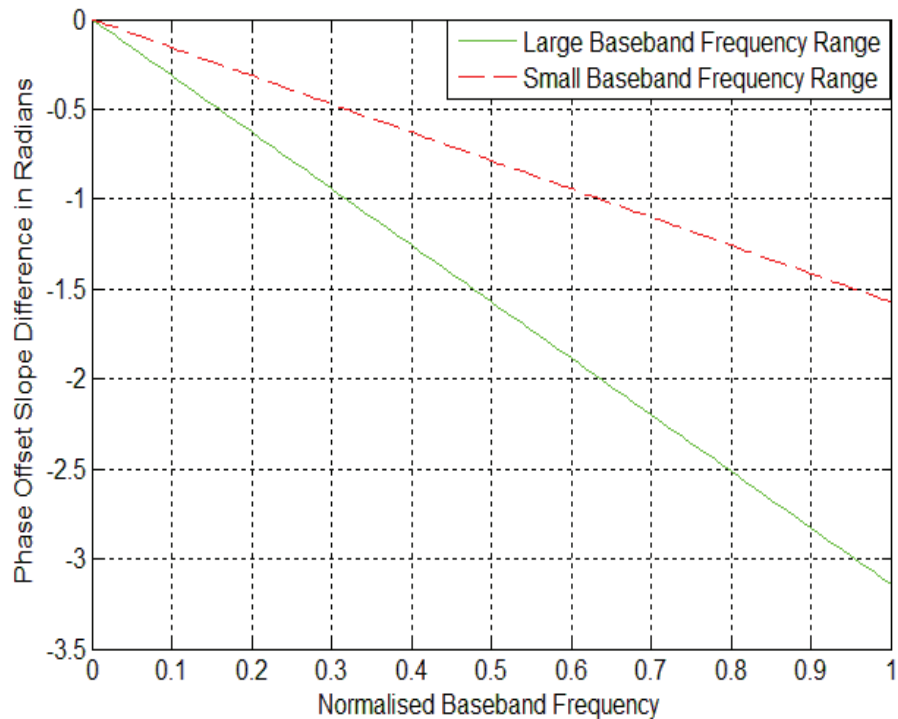


Figure 3.5: Phase Offset Slope Difference for Different Baseband Frequency Range

From the aforementioned discussion, the sufficient requirements resulting in a satisfactory sub-optimal channel matrix for a MU-MIMO system can be summarized as:

- The phase offset between the spatial signatures of the individual users on a particular receive antenna should be maximized.
- The slopes of phase offsets of individual users on respective receive antennas should be different.

These two different requirements concurrently affect the separability performance of a MU-MIMO system. Therefore, to interpret the separability performance of a MU-MIMO system based on spatial signatures it is beneficial to tie together both of the two requirements. The alignment angle ϕ between the spatial signatures of individual users on receive antenna array is one such criterion that signifies the separability performance of a MU-MIMO system. The analysis is carried out by considering a MU-MIMO system with two portable users and a uniform linear receive antenna array consisting of two receive antennas. This is depicted in Figure 3.6.

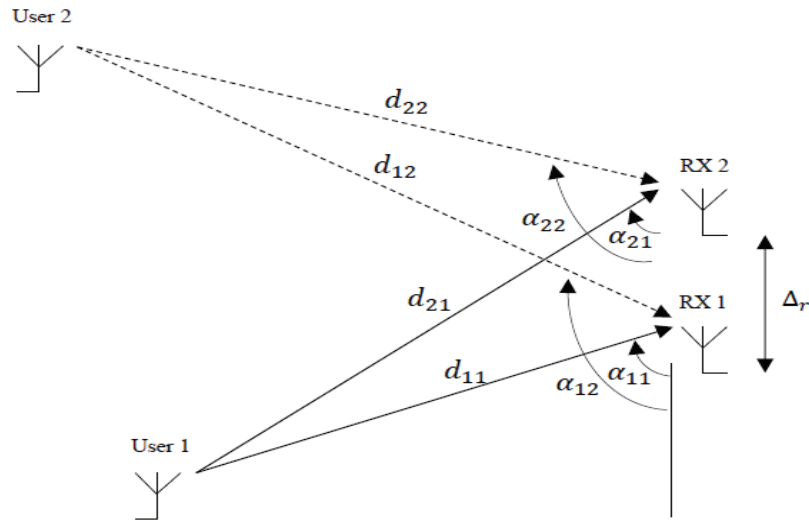


Figure 3.5: Phase Offset Slope Difference for Different Baseband Frequency Range

The channel transfer function matrix \mathbf{H}_P for a 2×2 MU-MIMO presented in equation (3.16) can be rewritten as

$$\mathbf{H}_P = \begin{bmatrix} e^{-j2\pi\frac{d_{11}}{\lambda}} & e^{-j2\pi\frac{d_{12}}{\lambda}} \\ e^{-j2\pi\frac{d_{21}}{\lambda}} & e^{-j2\pi\frac{d_{22}}{\lambda}} \end{bmatrix}, \quad (3.19)$$

where d_{NM} represents the LOS distance between receive antenna N and portable user M and λ represents the wavelength corresponding to baseband frequency of operation. The LOS distance of portable users to receive antenna N can be related in reference to receive antenna 1 as

$$d_{NM} = d_{1M} + (N - 1)\Delta_r \cos(\alpha_{NM}), \quad (3.20)$$

where Δ_r represents the separation between antennas of receive antenna array and α_{NM} is the angle of incidence of LOS signal from portable user M to receive antenna N. Using the relation presented in equation (3.20) the channel transfer function matrix \mathbf{H}_P presented in equation (3.19) can be modelled as

$$\mathbf{H}_P = \begin{bmatrix} e^{-j2\pi\frac{d_{11}}{\lambda}} & e^{-j2\pi\frac{d_{12}}{\lambda}} \\ e^{-j2\pi\frac{d_{11}}{\lambda}} e^{\frac{-j2\pi\Delta_r \cos(\alpha_{21})}{\lambda}} & e^{-j2\pi\frac{d_{12}}{\lambda}} e^{\frac{-j2\pi\Delta_r \cos(\alpha_{22})}{\lambda}} \end{bmatrix}, \quad (3.21)$$

the alignment angle ϕ between the spatial signatures for a 2×2 MU-MIMO system satisfies (see appendix A)

$$|\cos(\phi)| = \frac{1}{2} \left| e^{\frac{j2\pi(d_{11}-d_{12})}{\lambda}} + e^{\frac{j2\pi(d_{11}-d_{12})}{\lambda}} e^{\frac{j2\pi\Delta_r(\cos(\alpha_{21})-\cos(\alpha_{22}))}{\lambda}} \right|, \quad (3.22)$$

$$|\cos(\phi)| = \left| \frac{\sin\left(\frac{2\pi[\Delta_r \cos(\alpha_{21}) - \Delta_r \cos(\alpha_{22})]}{\lambda}\right)}{2\sin\left(\frac{\pi[\Delta_r \cos(\alpha_{21}) - \Delta_r \cos(\alpha_{22})]}{\lambda}\right)} \right|. \quad (3.23)$$

As can be seen in equation (3.23) the alignment angle ϕ is a function of separation distance among antennas of receive antenna array, difference between angle of incidence of LOS signals from individual portable users and wavelength corresponding to

baseband frequency of operation. When an alignment angle ϕ takes on a value such that $|\cos(\phi)|$ equals zero the separability performance of a MU-MIMO system is maximized and vice versa. As per equation (3.20)

$$\Delta_r \cos(\alpha_{21}) = d_{21} - d_{11} , \quad (3.24)$$

and

$$\Delta_r \cos(\alpha_{22}) = d_{22} - d_{12} , \quad (3.25)$$

using equations (3.24) and (3.25) the equation (3.23) can be rewritten as

$$|\cos(\phi)| = \left| \frac{\sin(2\pi f \tau_{\text{diff}})}{2\sin(\pi f \tau_{\text{diff}})} \right| , \quad (3.26)$$

where the parameter $\tau_{\text{diff}} = (\tau_{21} - \tau_{11} - \tau_{22} + \tau_{12})$ indicates a relationship among the propagation delays for a 2×2 MU-MIMO system. As per equation (3.26) the alignment angle ϕ can be related to a baseband frequency of operation f and the delay parameter τ_{diff} . Therefore, for a given value of delay parameter (i.e. for a specific location of portable users) an alignment angle can be changed by changing the baseband frequency of operation. The range of baseband frequency of operation is dependent upon the allocated user baseband bandwidth. Figures 3.6 and 3.7 show $|\cos(\phi)|$ plotted as a function of baseband frequency of operation for specific value of delay parameter. As can be seen when the allocated user bandwidth is increased from 40 MHz to 80 MHz the baseband frequency range of operation is increased resulting in better separability performance of a MU-MIMO system. In addition to this, equation (3.26) reveals that alignment angle is a periodic function of baseband frequency of operation. This is depicted in Figure 3.8, where value of $|\cos(\phi)|$ varies between one and zero for allocated user bandwidth of 160 MHz.

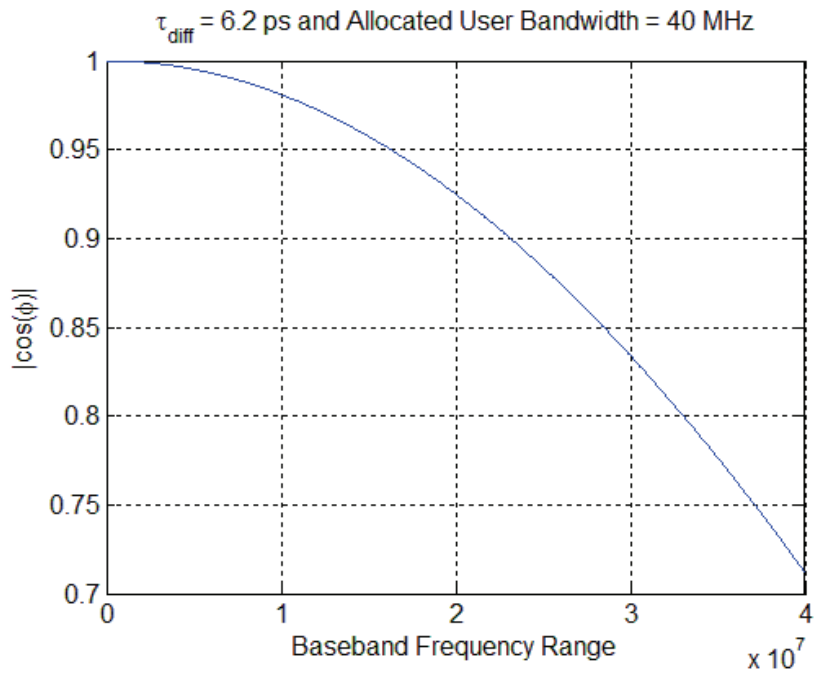


Figure 3.6: $|\cos(\phi)|$ vs. Small Allocated User Baseband Bandwidth

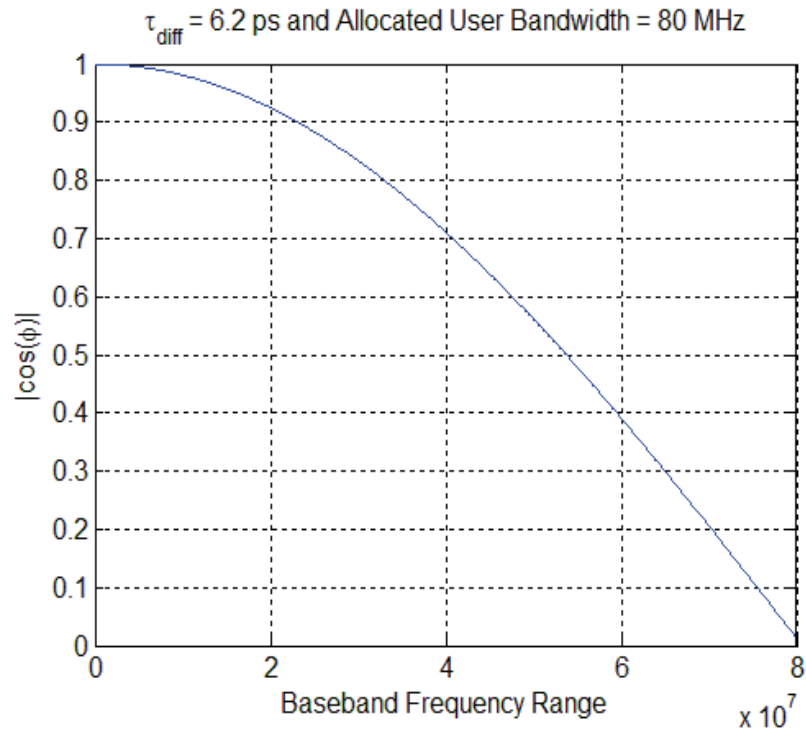


Figure 3.7: $|\cos(\phi)|$ vs. Large Allocated User Baseband Bandwidth

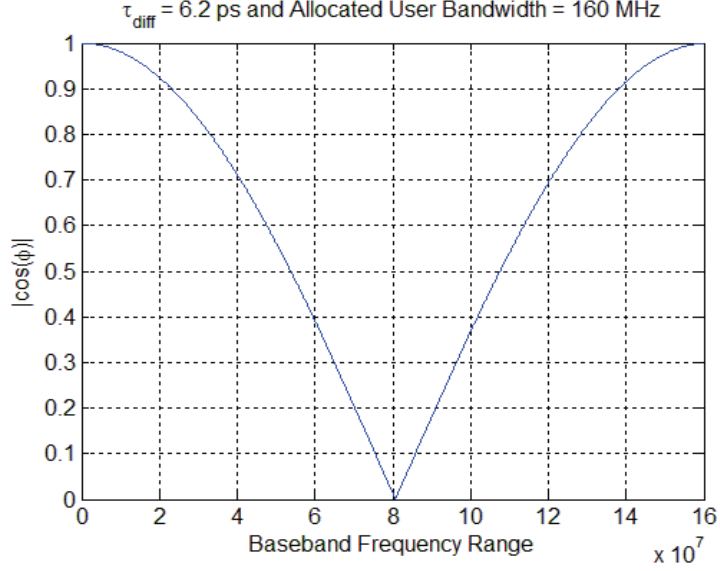


Figure 3.8: $|\cos(\phi)|$ vs. Allocated User Baseband Bandwidth

The aforementioned discussion concludes that the performance of a MU-MIMO system can be changed by changing the allocated user baseband bandwidth. However, the question arises that how much bandwidth should be allocated to obtain the satisfactory performance of a 2×2 MU-MIMO system. From equation (3.26) the required user bandwidth is calculated as

$$B_{\text{req}} = \frac{1}{|2 \tau_{\text{diff}}|} \cdot \quad (3.27)$$

The delay parameter τ_{diff} is dependent upon the location of the users. In the case of stationary users, the MU-MIMO system described by equation (3.27) can be used to calculate the required bandwidth such the MU-MIMO system performance is maximized. However in the case of portable users the delay parameter τ_{diff} changes with the location of the users resulting in different required bandwidths at different locations to maximize the performance of a MU-MIMO system. The result is that no particular value of bandwidth can maximize the performance of a MU-MIMO system at all the portable user

locations. The allocated user bandwidth should be selected such that it results in satisfactory performance at majority of the portable user locations. The criterion used to estimate the allocated user bandwidth that results in satisfactory performance at majority of portable user locations is presented in section 3.4 of the thesis.

3.3 The Channel Matrix H_M Analysis

The channel matrix H_M consists of the channel transfer function magnitude coefficients over the range of the allocated user baseband bandwidth. The received signal magnitude variations are guided by the variations in the magnitude coefficients of the channel. The variations in the magnitude coefficients of the channel matrix H_M are caused due to two different phenomena namely large-scale path loss and small-scale fading. Large-scale path loss is the gradual attenuation of signal strength with distance as the separation increases between the antennas. The small-scale fading is rapid fluctuations in the signal strength as the distance between signal source and receiver changes on the scale of few wavelengths. The ADC is used to digitize an incoming continuous-time baseband signal for further processing by a digital signal processor. The quantization process in an ADC introduces quantization error in the digitized signal. For an ADC employing uniform quantization, the quantization noise power is modelled as [46]

$$P_{QN} = \frac{\Delta^2}{12} \left(\frac{2B_w}{F_s} \right), \quad (3.28)$$

where P_{QN} is the quantization noise power, Δ is the quantization step size, B_w is the baseband one-sided bandwidth of an input signal and F_s denotes the sampling frequency for an ADC. The quantization step size Δ is dependent upon the maximum input signal

range and is modelled as [45, 46]

$$\Delta = \frac{A_{\max}}{2^b}, \quad (3.29)$$

where A_{\max} is the maximum input signal swing and b is the ADC resolution in bits. Using equation (3.29) in equation (3.28) and making an assumption that the ADC sampling frequency is twice the baseband input signal bandwidth, the quantization noise power is modelled as

$$P_{\text{QN}} = \frac{A_{\max}^2}{12(2^{2b})}; \quad (3.30)$$

next assuming that an input signal to an ADC is a Gaussian distributed signal with zero mean and variance ϑ^2 . For Gaussian distributed signals 99% of signal values lie within the range of -3ϑ to $+3\vartheta$. Figure 3.9 shows the Gaussian distributed signal with zero mean and variance of one. As can be seen most of the signal values lie within the range of -3 to $+3$.

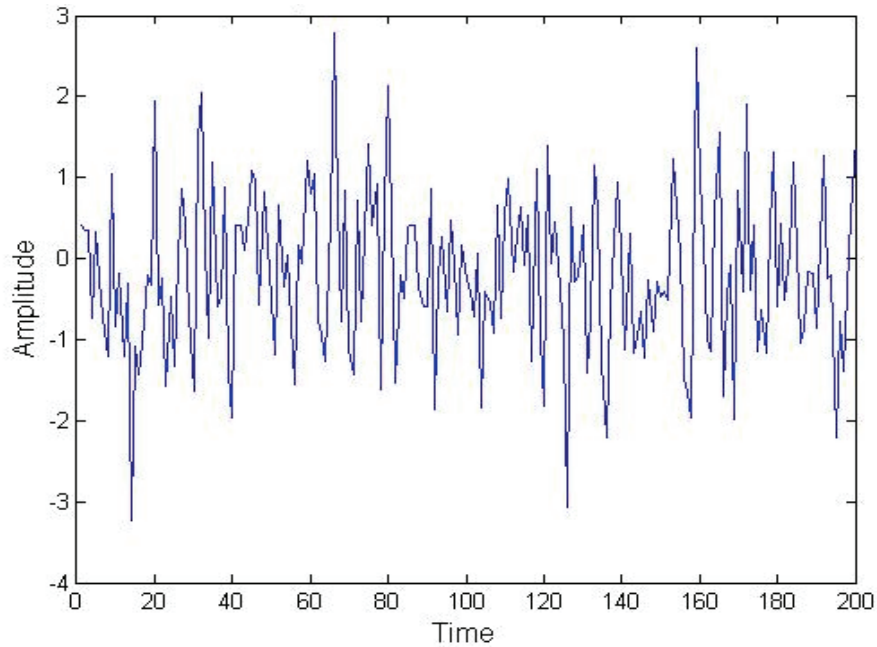


Figure 3.9: Gaussian signal with Zero Mean and Variance One

Therefore for an input Gaussian signal the maximum input signal range can be modelled as

$$A_{\max} = 2(3\vartheta), \quad (3.31)$$

using equation (3.31) in equation (3.30), the quantization noise power is modelled as

$$P_{\text{QN}} = \frac{36\vartheta^2}{12(2^{2b})}. \quad (3.32)$$

The signal-to-quantization noise ratio (SQNR) is modelled as

$$\text{SQNR} = \frac{\text{Signal Power}}{P_{\text{QN}}}. \quad (3.33)$$

Using equation (3.32) in equation (3.33) and making use of the fact that for an input Gaussian signal with zero mean the signal power equals the variance of the signal; the SQNR is modelled as

$$\text{SQNR} = \frac{2^{2b}}{3}. \quad (3.34)$$

From equation (3.34) it can be seen that the output SQNR increases exponentially with an increase in the ADC resolution. This is the case when an input signal to an ADC is being supplied from a single source. In a MU-MIMO system an input signal to an ADC consists of combination of signals from individual portable users. Let us consider a 2×2 MU-MIMO system with portable user 1 and portable user 2 signals being Gaussian distributed signals of zero mean and variance of ϑ_1^2 and ϑ_2^2 , respectively. For the purpose of analysis let us consider a configuration where a high-power signal is being received from portable user 2 whereas a low power signal is being received from portable user 1. Therefore, the signal received at an input of an ADC is a combination of a strong signal and a weak signal. To keep the clipping probability to a low value the maximum input signal range for an ADC should be at least equal to the signal range for the

strongest received signal. The maximum signal range for an ADC can be modelled as

$$A_{\max} = 2(3\vartheta_2), \quad (3.35)$$

using equation (3.35) in equation (3.32), the quantization noise power is modelled as

$$P_{\text{QN}} = \frac{3\vartheta_2^2}{2^{2b}}, \quad (3.36)$$

where ϑ_2^2 is signal power received from portable user 2. The minimum value of SQNR is modelled as

$$\text{SQNR}_{\min} = \frac{\text{Signal Power}_{\min}}{P_{\text{QN}}}, \quad (3.37)$$

where $\text{Signal Power}_{\min}$ denotes the minimum received signal power. The minimum signal power in this configuration is received from user 1 resulting in SQNR_{\min} as

$$\text{SQNR}_{\min} = \frac{(\vartheta_1^2)2^{2b}}{3\vartheta_2^2} \quad (3.38)$$

where ϑ_1^2 denotes the signal power received from portable user 1. To maintain a particular value of minimum required SQNR, the minimum required ADC resolution can be modelled as

$$b_{\min} = \frac{1}{2} \log_2 \left(3 \frac{\vartheta_2^2}{\vartheta_1^2} \text{SQNR}_{\min} \right). \quad (3.39)$$

Equation (3.39) indicates that the minimum required ADC resolution is directly dependent on the minimum required SQNR and the ratio of the maximum and the minimum received powers from portable users. For the fixed value of the minimum required SQNR the ADC resolution is dependent only on the ratio of the maximum to minimum received powers. The required ADC resolution increases logarithmically with an increase in the ratio of the received powers and vice-versa. The minimum required ADC resolution relation presented in equation (3.39) can be applied to any generalized

$N \times M$ MU-MIMO system. The generalized minimum required ADC resolution relation can be modelled as

$$b_{\min} = \frac{1}{2} \log_2 \left(3 \frac{\vartheta_{\max}^2}{\vartheta_{\min}^2} \text{SQNR}_{\min} \right), \quad (3.40)$$

where ϑ_{\max}^2 is the maximum received signal power and ϑ_{\min}^2 is the minimum received signal power. In this thesis, the portable users are permitted to move freely within the physical boundaries of an office environment. Due to the movement of portable users, large-scale path loss and small-scale fading are the two phenomena which determine the power received from a particular user depending upon its geographical location within an office environment.

As per large scale path loss model, the received signal power is dependent on the distance between the power source and the receive antenna. The Friis free space equation relates the free space received power at a particular distance from the source of the power [19]

$$P_r(d) = \frac{P_t G_t G_r \lambda^2}{(4\pi d)^2 L}, \quad (3.41)$$

where P_t is the transmitted power, $P_r(d)$ is the power received at a distance d from the source of power, λ is the wavelength, G_t and G_r are the transmitter and receiver antenna gains respectively and L denotes the system loss factor. The equation (3.41) indicates that for the constant values of all other parameters the received power is a function of the separation distance between transmit and receive antenna and falls off as a square of the separation distance d . Using equation (3.41) in equation (3.40), the minimum required ADC resolution using free space path loss model can be modelled as

$$b_{\min}^{\text{FSPL}} = \frac{1}{2} \log_2 \left(3 \frac{d_{\max}^2}{d_{\min}^2} \text{SQNR}_{\min} \right), \quad (3.42)$$

where d_{\max} is the maximum separation distance, d_{\min} is the minimum separation distance and b_{\min}^{FSPL} indicates the minimum required ADC resolution as per free space path loss model. In an indoor LOS MU-MIMO environment the physical boundaries of an environment control the maximum separation distance that can be achieved between a portable user and receiver antennas depending upon the location of a receiver. The minimum separation distance between a portable user and a receiver is constrained by the minimum possible separation allowed, which in this thesis is limited to a small value of 0.3 m due to limits imposed by physical dimensions of portable user and a receiver. This indicates that the minimum required ADC resolution due to free space path loss model is controlled by the physical boundaries of an office environment under consideration.

Small-scale fading is a phenomenon which results in rapid fluctuations of the received signal strength with small changes in travel distance. The rapid fluctuations in the signal strength are attributed to constructive and destructive combination of multiple copies of a same signal received at a receive antenna due to multipath propagation of a wireless signal. Due to movement of portable users the travel distance between the LOS component and multipath components of a signal changes, resulting in change of time delays for these components. The vectored combination of LOS and multipath components cause the receive signal strength to change with the movement of the portable user. Therefore, the small-scale fading due to motion of portable users is a spatial phenomenon. The small-scale fading phenomenon is highly influenced by the multipath structure of a wireless channel [2, 30]. In built-up urban outdoor environments

there is an abundance of multipath due to phenomena, such as reflection and diffraction, therefore small-scale fading greatly influences the fluctuations in the received signal strength. However, in an indoor environment presence of strong LOS component and fewer reflections result in reduced fluctuations in the signal strength due to small-scale fading [30]. The small-scale fading is also influenced by the bandwidth of a transmitted signal [19, 47, 48, 49]. It has been shown that for a given wireless channel the effect of small-scale fading is bandwidth dependent such that narrow band signals are affected more by small scale fading as compared to wideband signals [47, 48]. Rappaport [19] relates the small-scale fading effect on a particular signal to the delay spread of the channel. It states that if the inverse of the transmitted signal bandwidth is smaller than the root mean square (RMS) delay spread of the channel, the received signal will be distorted however the effect of small-scale fading on the received signal can be ignored and vice-versa. The RMS delay spread of the channel is dependent on different parameters such as the multipath structure of the channel and selected noise threshold. In an indoor environment such as being considered in this thesis the presence of strong LOS component and fewer reflections results in the small-scale fading effects that are not very prominent for indoor environments with a strong LOS component. Additionally, the small-scale fading is a spatial phenomenon occurring over smaller intervals of time therefore its effect on ADC resolution requirements for MU-MIMO system in indoor environments is not expected to be very prominent. Therefore, in this thesis the free space path loss is considered to be the major phenomenon that guides the ADC resolution requirements with small variations caused by small scale fading effects. The free space path loss being independent of allocated user baseband bandwidth, it is mainly the

geographical placement of portable users and receiver antennas that dictate the ADC resolution requirements.

3.4 90-50 MMB of an Office Environment

In section 3.2 it has been shown that the separability performance of a MU-MIMO system is dependent upon the parameter τ_{diff} . The attainable performance of a 2×2 LOS MU-MIMO system is maximized when the allocated user baseband bandwidth satisfies

$$B = \frac{0.5}{|\tau_{\text{diff}}|}. \quad (3.43)$$

The parameter τ_{diff} is a dynamic parameter that changes with the location of portable users. The ADC resolution requirements are also shown to be predominantly dependent upon the location of portable users in section 3.3. The minimum required ADC resolution is shown to be dependent upon the ratio of the powers of the strongest received signal to the weakest received signal. As per free space path loss model this is shown to be dependent on the square of ratio of the distances between the farthest and the nearest user. For the case of fixed user locations the optimal value of the user baseband bandwidth and minimum required ADC resolution can be calculated using equations (3.43) and (3.40) respectively, and therefore the performance of a fixed user MU-MIMO system can be optimized. However for the case of portable users the change in the location of users results in change of optimal values of baseband bandwidth and ADC resolution requirements. The question then arises what value of baseband bandwidth and ADC resolution should be used to maximize the performance of a portable user MU-MIMO system within an office environment. It is important to note that in such

scenarios the location of portable users is controlled by the physical boundaries of an office environment. Therefore it is significant to relate the baseband bandwidth and ADC resolution requirements of an indoor MU-MIMO system to the physical dimensions of an office environment. In the discussion to follow the ADC resolution requirements will be presented in terms of ADC dynamic range for the ease of comparison. The ADC dynamic range can be related to the ADC resolution expressed in bits as

$$\text{Dynamic range (dB)} = 6b, \quad (3.44)$$

where b indicates the ADC resolution expressed in bits.

In this thesis the author coins a new term called the 90-50 MU-MIMO bandwidth (90-50 MMB) which indicates the baseband bandwidth that results in an existence of an efficient MU-MIMO system over 90% of the locations within an office environment with approximately 50% usage of the dynamic range of the systems ADCs. A hypothesis is proposed which states that the 90-50 MMB of an office environment is inversely proportional to the maximum possible propagation delay between a portable user and a receive antenna within an office environment. This can be represented as

$$B_{90-50\text{MMB}} \propto \frac{1}{\tau_m}, \quad (3.45)$$

where τ_m indicates the maximum possible propagation delay between a portable user and a receive antenna within an office environment. The rationale behind the proposed relation is dual in nature and is explained as follows:

- The maximum possible propagation delay between portable user and receive antenna within an office environment closely approximates the maximum time difference that can be achieved between the arrival of LOS signals of portable users at a

particular receive antenna. Although, there is no direct relationship between the separability performance and time difference of arrival but the general trend is that more the separation better the separability performance and vice-versa. In addition to this, the maximum possible propagation delay is related to both the dimensions of an office space in a two dimensional scenario as being considered in this thesis. Therefore, it can be said that the maximum possible propagation delay relationship can be used to approximate the average required baseband bandwidth for optimal performance of a MU-MIMO system when portable users are separated in space. It is expected that in scenarios where number of portable users are comparable to the number of receive antennas; allocating baseband bandwidth approximated by relation presented in equation (3.45) would lead to the satisfactory performance over majority of the portable user locations.

- The maximum possible propagation delay between portable user and receive antenna within an office environment also closely approximate the maximum separation distance that can be achieved between the portable users. As per equations (3.40), (3.42) and (3.44) the maximum separation distance also indicates the maximum required dynamic range for the systems ADCs to maintain the minimum required SQNR. For the portable user locations where separation distance is small the required dynamic range would be smaller. In addition to this, using the maximum propagation delay to estimate the user baseband bandwidth would ensure that small scale fading effects can be ignored comfortably. The reason being that since the maximum propagation delay closely approximates the RMS delay spread in an indoor environment therefore allocating user bandwidth in accordance with

maximum propagation delay would ensure that the major multipath components of signal if any would be resolved. This would ensure that the ADC dynamic range requirements can be closely estimated based on the free space path loss model. The ADC dynamic range is estimated from 90-50 MMB using following relation:

$$\text{ADC}_{\text{DR}} = 3\log_2 \left(0.75 \frac{c^2 \tau_m^2}{d_{\min}^2} \text{SQNR}_{\min} \right), \quad (3.46)$$

where c denotes the speed of light in free space and d_{\min} is the minimum distance allowed between the transmit and receive antenna. It is expected that setting ADC dynamic range in accordance with the 90-50 MMB using relation presented in equation (3.46) would lead to approximately 50% usage of the total dynamic range for different portable user locations.

From the above discussion it can be said that a particular office environment has a distinctive average MU-MIMO bandwidth and ADC dynamic range requirements which are dependent on the physical dimensions of an office environment. Whenever allocated portable user baseband bandwidth and systems ADCs dynamic range are closer to the estimated values the MU-MIMO system performance is maximized. Allocating smaller user baseband bandwidth and ADC dynamic range would result in system performance degradation; whereas allocating higher baseband bandwidth and ADC dynamic range would result in inefficient usage of resources.

Chapter 4: MU-MIMO Prototype System Design and Implementation

In this chapter the design, hardware architecture and software implementation details of the prototype 2×2 MU-MIMO system used for indoor office environment measurements are discussed. Figure 4.1 shows the block diagram consisting of the major components of the prototype system.

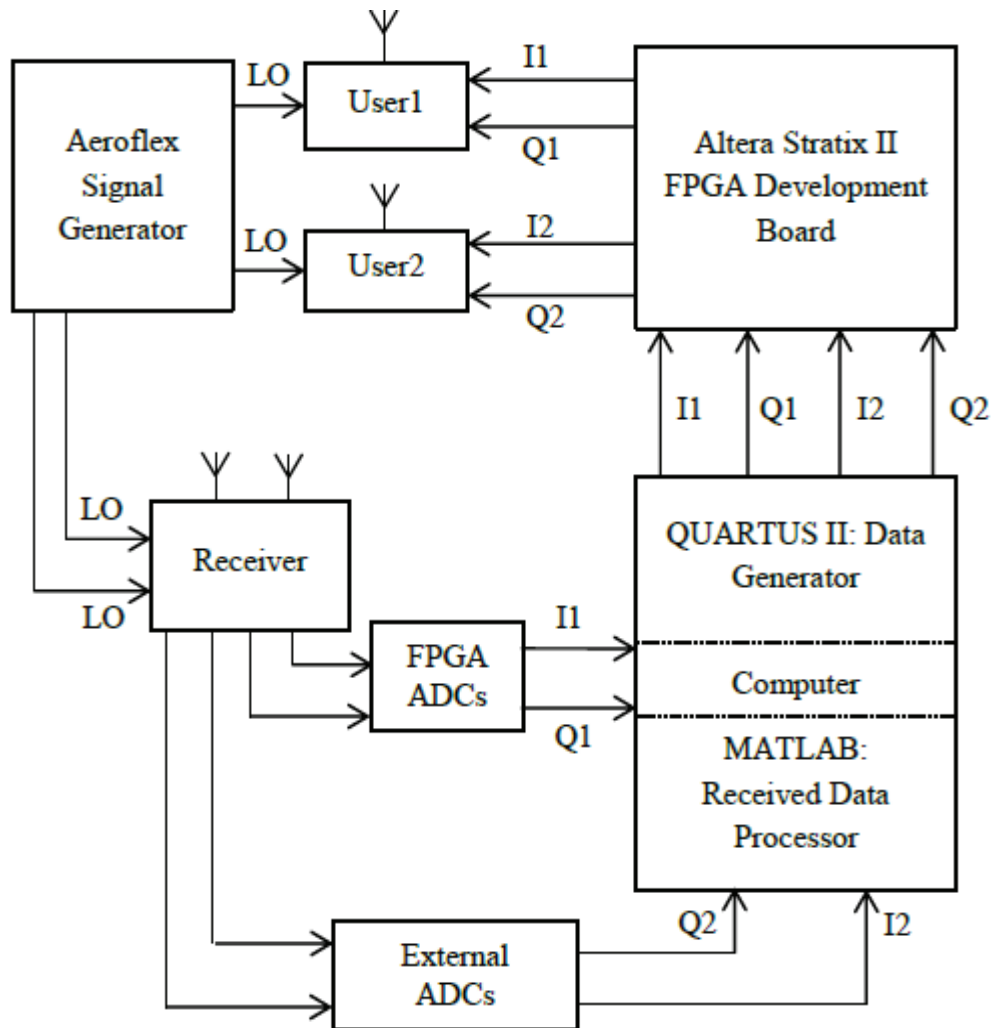


Figure 4.1: Block Diagram of a Prototype MU-MIMO System

It mainly consists of a computer system which is used for baseband data generation and received data processing. The Altera Stratix II FPGA development board

is used to send baseband data in the form of appropriate pulses to the portable users. In addition to this, the onboard ADCs are used to sample the demodulated data for received data processing using the computer system. The Aeroflex[®] signal generator is used to generate local oscillator (LO) signals for the portable users and the receiver. In addition to this, it is also used to provide a standard 10 MHz reference signal for the FPGA development board. The portable users are used to quadrature amplitude modulate the baseband data and transmit modulated data at RF. The receiver system is used to capture the RF modulated signal and perform QAM demodulation to recover the baseband data. This chapter is further divided into two sections. In the first section the design and hardware architecture development details of the prototype system are presented while the second section provides details on the software implementation part of the system.

4.1 Prototype System Design and Hardware Architecture

In this section the prototype system design module and hardware architecture details are provided. As can be seen in Figure 4.1 the prototype system can be mainly divided into three basic modules: portable user, receiver and baseband processing and control hub. Each of the modules is discussed in detail in subsections to follow.

4.1.1 Portable User

The portable-user module of the prototype system is constructed mainly using a Hittite HMC497LP4 wideband direct QAM modulator, a Mini-Circuits[®] ZX60-6013E-S+ wideband power amplifier (PA), a DC bias printed circuit board (PCB), a lab-designed monopole antenna capable of transmission in the amateur RF band of 1240 MHz – 1300 MHz, and 5 V and 12 V power supplies for the QAM modulator and PA respectively. All of these components are mounted on a wooden platform installed on a camera tripod

with inter-component connections made using appropriate length sections of RG-58 coaxial cable. Figure 4.2 shows the fully functional actual portable-user module located in the room GWD119 of Gillin Hall at the University of New Brunswick. Figure 4.3 shows the detailed setup diagram for the portable-user module presented in Figure 4.2.



Figure 4.2 (a): Portable User

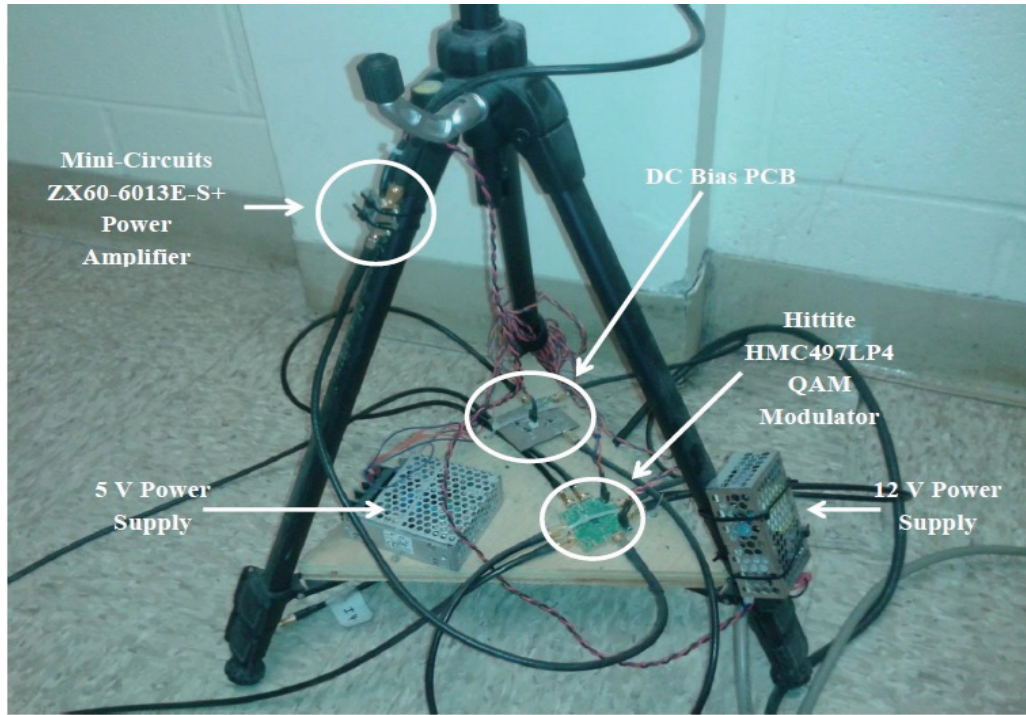


Figure 4.2 (b): Major Components of Portable User

Figure 4.2: Portable-User Module

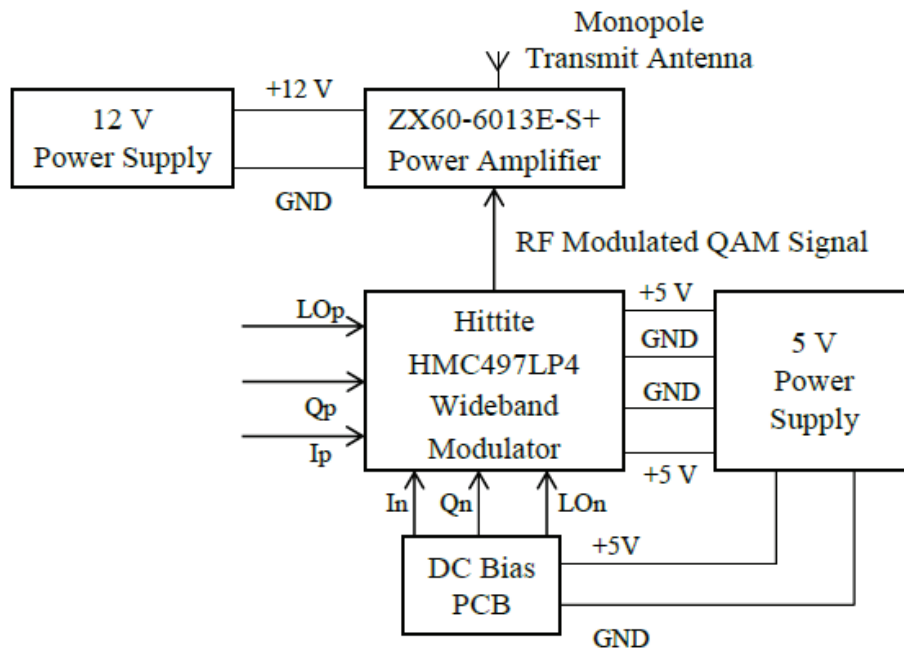


Figure 4.3: Setup Diagram for Portable-User Module

The Hittite HMC497LP4 wideband direct QAM modulator modulates two bits per symbol and acts as the heart of the portable-user module. Figures 4.4 and 4.5 show the evaluation PCB and schematic for the Hittite modulator [58]. It modulates the baseband inphase and quadrature signals being supplied by the FPGA board onto the local oscillator (LO) signal being supplied from the Aeroflex signal generator. The resultant RF QAM signal is amplified with the help of the Mini-Circuits ZX60-6013E-S+ PA before transmitting using a monopole antenna. The DC bias PCB is used to provide a 1.5 V DC bias to the BB_IN and BB_QN pins of the HMC497LP4 modulator.

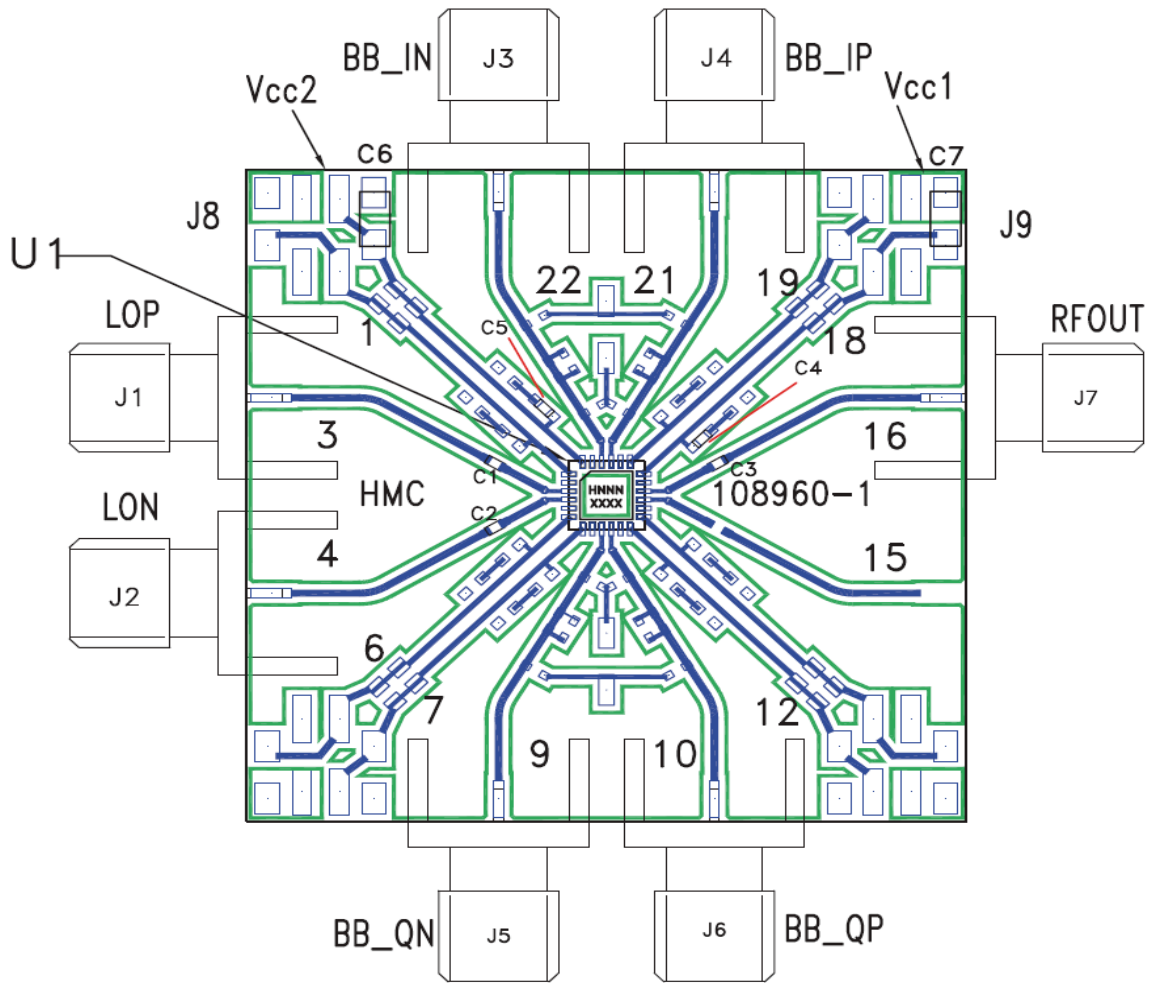


Figure 4.4: Hittite HMC497LP4 Wideband Modulator Evaluation PCB

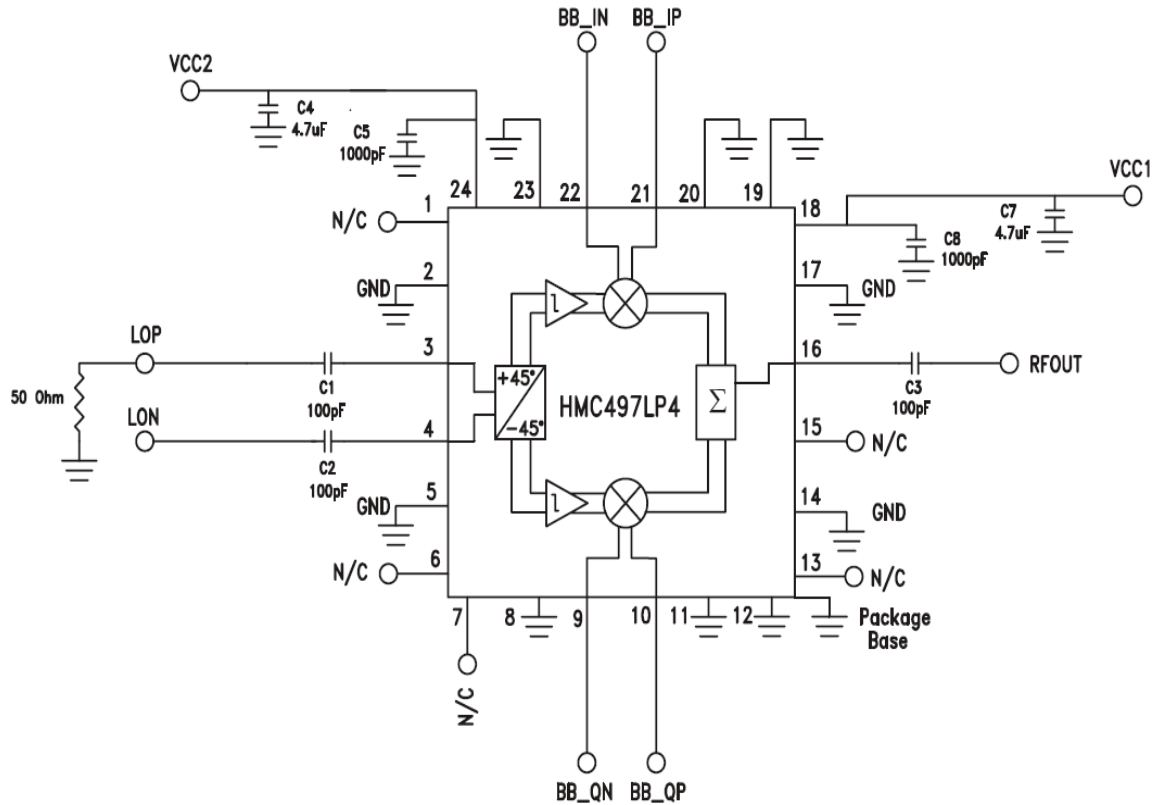


Figure 4.5: Hittite HMC497LP4 Wideband Modulator Schematic

4.1.2 Receiver

The receiver module of the prototype system is basically the reversed copy of the portable-user module with the Hittite HMC497LP4 wideband direct QAM modulator replaced with a Hittite HMC597LP4 wideband QAM demodulator. The receiver module is constructed mainly using a Hittite HMC597LP4 wideband QAM demodulator, a Mini-Circuits ZX60-6013E-S+ wideband PA, a monopole antenna, and 5 V and 12 V power supplies for the demodulator, PA respectively. All of these components are mounted on a wooden platform installed on a camera tripod with inter-component connections made using appropriate length sections of RG-58 coaxial cable. Figure 4.6 shows the fully functional actual receiver module. Figure 4.7 shows the detailed setup

diagram for the receiver module presented in Figure 4.6. The Hittite HMC597LP4 QAM demodulator acts as the heart of the receiver module. The monopole antenna is used to receive the RF modulated QAM signal transmitted by the portable-user module. The received RF QAM signal is amplified with the help of the Mini-Circuits ZX60-6013E-S+ PA before being supplied to the Hittite HMC597LP4 demodulator. It demodulates the received RF signal and separates out the baseband inphase and quadrature components of the signal onto the respective outputs accordingly. The Aeroflex signal generator is used to supply the LO carrier signal used for demodulation.

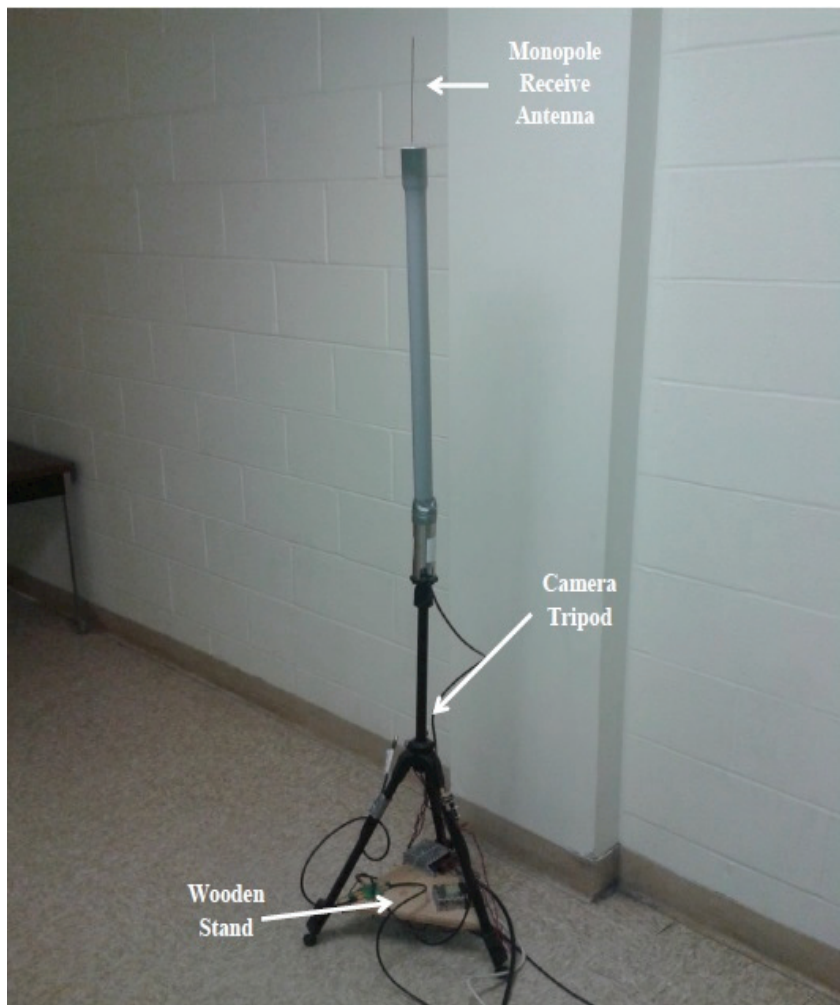


Figure 4.6 (a): Receiver

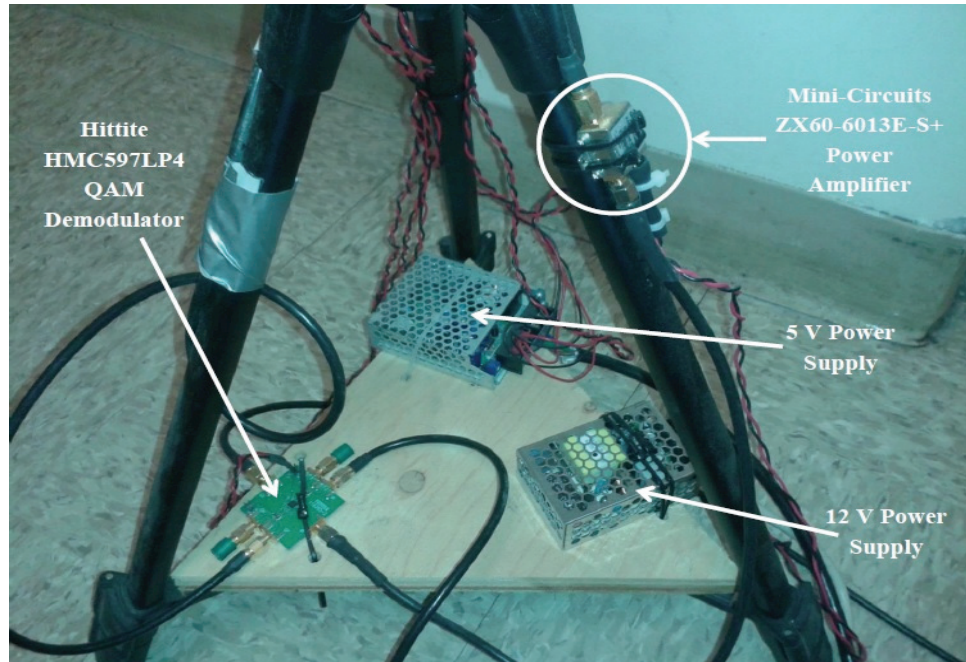


Figure 4.6 (b): Major Components of Receiver

Figure 4.6: Receiver Module

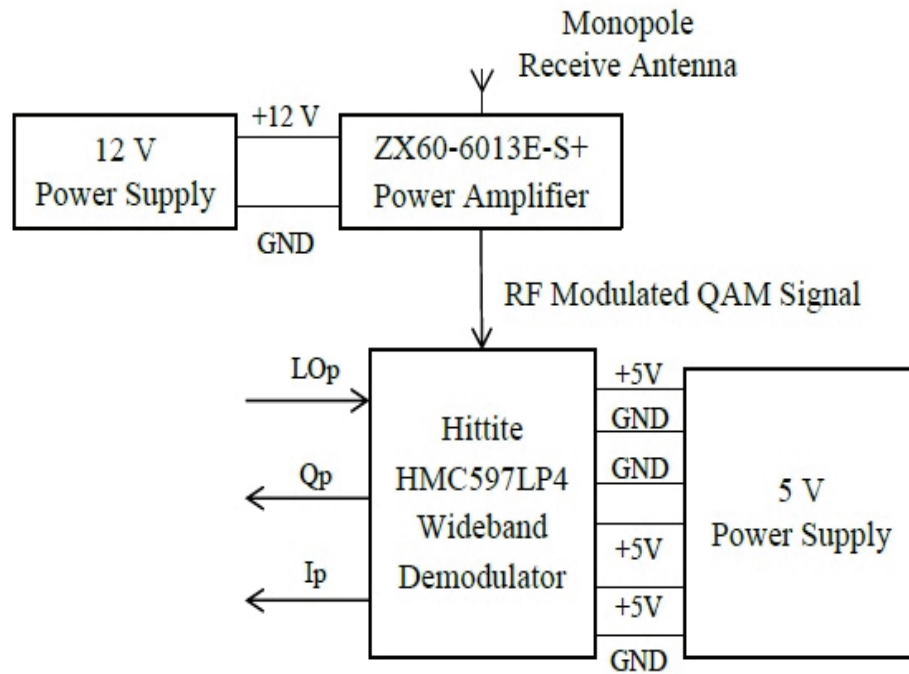


Figure 4.7: Setup Diagram for Receiver Module

Figures 4.8 and 4.9 show the evaluation PCB and schematic for the Hittite demodulator [59].

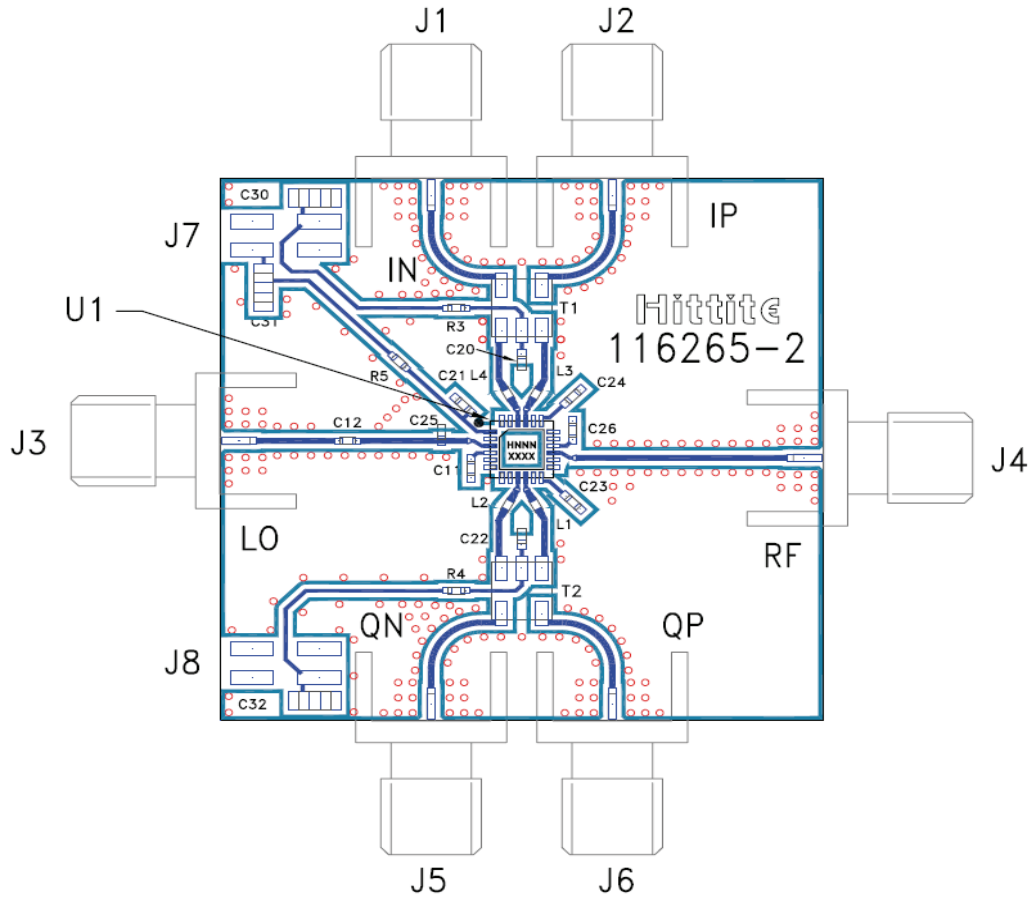


Figure 4.8: Hittite HMC597LP4 Wideband Demodulator Evaluation PCB

4.1.3 Baseband Processing and Control Hub

The baseband processing and control hub module of the prototype system consists of all the devices that are mainly used for baseband generation and processing of data as well as the devices that facilitate and control the communication among the portable user and the receiver modules of the prototype system. The baseband processing and control hub module mainly consists of an Altera Stratix II FPGA development board, a computer system installed with required software (mainly MATLAB and Quartus[®] II), an Aeroflex

signal generator, a signal conditioning PCB [21] and external ADC AD6645 daughter board. Figure 4.10 shows the actual fully functional baseband processing and control hub module. Figure 4.11 shows the detailed setup diagram for the module presented in Figure 4.10.

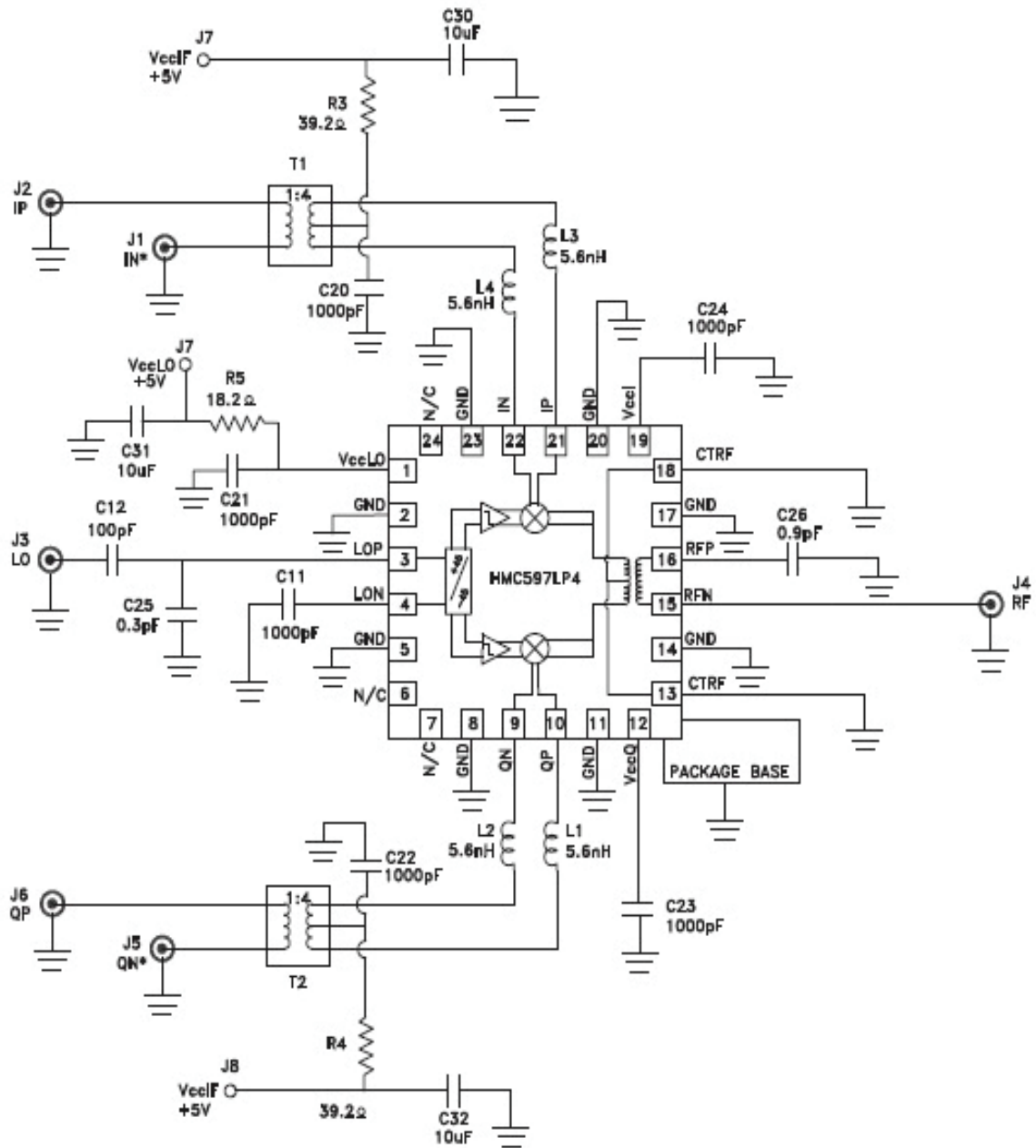


Figure 4.9: Hittite HMC597LP4 Wideband Demodulator Schematic

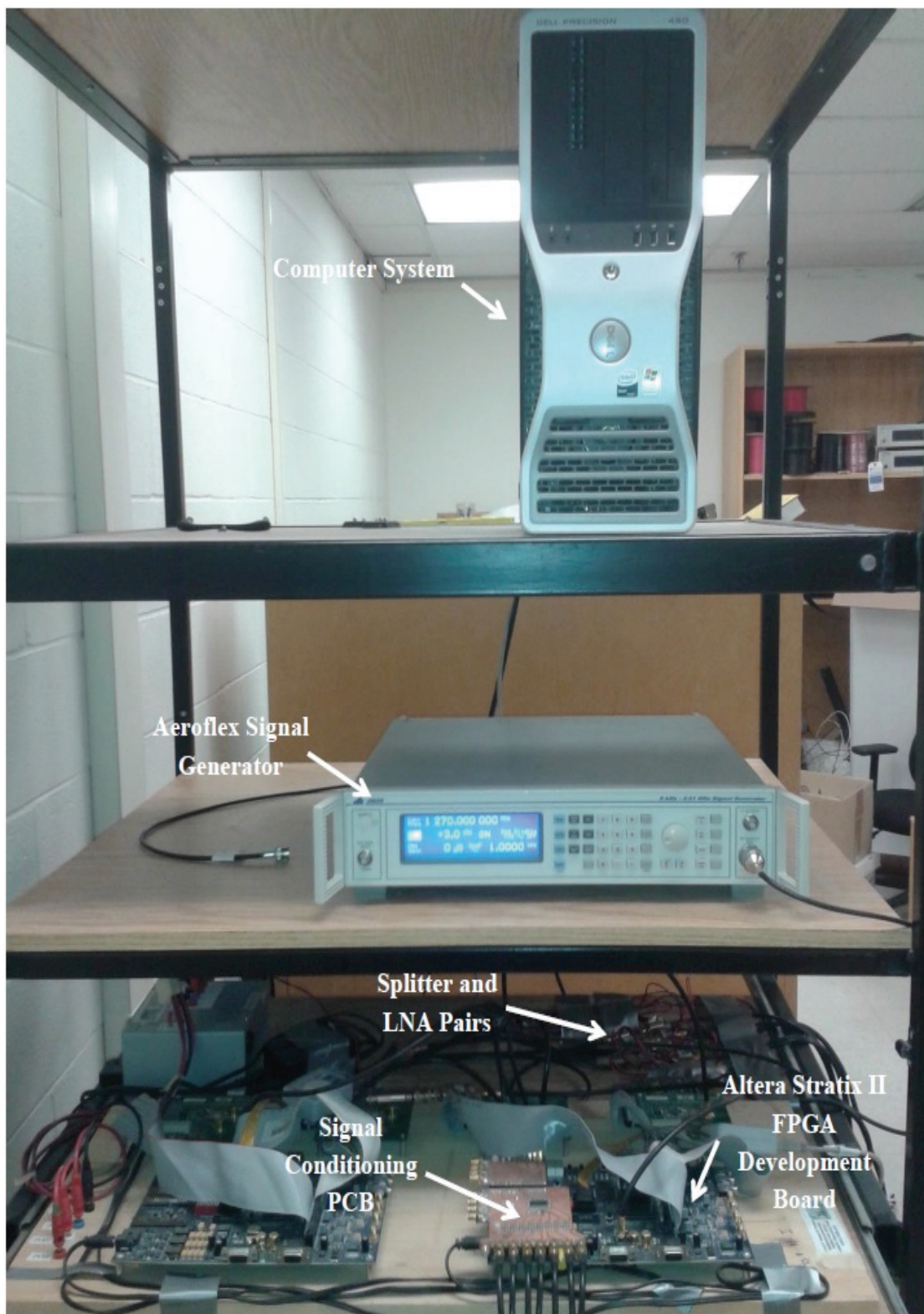


Figure 4.10: Baseband Processing and Control Hub Module

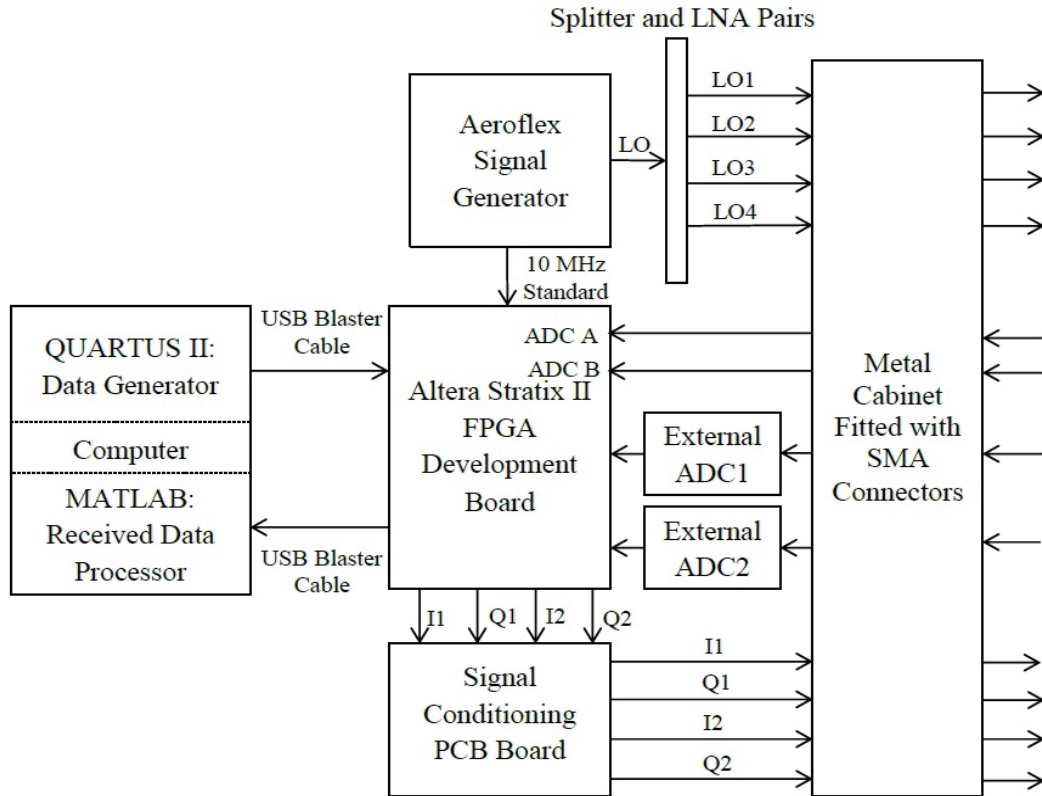


Figure 4.11: Setup Diagram for Baseband Processing and Control Hub Module

As can be seen in Figure 4.11 the computer system acts as the heart of the baseband processing and control hub module. The software package named Quartus II is used to generate soft-baseband data required for portable users in the form of software instructions. The universal serial bus (USB) blaster cable facilitates the transfer of soft-baseband data to the FPGA development board using a static random access memory (SRAM) object file (.sof). The Stratix II FPGA development board uses the soft-baseband data supplied by Quartus II in the form of software instructions and uses the low-voltage transistor-transistor logic (LVTTTL) standard to output baseband data on the general purpose input-output (GPIO) pins of the FPGA board. Since the Hittite HMC497LP4 wideband direct QAM modulator only accepts baseband data between

1.4 V_{DC} and 1.6 V_{DC} therefore the signal conditioning PCB developed by Harriman [21] is used to transform 0 V – 3.3 V LVTTTL baseband data from FPGA board to appropriate form before being supplied to Hittite HMC497LP4 QAM modulator. The Aeroflex signal generator serves a dual purpose: with the help of a splitter it is used to provide same local oscillator signal to all the portable-user modules and receiver module and additionally it is used to provide the external standard reference signal of 10 MHz to the FPGA development board. The FPGA development board ADCs along with two external AD6645 daughter boards are used to sample the baseband demodulated data received from the Hittite HMC597LP4 QAM demodulator used in the receiver module. The sampled data is transferred from the FPGA development board to the computer system for further baseband processing using MATLAB.

4.2 System Implementation

In the previous section the prototype MU-MIMO system design and hardware architecture details were presented. Figure 4.12 depicts the system implementation details for the prototype MU-MIMO system hardware architecture discussed in the previous section.

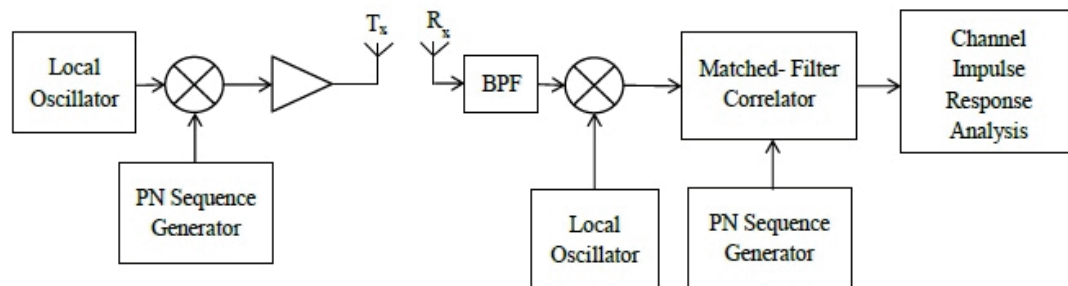


Figure 4.12: System Implementation for Prototype MU-MIMO

As can be seen the system has been implemented to function as a spread spectrum

matched filter correlator channel sounder. The reason for selecting this implementation method is that it allows for channel measurement using wideband probing signal while still using a narrowband system [19]. Now assuming $x(t)$ as the transmitted PN sequence, $h(t)$ as the impulse response of the wireless channel and $y(t)$ as an input to a matched filter correlator the functioning of an implemented system can be explained as follows

$$y(t) = x(t) * h(t); \quad (4.1)$$

now the impulse response $h_1(t)$ of a matched filter satisfies

$$h_1(t) = x(T_{PN} - t), \quad (4.2)$$

where T_{PN} indicates the period of the given PN sequence. Therefore the output of the matched filter can be modelled as

$$d(t) = y(t) * h_1(t), \text{ and} \quad (4.3)$$

$$d(t) = h(t) * \left(\int_0^t x(\tau)x(T_{PN} - t + \tau)d\tau \right); \quad (4.4)$$

next if we sample $d(t)$ at time $t = T_{PN}$ then

$$d(T_{PN}) = h(t) * \int_0^{T_{PN}} x(\tau)x(\tau)d\tau, \quad (4.5)$$

where $\int_0^{T_{PN}} x(\tau)x(\tau)d\tau$ is an auto-correlation function of a given PN sequence. Since an auto-correlation function for a given PN sequence is approximated by a dirac-delta function which attains peak at time $t = T_{PN}$. Therefore the output of the matched filter can be rewritten as

$$d(T_{PN}) = h(t) * \delta(t - T_{PN}); \quad (4.6)$$

next using the time shifting property of the dirac-delta function $\delta(t - T_{PN})$, the output of the matched filter can be rewritten as

$$d(T_{PN}) = h(t - T_{PN}). \quad (4.7)$$

Therefore the output of a matched filter is a delayed channel impulse response which can be further analyzed to approximate the performance of a MU-MIMO system. This provides an overview of the implementation method used for a prototype system. The actual details of the method of baseband soft-data generation, received baseband data processing and RS-232 control are provided in following subsections:

4.2.1 Baseband Soft-Data Generation

The baseband soft-data generation was carried out with the help of a Quartus II software package installed on the computer system. Since the prototype MU-MIMO system consists of two portable users with each portable user requiring two sets of data (i.e. in-phase component and quadrature component), therefore a total of four sets of baseband soft-data were required. The four sets of sequences known as maximum length PN sequences were generated and each sequence was used as a set of data. The two main reasons for selecting PN sequences as the set of data are: firstly they are somewhat spectrally flat sequences and secondly these sequences have a property such that autocorrelation function for a PN sequence is approximately same as that of white noise and also the cross correlation function for different PN sequences is basically a function with root mean square (RMS) value close to zero. As discussed before this property of PN sequences helps in the recovery of the wireless channel impulse response.

Despite the name pseudorandom noise (PN) sequence, the PN sequences have a periodic nature with number of bits $L = 2^n - 1$, where n denotes the degree of the PN sequence. The selection of the PN sequences of particular degree for this application is mainly guided by two major criteria named the multipath resolution and the coherence

time of the wireless channel. Although the wireless channel considered in this thesis is mostly LOS, still there are some multipath components present in the real wireless channel. For the implementation style used with the prototype system the period of the selected PN sequence should be such that the prototype system should be able to resolve at least the longest multipath propagation delay component [19]. The period for the given PN sequence is

$$T_{PN} = T_c L, \quad (4.8)$$

where T_{PN} and T_c denotes the period and chip duration of PN sequence respectively and L denotes the number of chips in a PN sequence. Since the period of the PN sequence should be greater than the longest multipath propagation delay component therefore [19]

$$T_c L > \tau_{max}, \quad (4.9)$$

where τ_{max} is the longest multipath propagation delay component. Therefore the minimum number of bits for the PN sequence that can be used can be rewritten as

$$L > \tau_{max} R_c, \quad (4.10)$$

where R_c is the chip rate of the PN sequence and satisfies $R_c = 1/T_c$. Therefore multipath resolution sets the lower limit on the number of chips in the PN sequence that can be used for given geographical area. As will be seen in the details provided regarding the positioning of the receive antennas the maximum separation between the receive antenna and portable user is found to be 6.52 m. Using a geometrical analysis the longest multipath propagation delay component for room GWD119 was found to be 69.8 ns. Since the maximum chip rate for the PN sequence is 30 MHz therefore the minimum number of bits for the PN sequence that needs to be used to satisfy the multipath resolution was found to be 2.094 bits.

Next the upper bound on the number of chips for the PN sequence is guided by the coherence time of the wireless propagation channel. The coherence time of the propagation channel is the time for which the channel impulse response is essentially invariant, i.e. channel acts as a static channel. The coherence time of the channel is inversely proportional to the Doppler spread of the channel. The coherence time and Doppler spread of a channel can be related as [19]

$$\tau_c = \frac{0.423}{f_m}, \quad (4.11)$$

where τ_c denotes the coherence time of the channel and f_m denotes the Doppler spread of the channel. The Doppler spread of the channel is related to the velocity of the user and carrier frequency of operation and can be modelled as

$$f_m = v_{\text{user}} \frac{f_c}{c}, \quad (4.12)$$

where v_{user} denotes the velocity of the user and f_c denotes the carrier frequency of operation and c denotes the speed of light. Since the carrier frequency of operation for this thesis is 1270 MHz and assuming the velocity of user to be 0.83 m/s the Doppler spread is calculated to be 3.51 Hz. Using this value of Doppler spread the coherence time of the channel is calculated to be 0.120 s. For a given PN sequence all bits experience the same channel if the period of the given PN sequence is small as compared with the coherence time of the channel. Therefore the maximum number of bits for a PN sequence can be calculated as

$$L < \frac{\tau_c}{T_c}, \quad (4.13)$$

next using the values provided above the maximum number of chips for a PN sequence is calculated to be 3 600 000. Using the values above the range for the number of bits of a

PN sequence that can be used can be expressed as

$$2^2 < L < 2^{22}. \quad (4.14)$$

It was decided to use a PN sequence with number of chips $L = 255$ in this thesis. The four sets of PN sequences were generated using a feedback shift register with number of stages equal to eight. Table 4.1 lists the primitive polynomials used for maximum length PN sequence generation.

Table 4.1: Primitive Polynomials

PN Sequence	Primitive Polynomial
I1	$x^8 + x^7 + x^6 + x^5 + x^2 + x + 1$
Q1	$x^8 + x^7 + x^6 + x^3 + x^2 + x + 1$
I2	$x^8 + x^7 + x^6 + x^5 + x^4 + x^2 + 1$
Q2	$x^8 + x^7 + x^6 + x + 1$

The generated baseband soft-data in the form of PN sequences was transferred to FPGA development board and eventually transmitted into RF spectrum with the help of transmit antenna at each portable user.

4.2.1 Received Baseband Data Processing

The received baseband data processing is mainly carried out with the help of MATLAB to recover the channel impulse response from the received data. Figure 4.13 shows the major steps carried out to obtain the impulse responses for the channel matrix. As can be seen the demodulated data received from the HMC597LP4 QAM demodulator is first sampled using ADCs and further transferred to the computer system with the help of the FPGA development board and USB blaster cable. The SignalTap[®] Logic Analyzer module of the Quartus II software is used to read the data received from the USB blaster cable. The received baseband data is transferred from the SignalTap Logic Analyzer

module into MATLAB for further processing. The received baseband data from different receive antennas is down-sampled to undo the oversampling operation that has been carried out at the ADCs. The under-sampled in-phase and quadrature components of the received data from same receive antenna are combined to form the complex baseband data for particular receive antenna. The complex baseband data for each receive antenna is used as an input to the matched filter correlator matched to each portable user. As explained in the implementation section of this chapter the output of the matched filter is the channel impulse response for particular portable user and receive antenna combination. The further analysis of the recovered channel impulse response matrix is carried out to analyze the performance of the prototype MU-MIMO system.

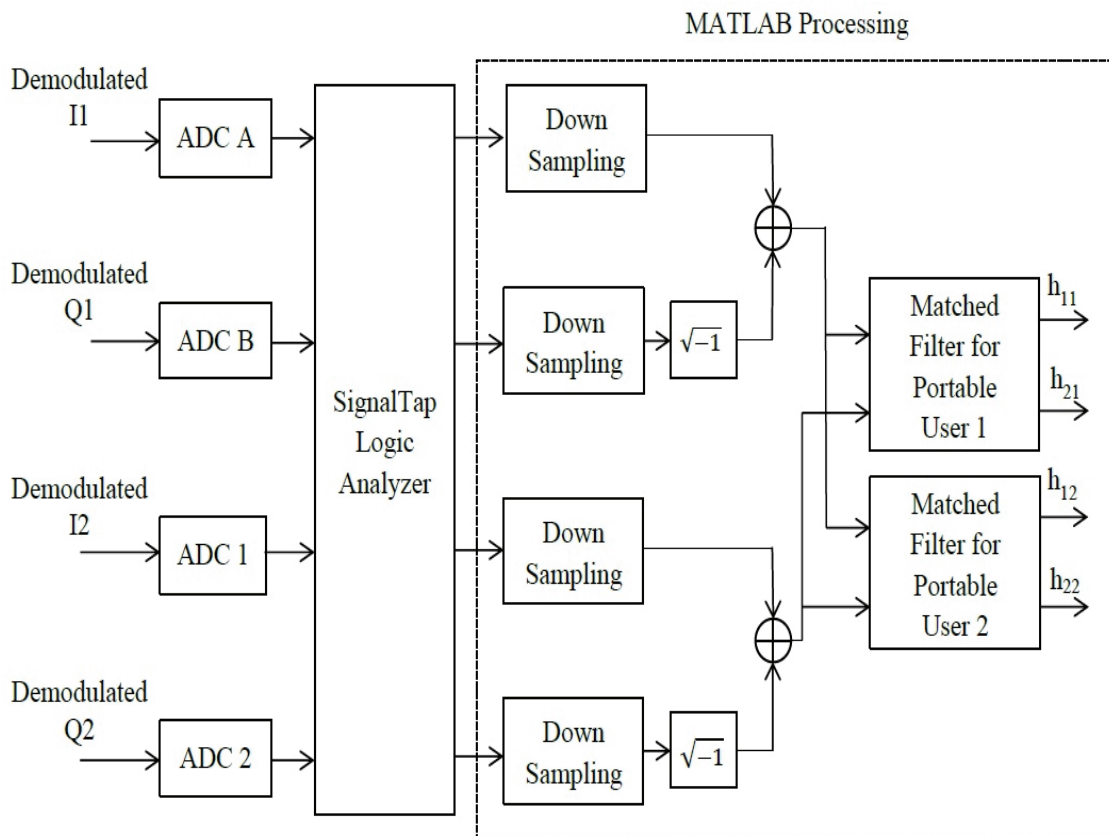


Figure 4.13: Received Signal Baseband Processing

4.2.1 RS-232 GUI Control

The RS-232 GUI control was developed with the help of the MATLAB GUI feature. The GUI control basically serves the two major purposes: firstly it is used to control the local oscillator RF power and carrier frequency by controlling the functioning of the signal generator and secondly it is used to facilitate the data collection by automating the major steps performed during data collection. The RS-232 GUI developed with the help of MATLAB is depicted in Figure 4.14. As can be seen the signal generator section of the control can be used to set the carrier frequency of operation and RF power of the output of the signal generator. This helps to set the desired carrier frequency and output RF power when system is initially powered-on or during any session of operation. The data collection section of the control is used to automatically transmit the author's amateur radio callsign in the form of Morse code at a rate of six words per minute. Since the amateur RF band is used for RF transmissions therefore the author is required to transmit the callsign at the start, end and after every thirty minutes of the RF transmission session. Therefore, the Morse code transmission control facilitates the management of RF band of operation. Despite the automation of callsign transmission the author is still required to listen for the presence of other users in the band of operation before start of any RF transmission. The reason for this is that the amateur users are secondary users in the 1240 MHz – 1370 MHz band. The GUI is also used to select the number of readings to be taken, the number of periods of data to be collected and the portable user baseband bandwidth to be used for particular session of operation. This greatly facilitates and automates the data collection operation required for performance analysis of the prototype MU-MIMO system.

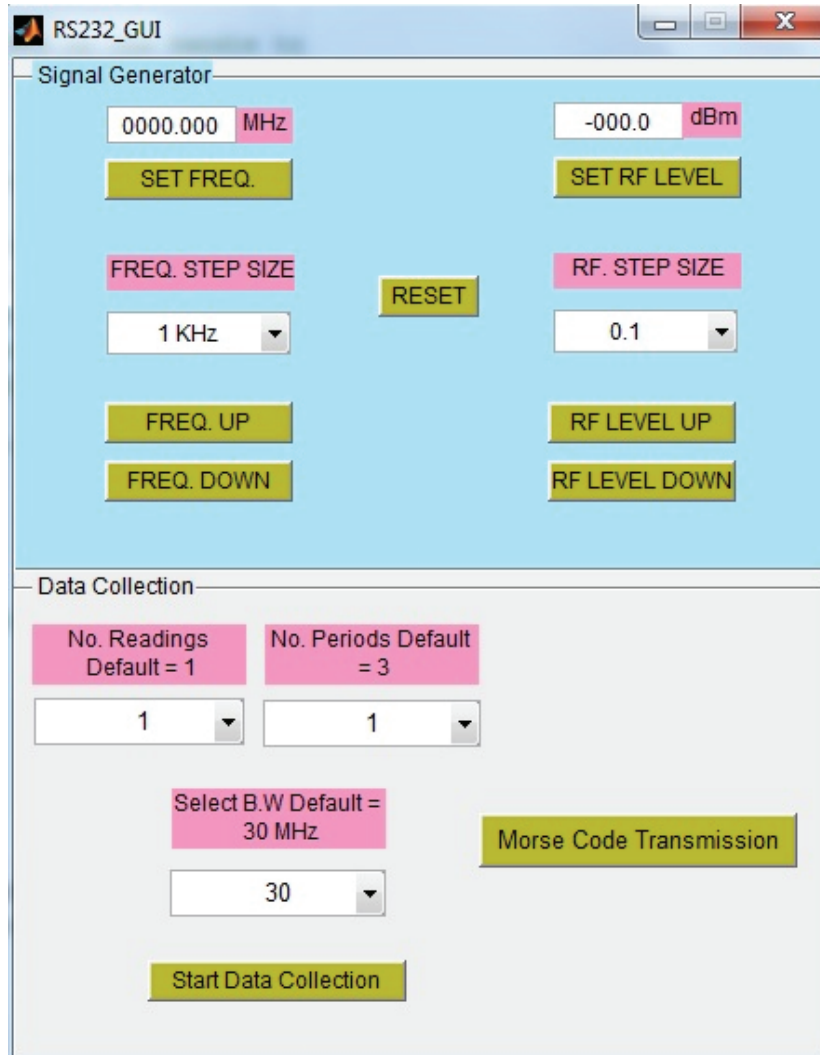


Figure 4.14: RS-232 GUI Control

Chapter 5: Simulation Results

In this chapter, the simulation results are presented. A simulation model was created with the help of MATLAB to approximate the optimal required baseband bandwidth, ADC dynamic range requirements for different portable user locations and to see the effect of different allocated portable user baseband bandwidths on the separability performance of a MU-MIMO system. In addition, the simulation model is used to access the precision of the theoretically proposed hypothesis in equation (3.45) to approximate the 90-50 MMB of an office environment. In this simulation a 2×2 MU-MIMO system model with uniform linear antenna array for a receiver has been considered. The dimensions of an office environment under consideration in the x , y and z directions are defined as d_x , d_y and d_z and are same as of room GWD119. This is depicted in Figure 5.1 and would be referred to as an office environment from this point onwards in this thesis.

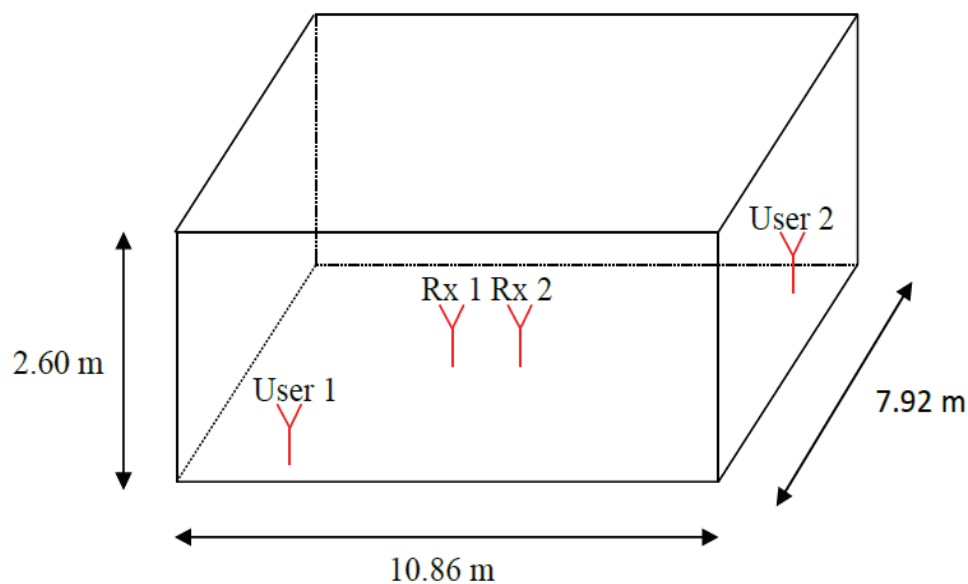


Figure 5.1: Office Environment under Analysis

As can be seen in Figure 5.1, the office environment is modelled as an empty room with the exception of two portable users each equipped with a single transmit antenna and a uniform linear antenna array receiver consisting of two receive antennas. The receive antennas are separated on the scale of carrier wavelength λ_c . The RF measurements in this thesis are conducted using the amateur radio band of 1240 MHz - 1300 MHz employing double sideband quadrature amplitude modulators; therefore for simulation purposes the carrier frequency of 1270 MHz is used leading to a receive antenna separation of 0.23 m. In addition, the receiver is situated in the middle of the office environment with the receive antennas at a height of 1.6 m above the floor. There are two individual portable users with each equipped with a single transmit antenna. The height of the portable user antennas above the floor is same as that of the receive antennas. The portable users are independent of each other and can be present at any location within the physical boundaries of an office environment under consideration. Due to the physical dimensions of portable users and the receiver the minimum separation distance of 0.3 m is always assumed to exist among portable user antennas, receive antennas and the wall. The transmit and receive antennas are assumed to be monopole antennas having an omnidirectional radiation pattern. The transmit power for individual portable users is set to a value of -17.4 dB. For the purpose of simulations the resulting 2×2 MU-MIMO channel matrix \mathbf{H}_P is modelled as

$$\mathbf{H}_P^k = \begin{bmatrix} e^{-j2\pi f(k)\tau_{11}} & e^{-j2\pi f(k)\tau_{12}} \\ e^{-j2\pi f(k)\tau_{21}} & e^{-j2\pi f(k)\tau_{22}} \end{bmatrix}, \quad (5.1)$$

where k represents the discrete sample point index, $f(k)$ represents the discrete frequency points over the baseband frequency range and \mathbf{H}_P^k represents the channel

matrix \mathbf{H}_P sampled at discrete frequency points. For the separability performance analysis of matrix \mathbf{H}_P^k a set of condition numbers is computed for individual frequency sample points as represented below

$$\text{cond}(k) = \frac{\sigma_{\max}(\mathbf{H}_P^k)}{\sigma_{\min}(\mathbf{H}_P^k)}, \quad (5.2)$$

where σ_{\max} and σ_{\min} are the maximum and minimum singular values of channel matrix \mathbf{H}_P^k . The resulting condition number cond is calculated by obtaining the average of a set of condition numbers calculated at individual frequency sample points. The condition number corresponding to particular location of portable user for the case of particular allocated user bandwidth is computed in similar fashion. The ADC dynamic range requirements analysis is carried out by analyzing the received power calculations for receiver antennas corresponding to particular locations of portable users. The dynamic range requirements for the ADC corresponding to particular receive antennas is calculated as

$$\text{DR_ADC}_N(u) = 3 \log_2 \left(3 \frac{\max(P_{N1}, P_{N2})}{\min(P_{N1}, P_{N2})} \text{SQNR}_{\min} \right), \quad N = 1, 2 \quad (5.3)$$

where u is a portable user location index, P_{N1} indicates the power received at antenna N due to power transmitted by portable user 1 and where P_{N2} indicates the power received at antenna N due to power transmitted by portable user 2. The required minimum and maximum ADC dynamic range for the system is computed as

$$\text{DR_ADC}_{\min} = \min (\text{DR_ADC}_1(u), \text{DR_ADC}_2(u)) , \quad (5.4)$$

$$\text{DR_ADC}_{\max} = \max (\text{DR_ADC}_1(u), \text{DR_ADC}_2(u)) . \quad (5.5)$$

To simulate the movability feature of the portable users considered in this thesis a grid of probable user locations was designed. The separation between the points of a grid

is determined by the size of an office environment and the total number of portable user locations. In this thesis the number of locations is fixed such that as the size of an office environment increases the separation among the points of a grid increases and vice versa. Additionally, the separation among the grid points along the x and z directions is guided by the ratio of the dimensions d_x and d_z of an office environment such that

$$\frac{d'_x}{d'_z} = \frac{d_x}{d_z}, \quad (5.6)$$

where d'_x and d'_z is the separation among portable user locations along dimensions d_x and d_z of an office environment respectively. The setting of grid point separation in accordance with the relation presented in equation (5.6) ensures that grid point spacing is proportionate as per the office environment dimensions. This is depicted with the help of Figure 5.2.

x - Receiver Antenna Location

o - Portable User Location

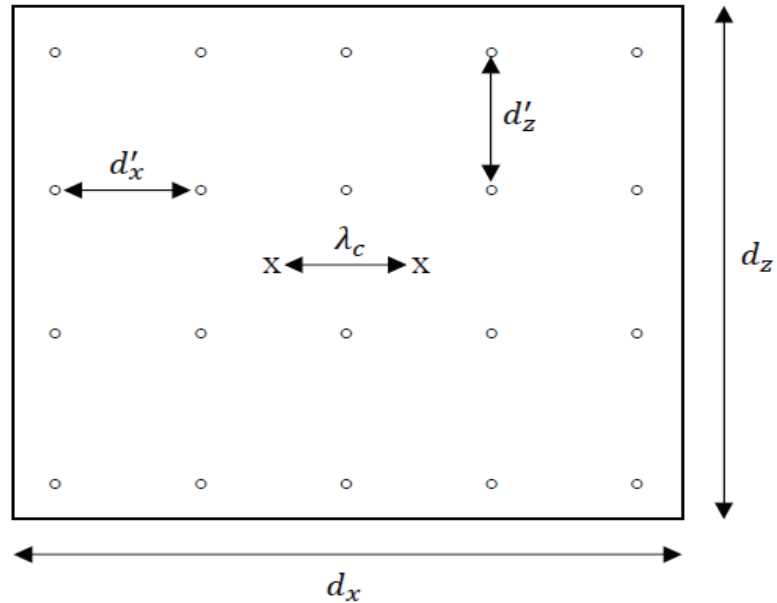


Figure 5.2: Grid of Portable User Locations

The set of simulations is carried out using the above mentioned portable user and receiver operational parameters. For the purpose of simulations, the number of portable user locations is fixed to 500 and portable users are distributed within the physical boundaries of an office environment guided by the grid of user locations. The simulations are divided into different sets for the purpose of analysis:

- The first set of simulations is carried out to perceive the overall trend of required baseband bandwidth resulting in an ideal channel transfer function matrix. The results are also presented by scaling an office environment to different sizes such as to see the effect of size of an office environment on the bandwidth requirements.
- The second set of simulations is carried out to analyze the effect of dimensions of an office environment on the ADCs dynamic range requirements.
- The third set of simulations consists of analysis of performance of a MU-MIMO system for different values of allocated portable user baseband bandwidths.

5.1 Required Baseband Bandwidth Trend

As per equations (3.26) and (3.27) the different portable user locations result in different baseband bandwidth requirements for the optimized channel matrix \mathbf{H}_p^k presented in equation (5.1). It is important to observe the bandwidth requirement of different portable user locations because it reflects the general bandwidth requirements of an office environment. The simulations are carried out to present the results in terms of the percentage of portable user locations contributing to a particular value of required user bandwidth. Figure 5.2 shows the effect of portable user locations on the optimal baseband bandwidth requirement for a 2×2 MU-MIMO system present in an office environment depicted in Figure 5.1.

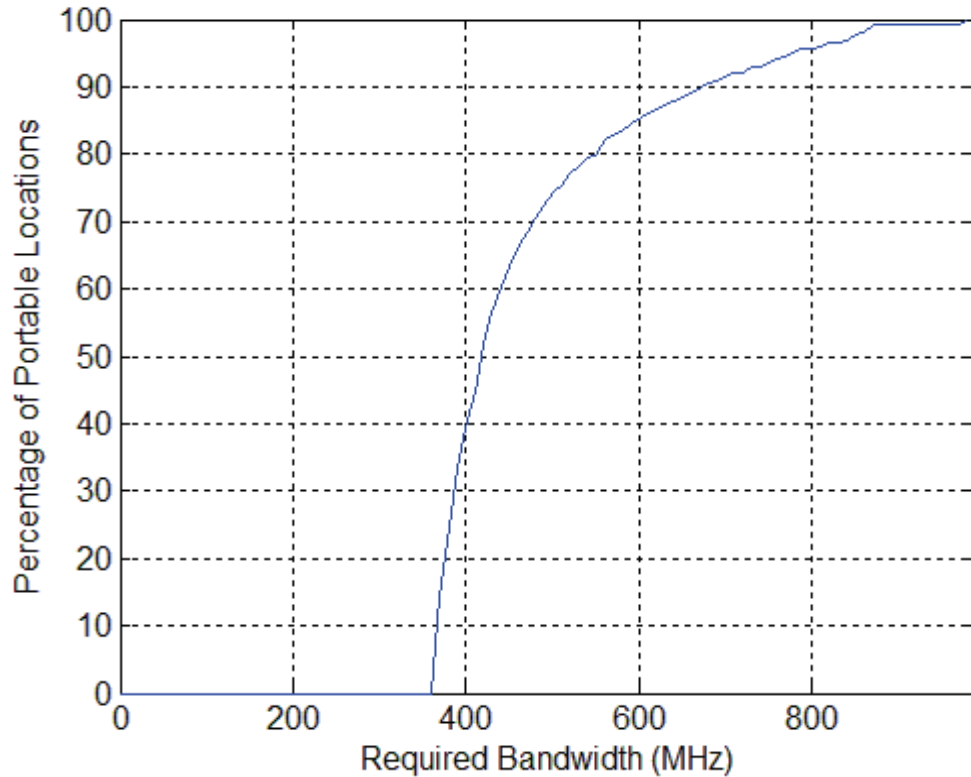


Figure 5.2: Bandwidth Requirement for Office Environment with No Room Scaling

As can be seen for 50% of the portable user locations the optimal value of baseband bandwidth requirement for a 2×2 MU-MIMO system under analysis lies in the range of 360 MHz – 420 MHz. Another 30% of the portable user locations contribute to optimal baseband bandwidth requirement in the range of 430 MHz – 550 MHz whereas rest of 20% of the portable user locations contributes to the remaining optimal baseband bandwidth requirements in the range of 550 MHz – 970 MHz. This shows the general trend of baseband bandwidth requirements for an office environment under consideration for the given setup of receiver and portable user locations. It is also important to see the effect of office environment dimensions on the baseband bandwidth requirements. Figures 5.3, 5.4 and 5.5 show the optimal baseband bandwidth

requirement results for an office environment for the case when the dimension d_x is scaled by half, d_z is scaled by half and both d_x and d_z are scaled by half respectively. For the purpose of clarity and simplicity the results from this point onwards in this thesis will be referred using following notations:

- Office environment with dimensions presented in figure 5.1: oe_case1
- Office environment with dimension d_x scaled by half: oe_case2
- Office environment with dimension d_z scaled by half: oe_case3
- Office environment with dimensions d_x and d_z scaled by half: oe_case4

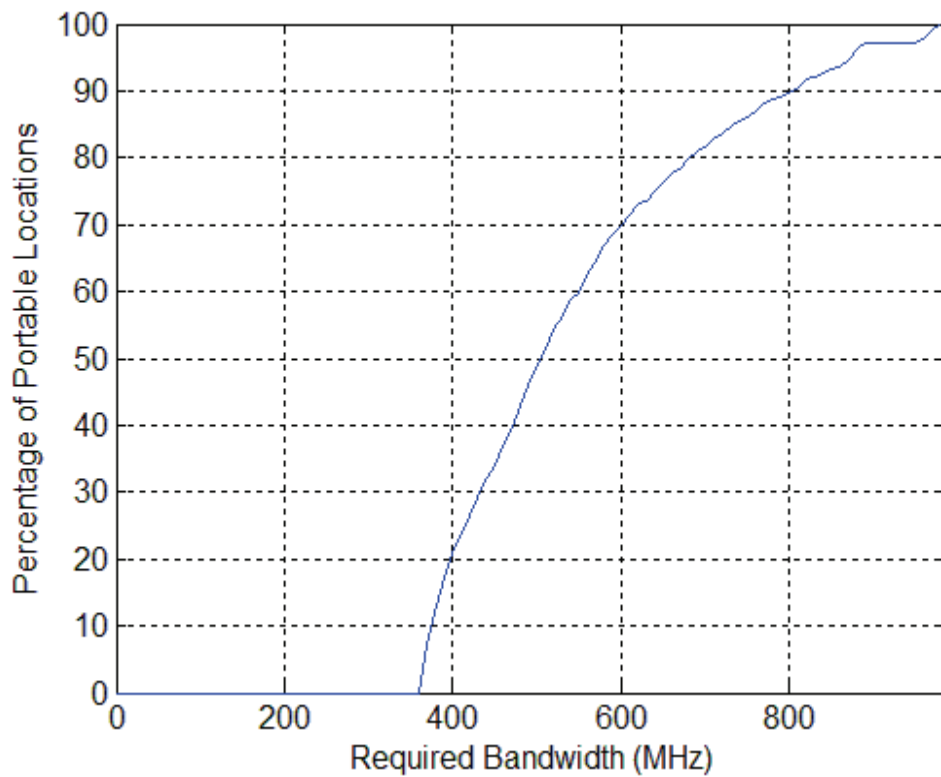


Figure 5.3: Bandwidth Requirement for oe_case2

Figure 5.6 presents the comparison of the results presented in Figures 5.2, 5.3, 5.4 and 5.5 for oe_case1, oe_case2, oe_case3 and oe_case4.

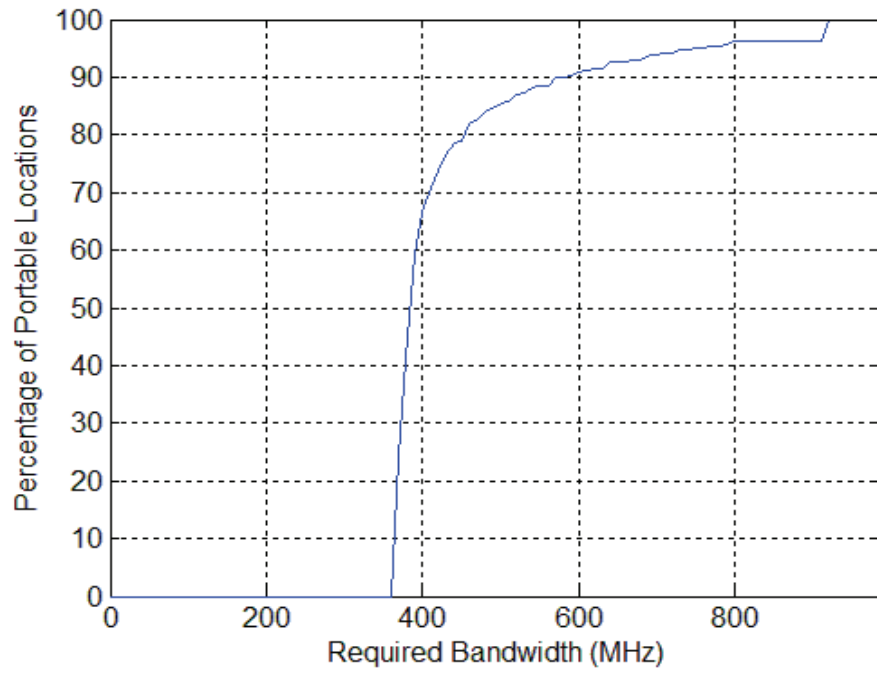


Figure 5.4: Bandwidth Requirement for oe_case3

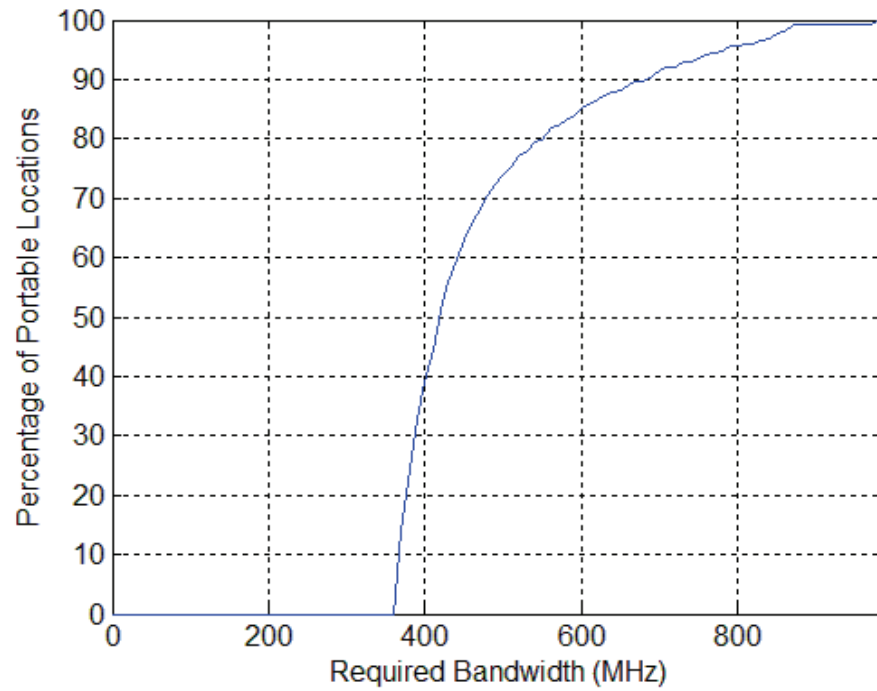


Figure 5.5: Bandwidth Requirement for oe_case4

It is directly evident that the bandwidth requirements changes with the change in the dimensions of an office environment. This can be related to a change in the angle of incidence of portable users on receive antennas due to change in the physical dimensions.

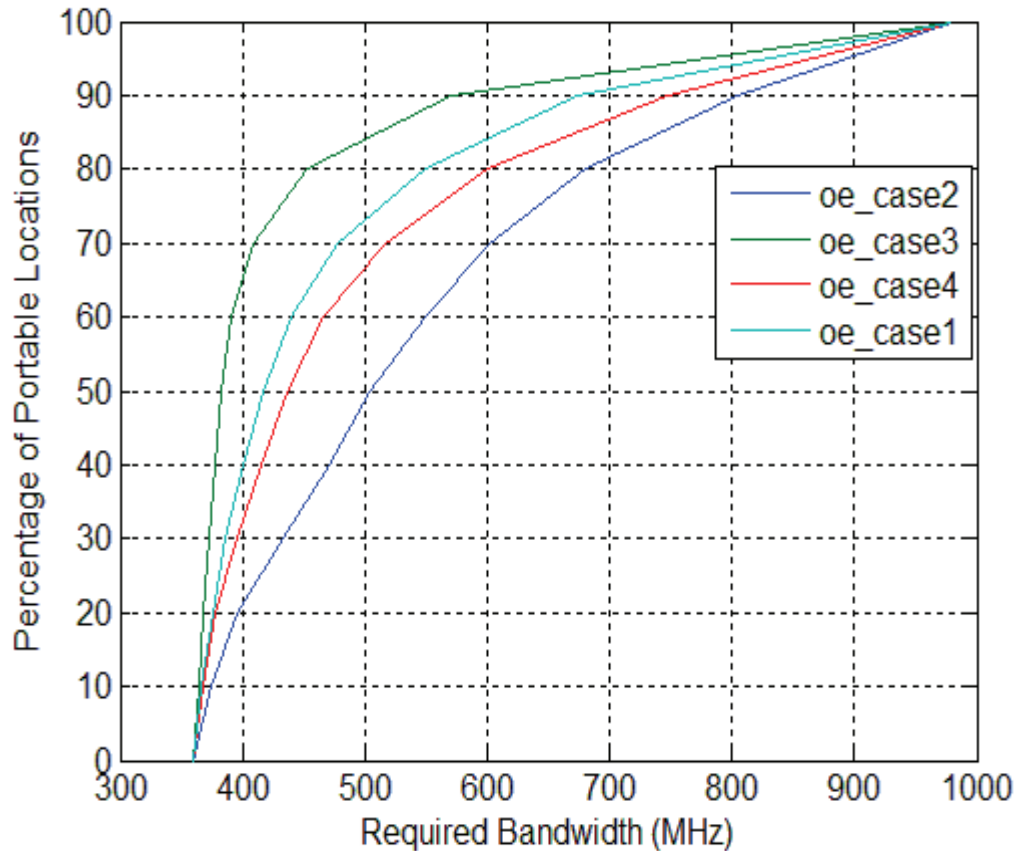


Figure 5.6: Comparison of Bandwidth Requirement Results

A closer examination of the results presented in Figure 5.6 reveals that the bandwidth requirements of an office environment increases with the decrease in the dimensions of an office environment. This is as per theoretical analysis predictions since an office environment with smaller dimensions would result in smaller changes in angle of incidences of portable users on receive antennas therefore resulting in higher bandwidth requirements. The presented results also reveal the effect of change in

particular dimension of an office environment on the bandwidth requirements. It can be clearly seen that the decrease in the dimension of an office environment along the axis of receive antenna array results in an increase in the bandwidth requirements. This is attributed to the fact that a decrease in the dimension along the axis of the receive antenna array results in a decrease of portable user locations having large angle of incidence differences as presented in equation (3.23). Similarly, the decrease in the dimension perpendicular to the axis of the receive antenna array results in decrease in the bandwidth requirements. This can again be attributed to the fact that the decrease in the dimension perpendicular to the receive antenna array axis results in increase of portable user locations having large angle of incidence differences as presented in equation (3.23). The first set of simulations provided an insight into the general bandwidth requirement trends for an office environment. Additionally, it also showed the effect of changes in the physical dimensions of an office environment on the bandwidth requirement results.

5.2 ADCs Dynamic Range Requirements

In the next set of simulations the effect of changes in the dimensions of an office environment on the systems ADCs dynamic range requirements is analyzed. The analysis is first carried out by computing the ratio of the powers received from portable users on a particular receive antenna. The results are presented in terms of the maximum power ratio of the portable users for ADC1/ADC2 versus normalized maximum distance ratio of portable users within an office environment, where ADC1 and ADC2 are the two ADCs used by two different receive antennas. Figures 5.7, 5.8, 5.9 and 5.10 present the power ratio results for *oe_case1*, *oe_case2*, *oe_case3* and *oe_case4*. It is clearly evident from the presented results that the power ratio of the portable users increases with an

increase in the dimensions of an office environment. This is in accordance with the theoretical analysis carried out in section 3.3 of the thesis.

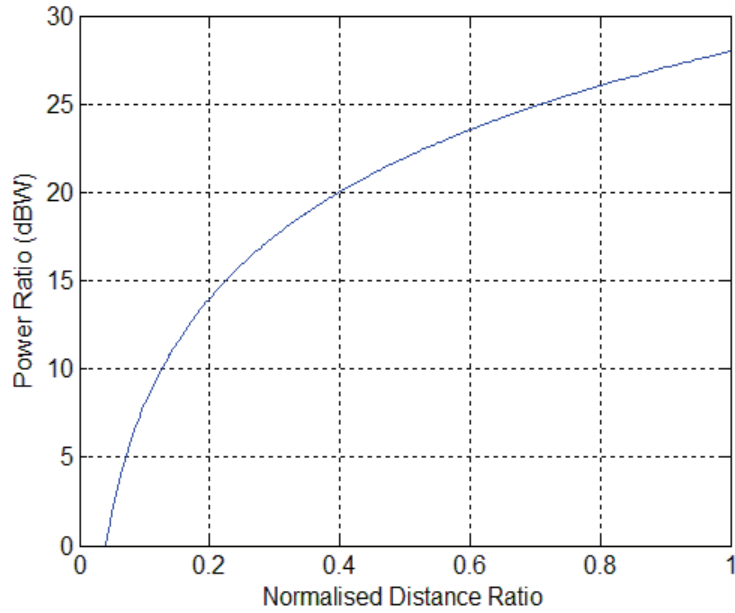


Figure 5.7: Power ratio for oe_case1

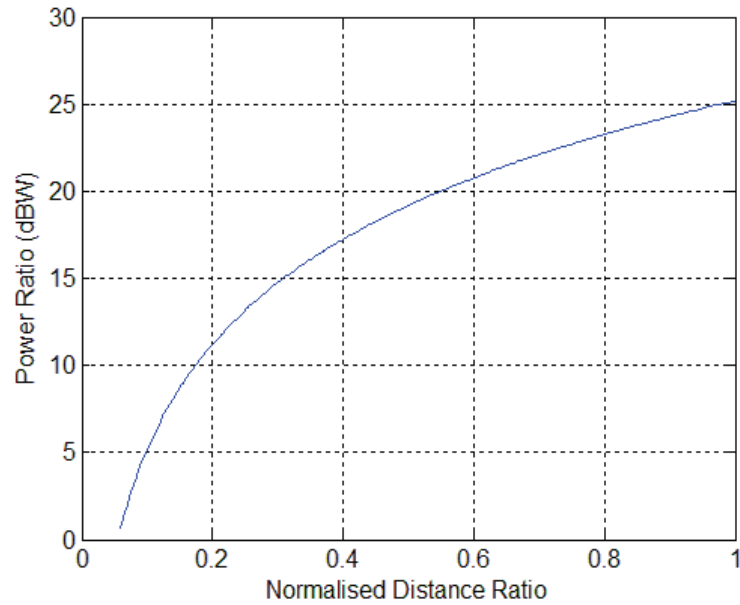


Figure 5.8: Power ratio for oe_case2

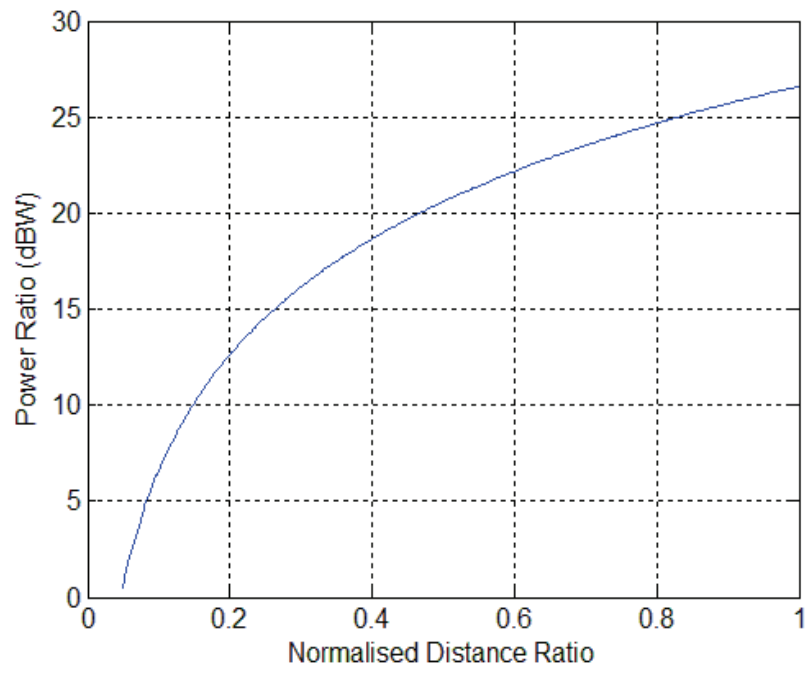


Figure 5.9: Power ratio for oe_case3

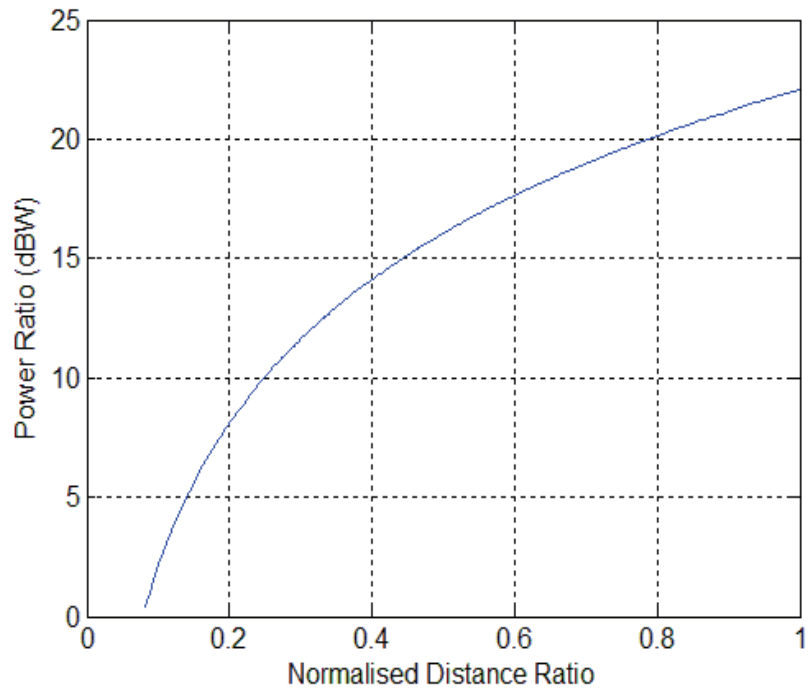


Figure 5.10: Power ratio for oe_case4

The ADC dynamic range requirements for portable user locations for the oe_case1, oe_case2, oe_case3 and oe_case4 are presented in Figures 5.11, 5.12, 5.13 and 5.14. The results are presented in terms of the percentage of the portable user locations resulting in particular ADC dynamic range requirements. The presented results are computed using the relation presented in equations (5.4) and (5.5).

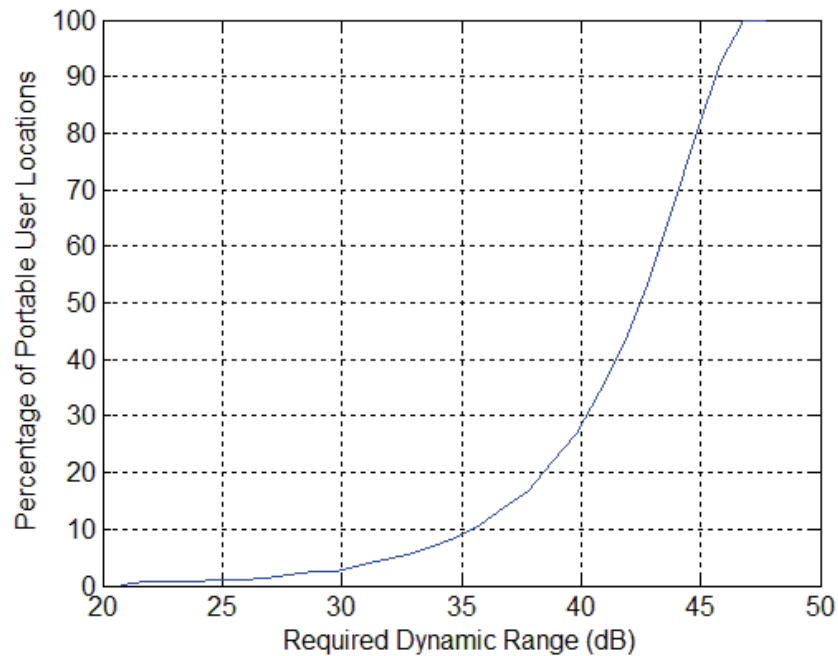


Figure 5.11: ADC Dynamic Range Requirements for oe_case1

As can be seen in Figures 5.11, 5.12, 5.13 and 5.14 the presented results show a common trend of decrease in the ADC dynamic range requirements with the decrease in the dimensions of an office environment. This is again in accordance with the theoretical analysis carried out in section 3.3 of the thesis. The reason being the fact that an office environment with larger dimensions allows for larger separation among portable users as compared to an office environment with smaller dimensions.

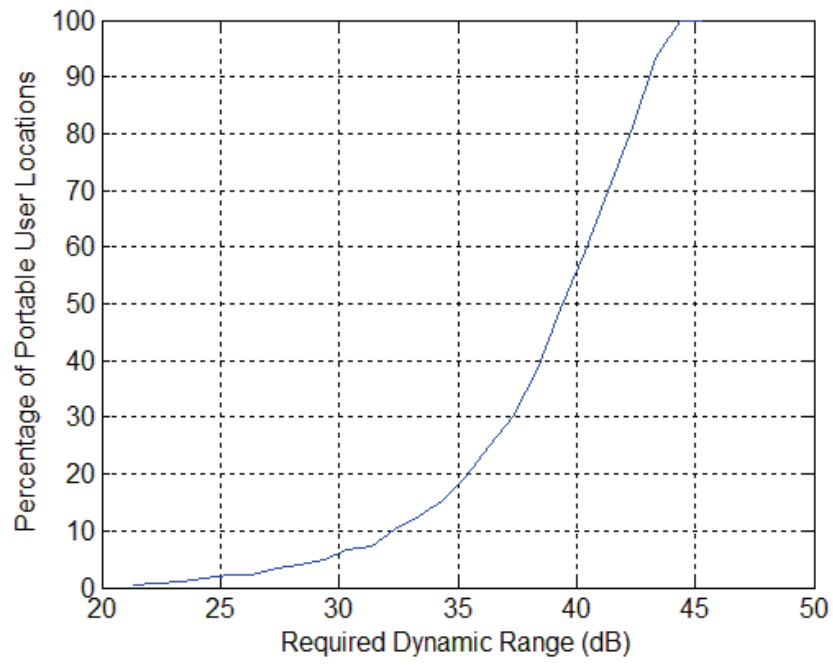


Figure 5.12: ADC Dynamic Range Requirements for oe_case2

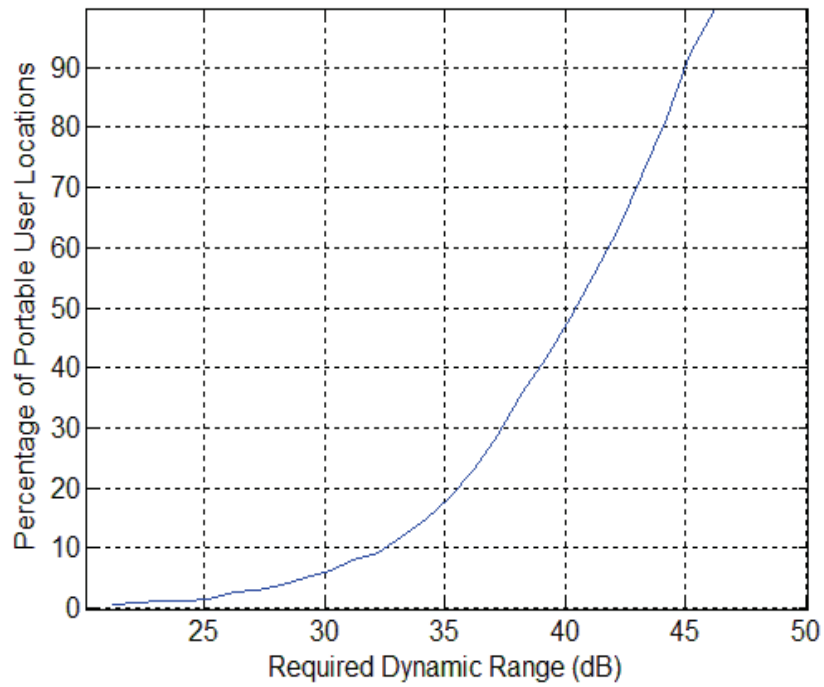


Figure 5.13: ADC Dynamic Range Requirements for oe_case3

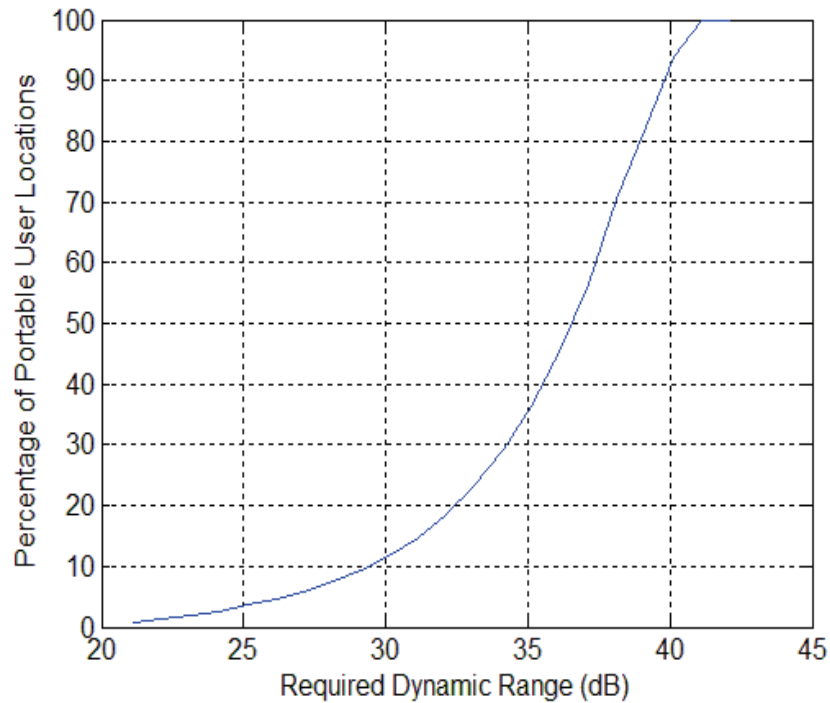


Figure 5.14: ADC Dynamic Range Requirements for oe_case4

The important aspect of the presented results is that the ADC dynamic range requirements are purely dependent on the physical separation of portable users within an office environment. This is in contrast with the bandwidth requirement results where bandwidth requirements are dependent on the physical separation as well as the separation of angle of incidence of portable users on receive antennas.

The above presented two sets of simulation results show the dependence of bandwidth requirement and ADC dynamic range requirement on the physical dimensions of an office environment. It is important to mention here that the baseband bandwidth requirement results are calculated using an optimal condition of having a MU-MIMO channel matrix condition number equal to one. In an office environment with portable users the MU-MIMO channel matrix cannot be optimized for all the user locations for

particular allocated user baseband bandwidth. Therefore, it seems more meaningful to present results in terms of resulting condition numbers for different portable user locations for the case of different allocated user baseband bandwidths.

5.3 MU-MIMO System Performance Results

In the next set of simulation results the effect of an allocated portable user baseband bandwidth on the resulting condition number of the channel matrix for a 2×2 MU-MIMO system is analyzed. Figures 5.15 and 5.16 present results for `oe_case1` and `oe_case4`, respectively. The results are presented in terms of the percentage of the portable user locations that contribute to a particular resulting value of a condition number for different values of allocated user baseband bandwidths. As can be seen the trends followed by the resulting condition numbers due to change of allocated portable user bandwidths is comparable for different office environments. In accordance with the theoretical analysis an increase in the allocated user baseband bandwidth results in an improvement in the separability performance of a MU-MIMO system receiver. This is reflected by an increase in the percentage of portable user locations resulting in lower values of condition number for larger values of the allocated user baseband bandwidths. Table 5.1 presents the data recovered from Figures 5.15 and 5.16 in a tabulated form. The data has been arranged to show the effect of allocated user baseband bandwidth on the resulting condition number of the MU-MIMO channel matrix for different office environments. Following trends are observed for 90% of the portable user locations for two different office environments:

- The condition numbers are relatively high for allocated user baseband bandwidths of 10 MHz and 20 MHz whereas for the allocated user baseband bandwidths of 30

MHz, 60 MHz and 90 MHz the resulting condition numbers are reduced considerably.

- The improvement in the condition numbers tends to saturate with the higher allocated user baseband bandwidths.
- The resulting condition numbers are smaller for office environment with larger dimensions as compared to office environment with smaller dimensions.

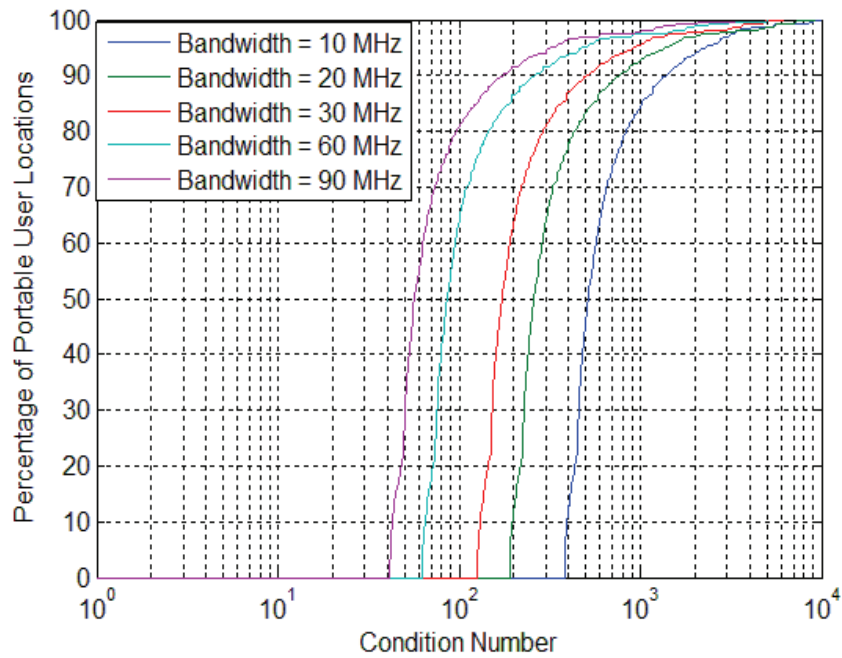


Figure 5.15: Effect of Allocated User Bandwidth for oe_case1

Table 5.1: Allocated User Bandwidth Effect on System Performance

Allocated User Bandwidth	Percentage Portable User Locations	Maximum Condition Number for oe_case1	Maximum Condition Number for oe_case4
10 MHz	90%	1404	2014
20 MHz	90%	799	1083
30 MHz	90%	511	759
60 MHz	90%	264	388
90 MHz	90%	176	260

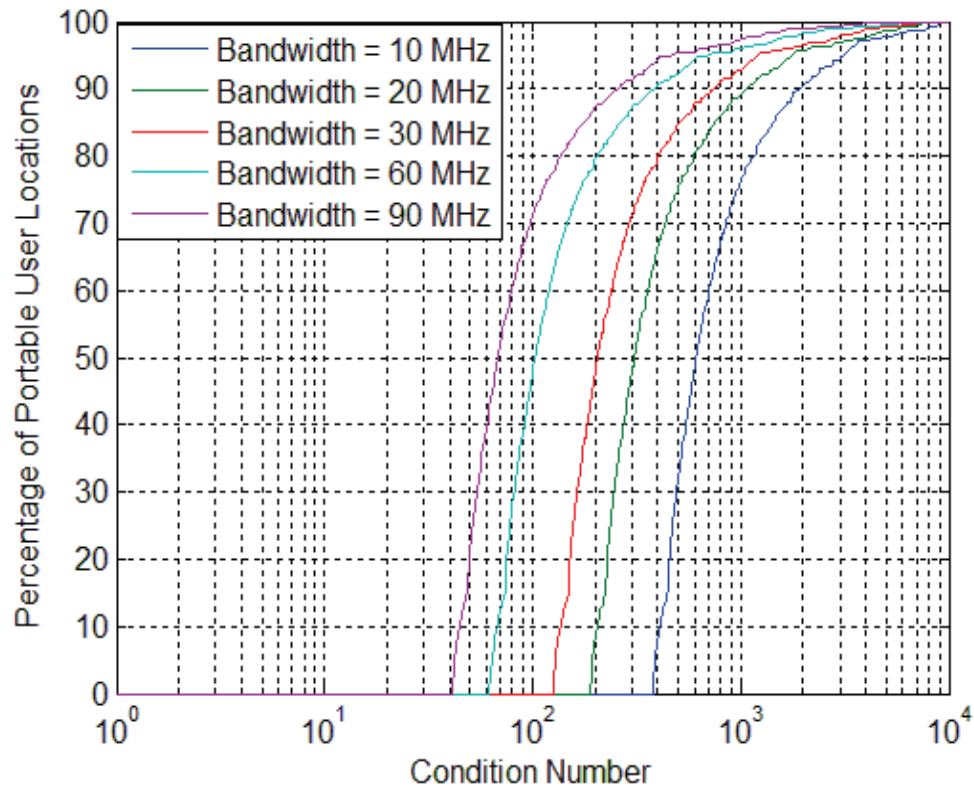


Figure 5.16: Effect of Allocated User Bandwidth for oe_case4

Table 5.2 presents the data recovered from Figures 5.11 and 5.14. The data has been arranged to show the effect of physical dimensions of an office environment on the required dynamic range of the systems ADC's. The following trends are observed for three different office environments:

- The minimum and maximum required ADC dynamic range increases with an increase in the dimensions of an office environment.
- The difference between the minimum and maximum required ADC dynamic range increases with an increase in the dimensions of an office environment.

From the aforementioned discussion, it is concluded that with an increase in the dimensions of an office environment the baseband bandwidth requirements are relaxed

whereas the ADC’s dynamic range requirements become more stringent. This attests to the theoretical predictions that every office environment has average baseband bandwidth and ADC dynamic range requirements that are needed for the existence of an efficient MU-MIMO system within an office environment.

Table 5.2: Office Environment Physical Dimensions Effect on ADC Dynamic Range Requirements

ADC Dynamic Range (dB)	oe_case1	oe_case4
Minimum Required ADC Dynamic Range	20.79	21.13
Maximum Required ADC Dynamic Range	47.79	42.15

Using the relation presented in equation (3.45) the predicted value of 90-50 MMB for oe_case1 is 45 MHz and for oe_case4 is 89 MHz. The data presented in table 5.1 shows that the resulting condition numbers within the allocated user baseband bandwidth range of 30 MHz to 60 MHz for oe_case1 and 60MHz to 90 MHz for oe_case2 are comparable. Additionally, the predicted value of dynamic range for ADCs using the relation presented in equation (3.40) is 41.5 dB and 35.6 dB for oe_case1 and oe_case4 respectively. The results presented in Figure 5.11 show the usage of 41.5 dB of ADC’s dynamic range for approximately 40% of the portable user locations for oe_case1. Similarly, the results presented in Figure 5.14 shows the usage of 35.6 dB of the ADC’s dynamic range for approximately 40.8% of the portable user locations for oe_case4. These values being closer to the expected 50% of the usage therefore attests to the theoretical predictions. The ADC dynamic range requirement results presented above are based purely on free space path loss model using the power exponent factor of 2. The

free space path loss model is a base model for signal propagation but in real indoor environments there is always some presence of multipath components in addition to strong LOS component. Figures 5.17 and 5.18 present the results to analyze the effect of multipath components in the presence of strong LOS component on the ADC dynamic range requirements. The simulations are carried out using a Log-distance path loss model having a power exponent factor of 1.6 and normal random variable having a standard deviation of 5.8 dB [19].

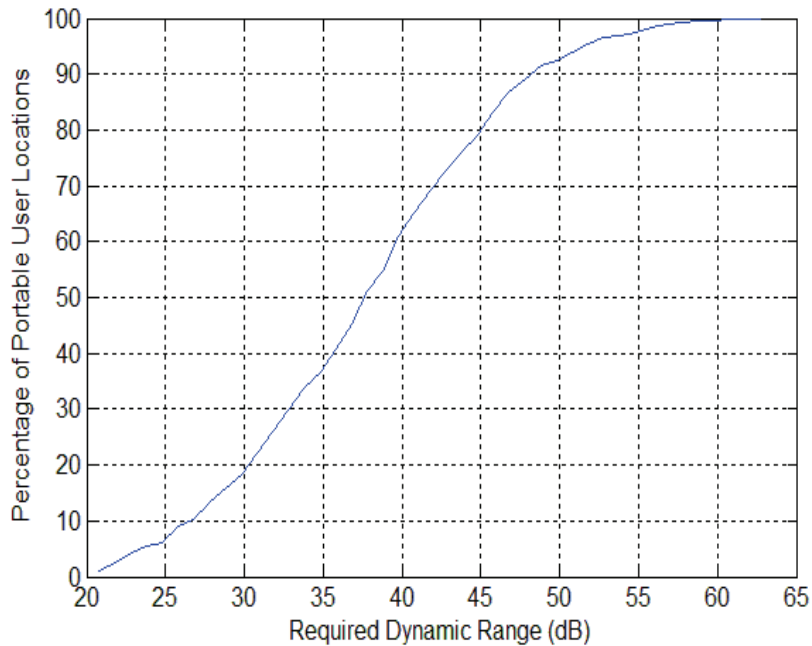


Figure 5.17: ADC Dynamic Range Requirements for oe_case1 with Multipath Effects

The results presented in Figure 5.16 shows the usage of 41.5 dB of the ADC’s dynamic range for approximately 69% of the portable user locations for oe_case1. Similarly, the results presented in Figure 5.17 shows the usage of 35.6 dB of the ADC’s dynamic range for approximately 63.5% of the portable user locations.

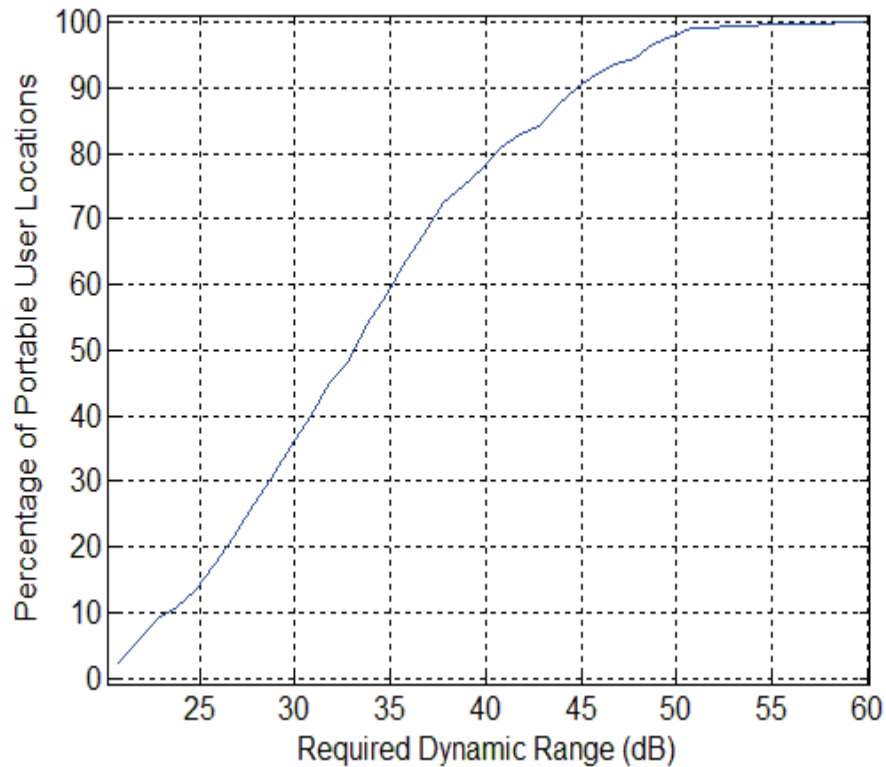


Figure 5.17: ADC Dynamic Range Requirements for oe_case4 with Multipath Effects

This indicates that the ADC dynamic range usage improves in the presence of multipath components as compared to the usage predicted by the free space path loss model. This is in accordance with the theoretical analysis which states that the presence of multipath components results in rapid fluctuations of received signal strength often resulting in decrease in the received signal power [19]. Summarizing the above presented simulation results it can be stated that:

- If the allocated user baseband bandwidth and ADC dynamic range is too small the system performance is degraded.
- System performance along with bandwidth and ADC dynamic range utilization is

improved by allocating user baseband bandwidth and ADC dynamic range in accordance with the 90-50 MMB.

- Excessive allocation of higher baseband bandwidths and ADC dynamic range would result in improved system performance however it results in inefficient usage of resources.

In the next chapter, the measurement results would be presented and comparison of the presented analytical, simulation and measurement results would be carried out to show the effect of allocated user baseband bandwidth on MU-MIMO system performance.

Chapter 6: Measurement Results

In this chapter, the results obtained by processing the data collected using a prototype 2×2 MU-MIMO system discussed in chapter 4 are presented. Data is collected by taking measurements in the amateur RF band of 1240 MHz – 1300 MHz. The maximum available RF passband bandwidth is limited to 60 MHz in this band and the prototype portable users employ double-side-band QAM modulators. Due to the modulators, the maximum possible baseband bandwidth that can be used is 30 MHz. Due to this limitation, measurement results would be presented for three different cases of allocated user baseband bandwidths of 10 MHz, 20 MHz and 30 MHz. The office environment dimensions and other assumptions such as receive antenna separation, receive and portable user antenna height above the floor have already been presented in the chapter 5 of the thesis. In comparison to the 500 portable user locations considered for simulation results the measurement results are computed using 50 different portable user locations. The results are presented by conducting RF measurements for office environments `oe_case1` and `oe_case4`.

6.1 Anechoic Chamber Results

The propagation properties of `oe_case1` and `oe_case4` are mostly LOS however due to reflection from surfaces, walls and windows there is a small presence of multipath components. To comprehend the effect of multipath components it was decided to first carry out RF measurements in an anechoic chamber located in room H209 in Head Hall at the University of New Brunswick. Figure 6.1 shows the prototype 2×2 MU-MIMO system located inside an anechoic chamber. The anechoic chamber dimensions are not exactly similar to GWD119 dimensions however they are analogous to GWD119

dimensions so that measurement results for the anechoic chamber and GWD119 are comparable.

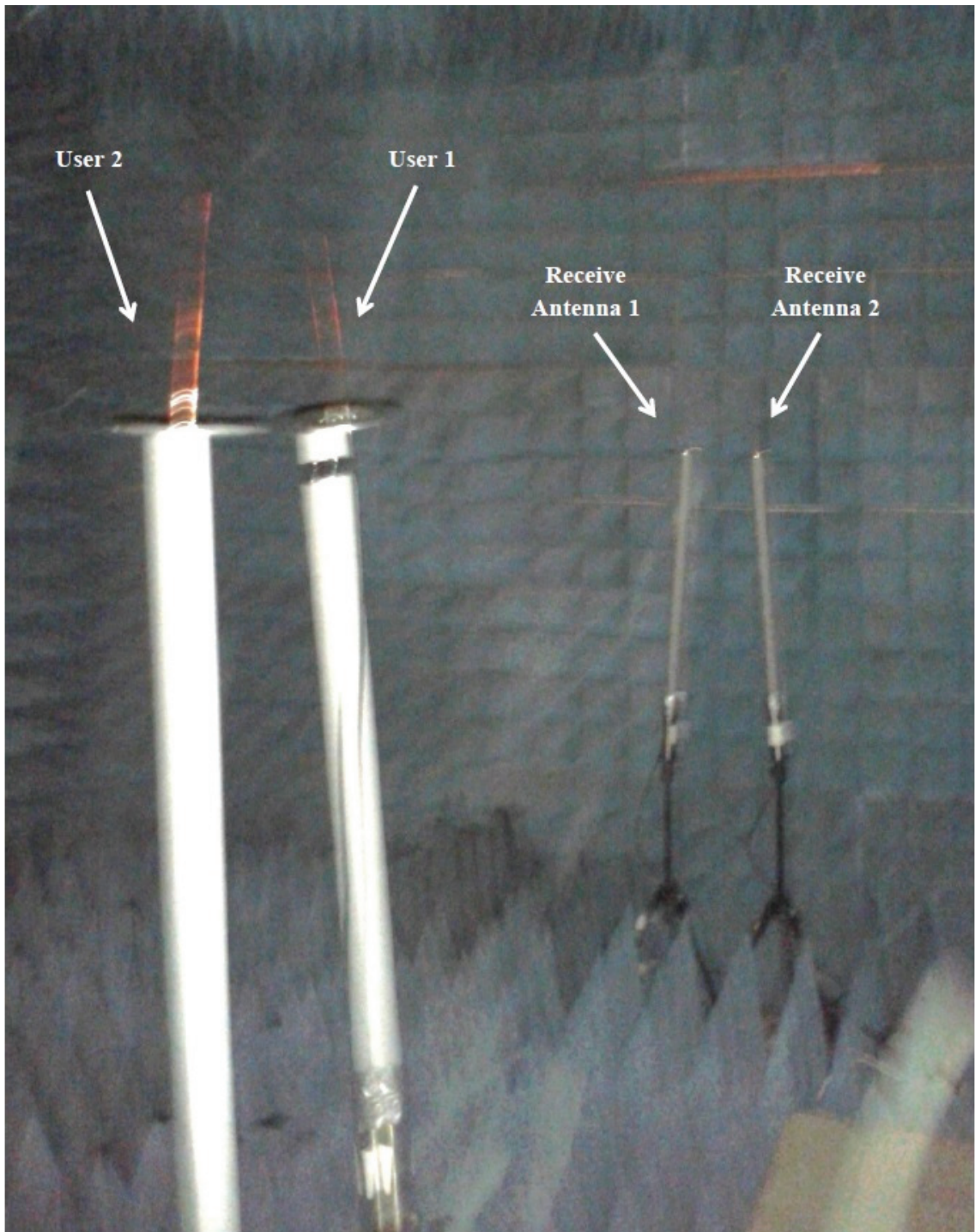


Figure 6.1: Prototype MU-MIMO System Setup inside Anechoic Chamber

Figures 6.2 and 6.3 present anechoic chamber measurement results for oe_case1 and oe_case4 in terms of the percentage of portable user locations that contribute to a particular value of a condition number for different values of allocated user baseband bandwidths. As can be seen the anechoic chamber results for oe_case1 and oe_case4 follow the same trend as followed by simulation results presented in the previous chapter.

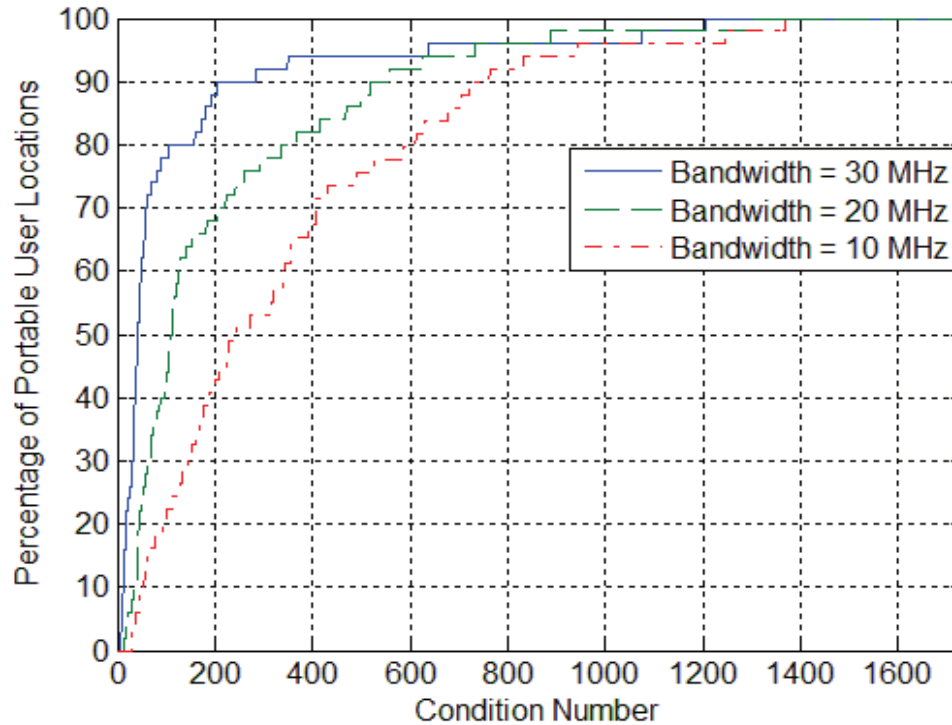


Figure 6.2: Condition Number vs. Allocated User Bandwidths for Anechoic Chamber for oe_case1

Table 6.1: Allocated User Bandwidth Effect on System Performance inside Anechoic Chamber for oe_case1

Allocated User Bandwidth	Percentage Portable User Locations	Maximum Condition Number
10 MHz	90%	762
20 MHz	90%	555
30 MHz	90%	205

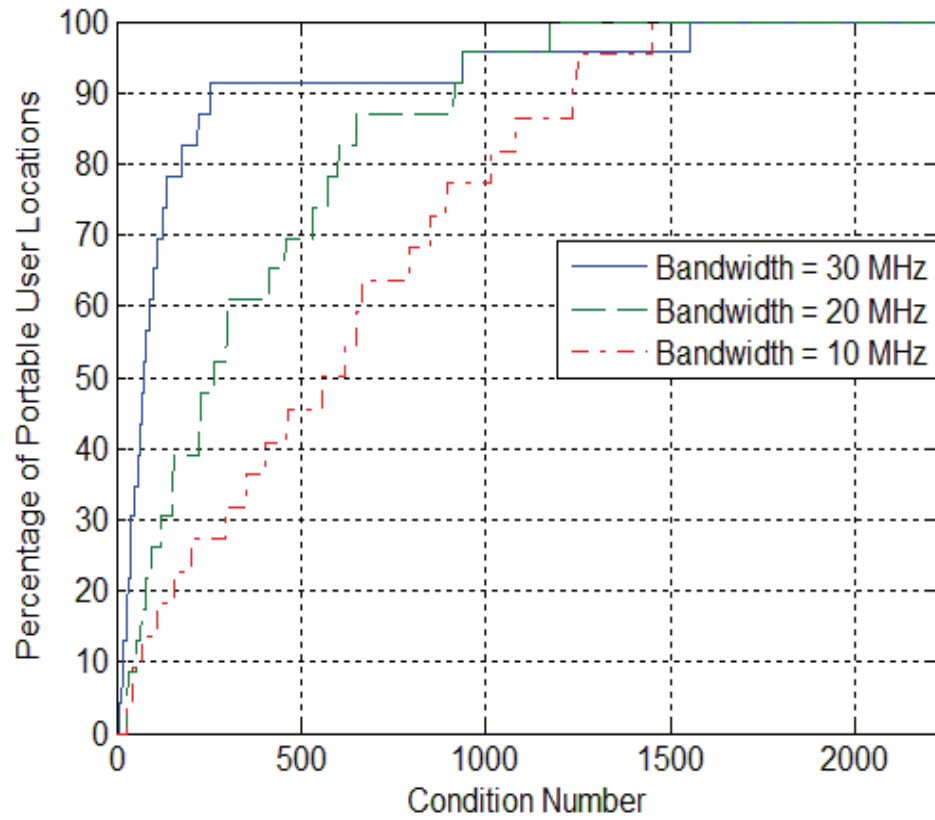


Figure 6.3: Condition Number vs. Allocated User Bandwidths for Anechoic Chamber for oe_case4

Table 6.2: Allocated User Bandwidth effect on System Performance inside Anechoic Chamber for oe_case4

Allocated User Bandwidth	Percentage Portable User Locations	Maximum Condition Number
10 MHz	90%	1233
20 MHz	90%	914
30 MHz	90%	253

Tables 6.1 and 6.2 presents the data recovered from Figures 6.2 and 6.3, respectively, in the tabulated form.

6.2 Office Environment Results

The RF measurements were taken within an office environment GWD119. Figure 6.4 shows the prototype 2×2 MU-MIMO system located inside an office environment GWD119.

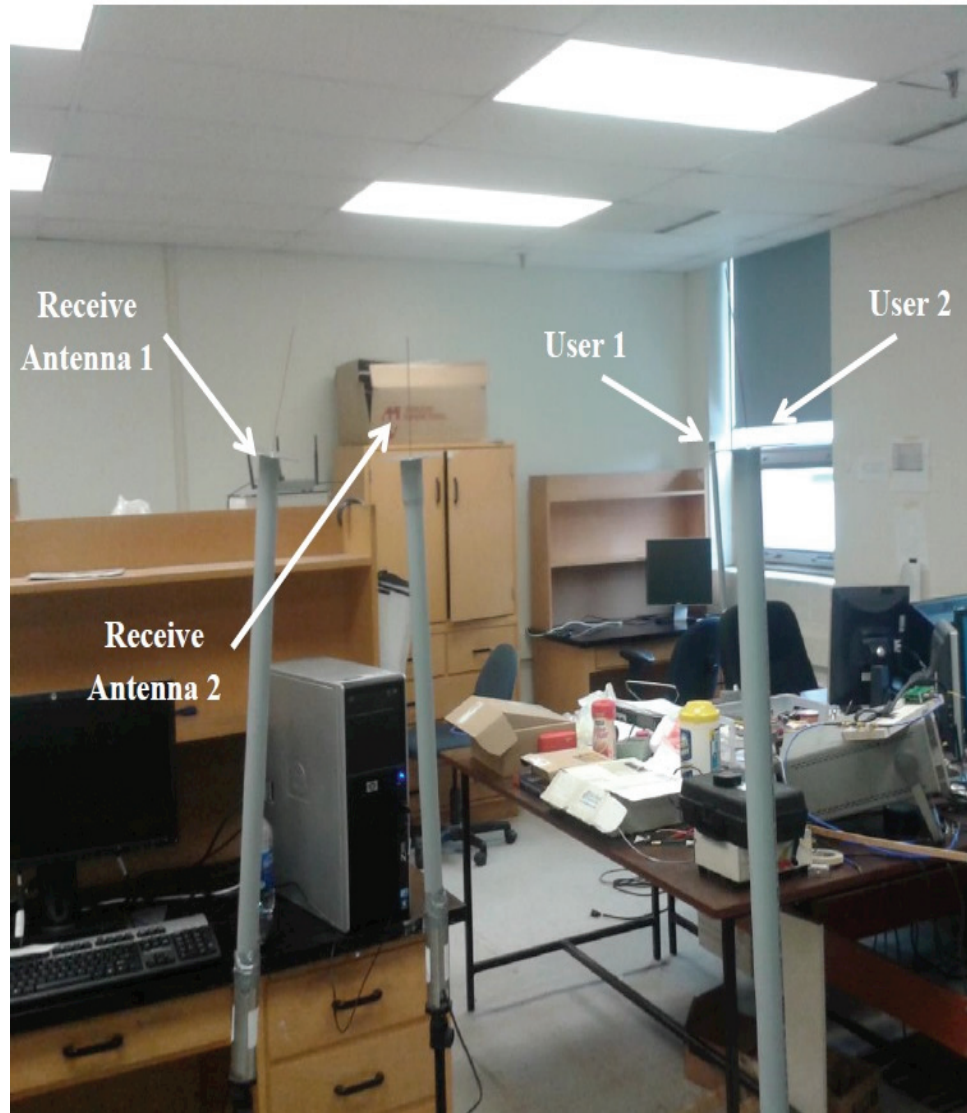


**Figure 6.4: Prototype MU-MIMO System Setup inside Office Environment
GWD119**

Figures 6.5 and 6.6 present GWD119 measurement results for oe_case1 and

oe_case4 in terms of the percentage of the portable user locations that contribute to a particular value of a condition number for different values of allocated user baseband bandwidths. Tables 6.3 and 6.4 presents the data recovered from Figures 6.5 and 6.6, respectively in the tabulated form.

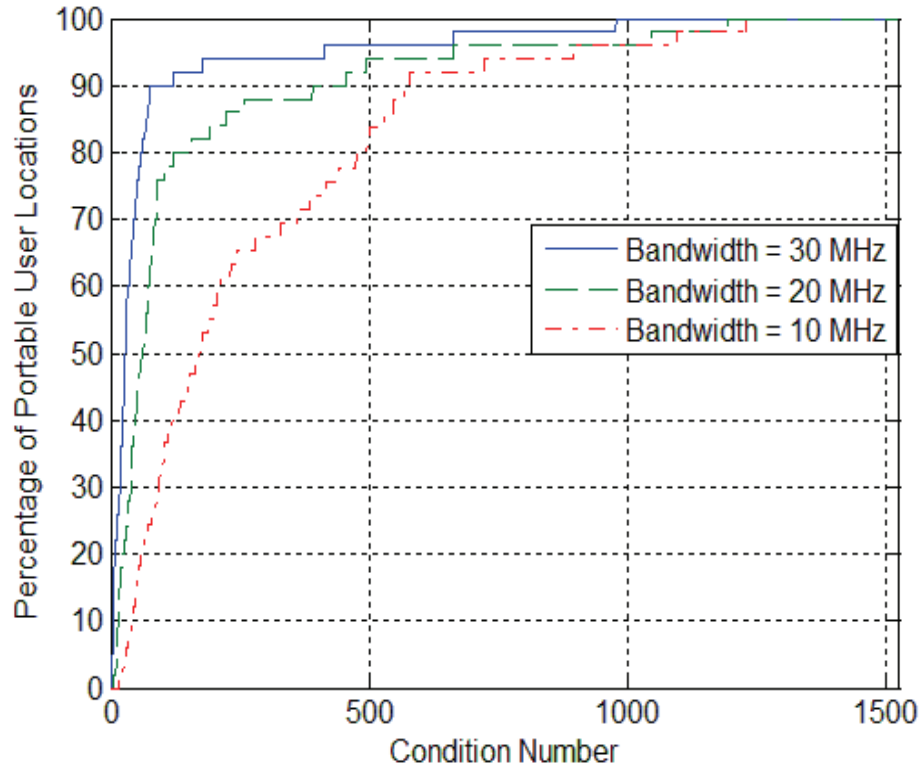


**Figure 6.5: Condition Number vs. Allocated User Bandwidths for GWD119 for
oe_case1**

**Table 6.3: Allocated User Bandwidth effect on System Performance inside GWD119
for oe_case1**

Allocated User Bandwidth	Percentage Portable User Locations	Maximum Condition Number
10 MHz	90%	577
20 MHz	90%	455
30 MHz	90%	83

**Table 6.4: Allocated User Bandwidth effect on System Performance inside GWD119
for oe_case4**

Allocated User Bandwidth	Percentage Portable User Locations	Maximum Condition Number
10 MHz	90%	1319
20 MHz	90%	1111
30 MHz	90%	139

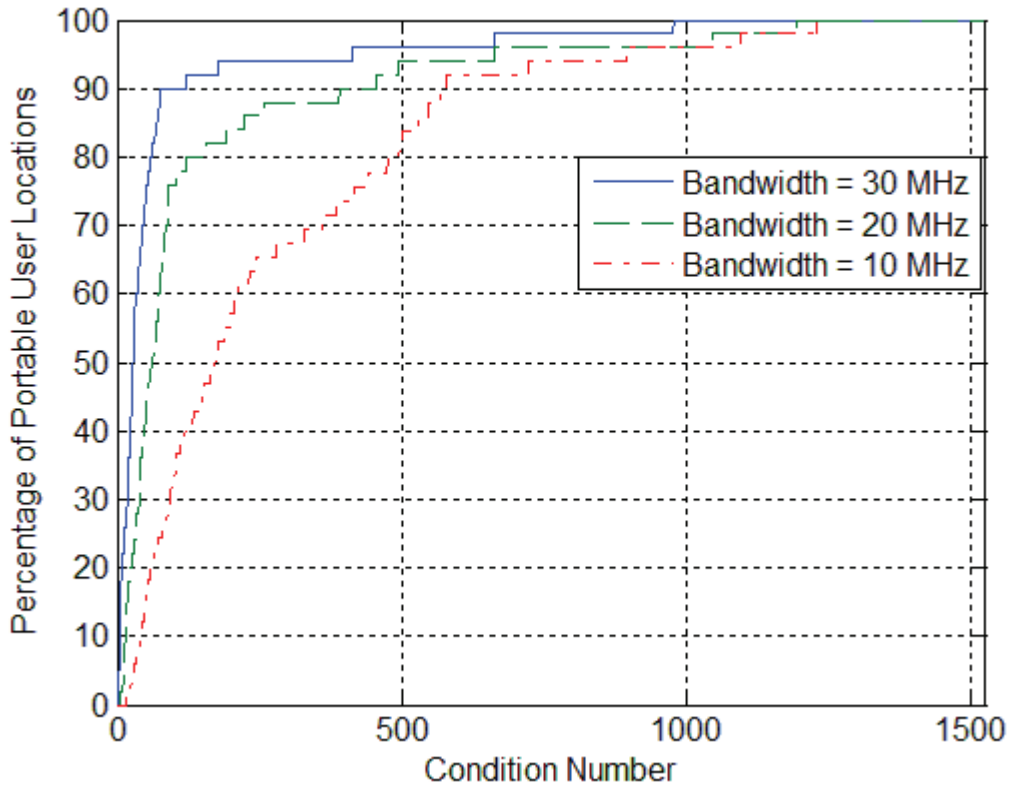


**Figure 6.6: Condition Number vs. Allocated User Bandwidths inside GWD119 for
oe_case4**

As can be seen the results presented in Figures 6.2, 6.3, 6.5 and 6.6 follow the collective trend of improvement in the performance of a MU-MIMO system with an increase in the allocated user baseband bandwidth. This attests to the theoretical analysis

results presented in chapter 3 of the thesis. Additionally, the measurement results presented in tables 6.1, 6.2, 6.3 and 6.4 attests the effect of dimensions of an office environment on the bandwidth requirements as predicted by theoretical and simulation analysis.

Further analysis is carried out by presenting the comparison of simulation, anechoic chamber and GWD119 results for `oe_case1` and `oe_case4`. Figures 6.7 and 6.8 present results in terms of maximum condition number of the recovered channel matrix H_p for particular allocated user baseband bandwidth for 90% of the portable user locations for `oe_case1` and `oe_case4` respectively.

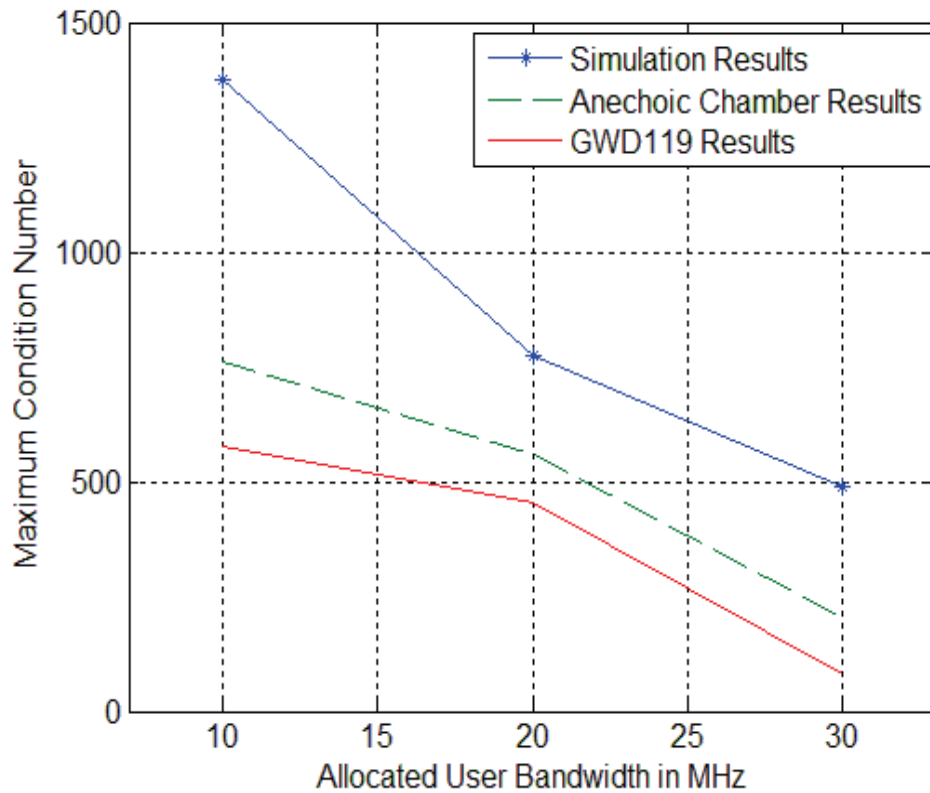


Figure 6.7: Maximum Condition Number for 90% Portable User Locations for `oe_case1`

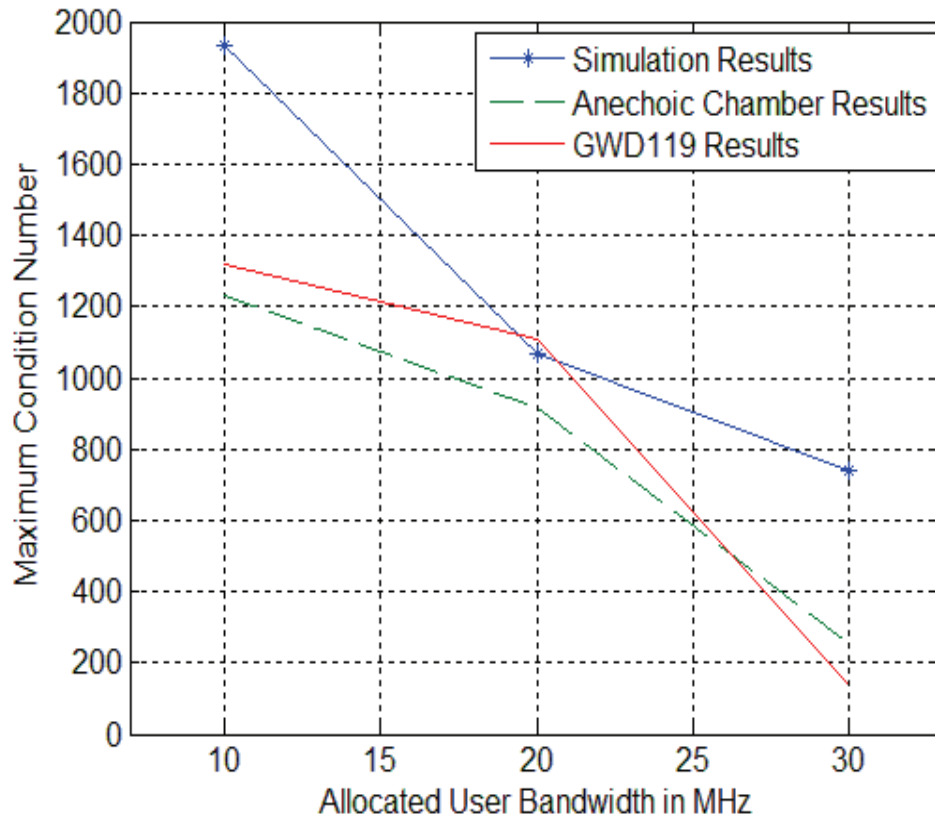


Figure 6.8: Maximum Condition Number for 90% Portable User Locations for `oe_case4`

The presented results show that for 90% of portable user locations within an office environment the condition number of the recovered channel matrix is reduced as the allocated user baseband bandwidth is increased. The simulation results predict an almost linear decrease in condition number of a channel matrix for allocated user baseband bandwidth range. However, anechoic chamber and measurement results show greater decrease in condition number when allocated user baseband bandwidth is increased from 20 MHz to 30 MHz as compared to increase from 10 MHz to 20 MHz. This difference can be attributed to small scale fading or pathological situations that may

exist for MU-MIMO systems [29]. These situations exist when:

- Portable users are geographically located very close to each other,
- Receive antennas are geographically located very close to each other,
- Portable users are geographically located in symmetric conditions with respect to receive antennas, or
- Receive antennas are geographically located in symmetric conditions with respect to portable users.

Whenever these situations exist for a MU-MIMO system the parameter τ_{diff} in equation (3.26) becomes zero, resulting in no improvement in the condition number of a channel matrix \mathbf{H}_p for any value of allocated user baseband bandwidth. For the MATLAB simulation analysis the pathological situations can be realized perfectly resulting in no improvement in the performance of MU-MIMO systems for any value of allocated user baseband bandwidth. However for measurement results these situations cannot be realized perfectly resulting in some difference of path lengths resulting in some performance improvement for higher allocated portable user baseband bandwidths as compared to smaller allocated portable user baseband bandwidths. In addition to this, the presented results reveal small improvement in the performance of a MU-MIMO system for GWD119 measurement results as compared to anechoic chamber results for oe_case1. As discussed before the GWD119 has a small presence of multipath components as compared to the anechoic chamber. The presence of multipath components adds to stochastic nature of the MU-MIMO channel matrix that results in improved system performance [4] [5]. Therefore, the improvement in the performance of a MU-MIMO system in GWD119 as compared to the anechoic chamber can be attributed to small

presence of multipath components that may exist for `oe_case1`. Interestingly, the results presented for `oe_case4` reveal a mix trend of improvement for anechoic chamber and GWD119 measurement results. For the allocated user baseband bandwidth of 10 MHz and 20 MHz it shows small improvement in anechoic chamber results as compared to GWD119 measurement results. However for the allocated user baseband bandwidth of 30 MHz it shows small improvement in the GWD119 results as compared to anechoic chamber results. This is different as compared to results presented for `oe_case1`. One reason for this could be that the `oe_case4` GWD119 measurement results were computed by limiting the portable users within the imaginary boundaries considered within GWD119 as compared to actual physical boundaries in the case of `oe_case1` results. This means that the effect of multipath components resulting due to reflection from physical boundaries is reduced which causes the reduction in the improvement of GWD119 measurement results for `oe_case4`. The small difference in performance improvement for anechoic chamber and GWD119 measurement results for `oe_case1` and `oe_case4` is attributed to multipath components and is random in nature.

Next, to see the overall trend of MU-MIMO system performance the measurement results are presented for different percentages of portable user locations for `oe_case1` and `oe_case4`. Figures 6.9 and 6.10 present measurement results for `oe_case1` and `oe_case4` respectively. The results are presented in terms of maximum condition number for a particular percentage of number of portable user locations for different allocated portable user baseband bandwidths. The results presented for `oe_case1` and `oe_case4` show that as the percentage of portable user locations is increased the maximum condition number for a channel matrix is increased and vice versa.

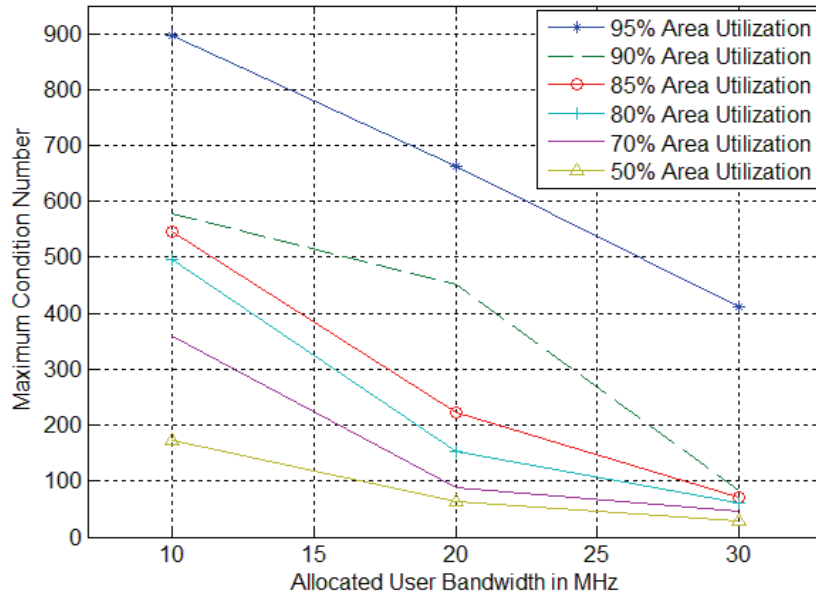


Figure 6.9: Maximum Condition Number for different Percentages of Portable User

Locations for oe_case1

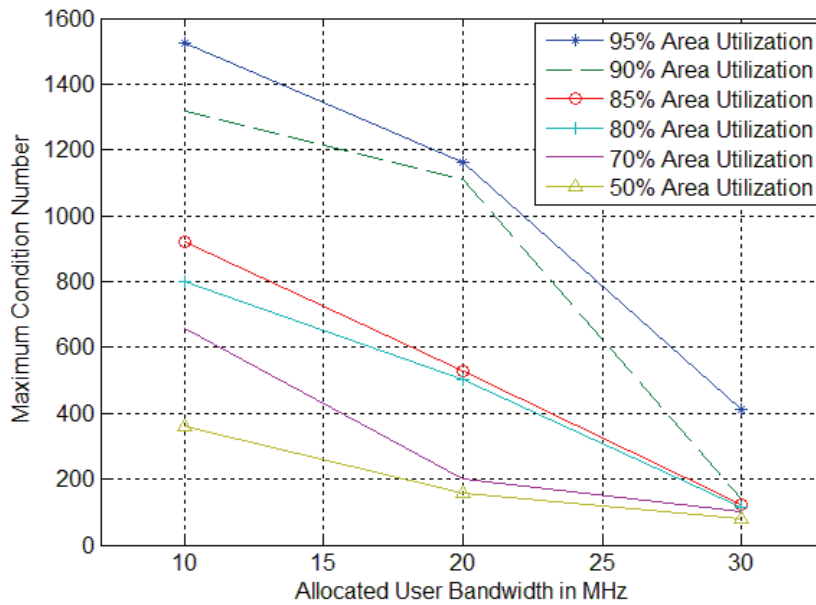


Figure 6.10: Maximum Condition Number for different Percentages of Portable

User Locations for oe_case4

In addition to this, it can also be seen that for smaller percentage of portable user locations the range of condition numbers for different allocated user bandwidths is small whereas for a larger percentage of portable user locations the range of condition numbers is increased. This can be attributed to the fact that a bandwidth efficient MU-MIMO system exists over larger percentage of portable user locations, which includes situations due to fading and pathological cases that generally result in higher condition numbers. Since for such situations the effect of a change of allocated user baseband bandwidth is more prominent, therefore the amount of change in the condition number for different allocated user baseband bandwidths is higher. In addition to this, since the situations are known to result in higher condition numbers for the channel matrix \mathbf{H}_P , therefore for a larger percentage of portable user locations the maximum condition number for the respective allocated user bandwidths is increased as well. Therefore a tradeoff exists, for a larger percentage of portable user locations the performance of a MU-MIMO system is degraded whereas for lower percentage of portable user locations the MU-MIMO system performance is improved at the cost of coverage area reduction. This trend is more prominent for smaller allocated portable user baseband bandwidths as compared to larger allocated user baseband bandwidths.

Next, the measurement results are presented for oe_case1 and oe_case4 to analyze the effect of office environment dimensions and allocated user baseband bandwidth on systems ADCs dynamic range requirements. The Figures 6.11 and 6.12 present received power ratio measurement results for oe_case1 and oe_case4. The results are presented in terms of received power ratio of portable users for normalized distance ratio that exist between portable users and receive antenna. Additionally, the comparison of received

power ratios for different allocated user baseband bandwidths and theoretical prediction based on normalized distance ratio is presented.

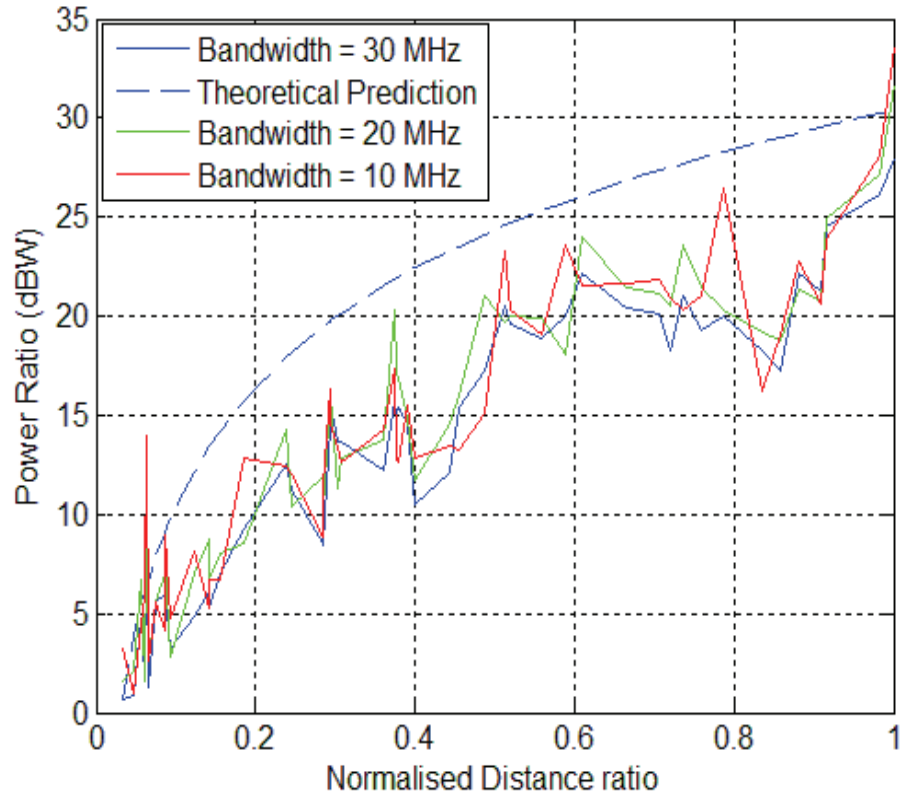


Figure 6.11: Received Power Ratio vs. Normalized Distance Ratio for oe_case1

As can be seen, the measurement results follow the same trend of increase in the received power ratio for increased distance ratio as predicted by theoretical analysis. The comparison of results presented in Figures 6.11 and 6.12 also shows that the received power ratio results for oe_case4 follow closely the theoretical predications as compared to oe_case1. This can be attributed to reduction in multipath components for oe_case4 due to absence of actual physical boundaries for the case of oe_case1 measurement results. Additionally, the presented results for oe_case1 and oe_case4 follow the

collective trend of reduced variation in power ratio results for increased user allocated bandwidth. This is in accordance with the theoretical analysis which states that the variations in the received signal power levels due to multipath effects are reduced for increase allocated user bandwidths. The received signal power ratio values for oe_case1 and oe_case4 are presented in Appendix D.

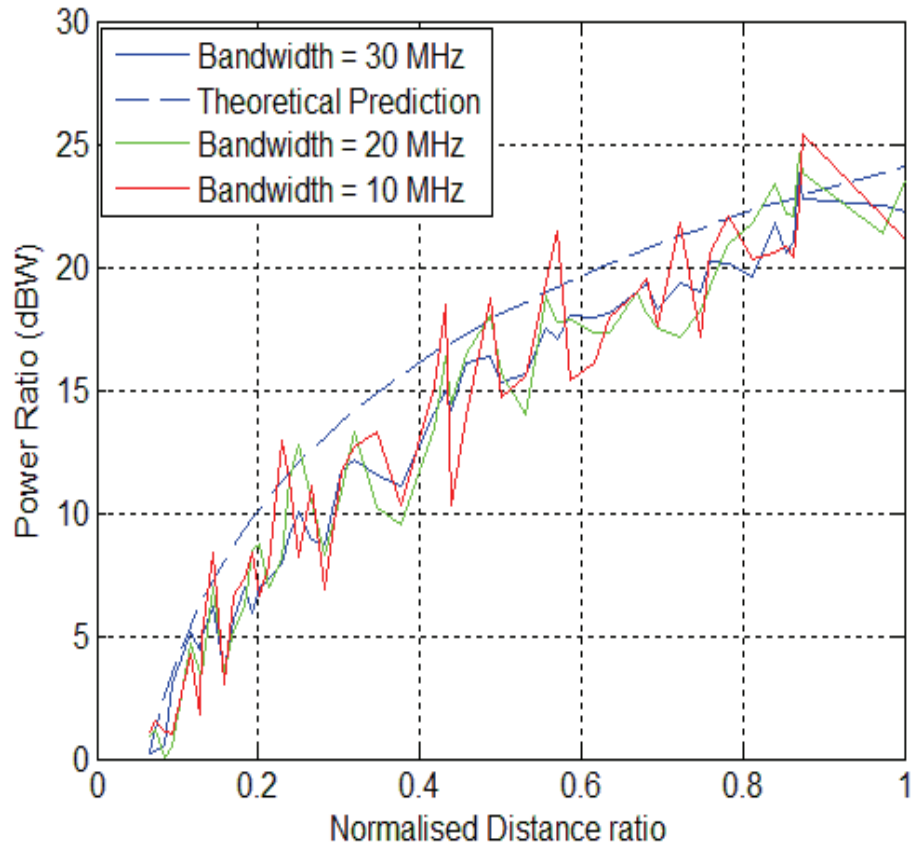


Figure 6.12: Received Power Ratio vs. Normalized Distance Ratio for oe_case4

Next, the relation presented in equation (3.40) is used to compute the ADC dynamic range requirement results by using the received power ratio measurement results. The results are presented in terms of ADC dynamic range requirement's for percentage of portable user locations for different allocated user baseband bandwidths.

The Figures 6.13 and 6.14 present ADC dynamic range requirement results for oe_case1 and oe_case4.

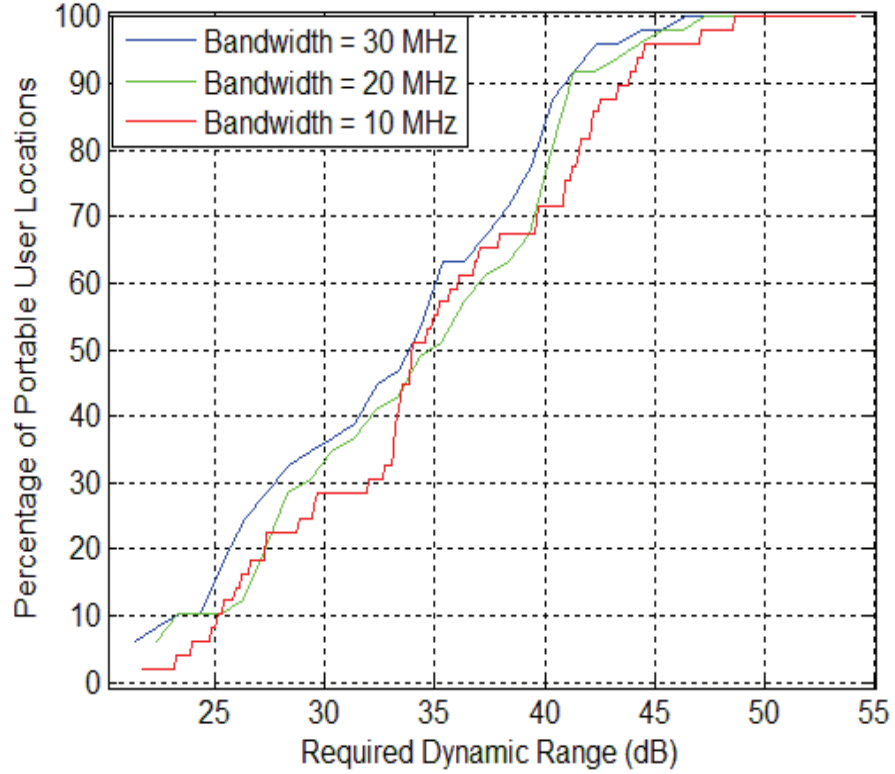


Figure 6.13: ADC Dynamic Range Requirements for oe_case1

The table 6.5 provides the data recovered from Figures 6.13 and 6.14 is the tabulated form.

Table 6.5: ADC Dynamic Range Requirements

Allocated User Bandwidth	Required ADC Dynamic Range (dB)	oe_case1	oe_case4
10 MHz	Min Required DR	22.13	22.16
	Max Required DR	54.13	45.46
20 MHz	Min Required DR	22.31	20.74
	Max Required DR	49.31	43.74
30 MHz	Min Required DR	21.36	20.93
	Max Required DR	47.36	42.93

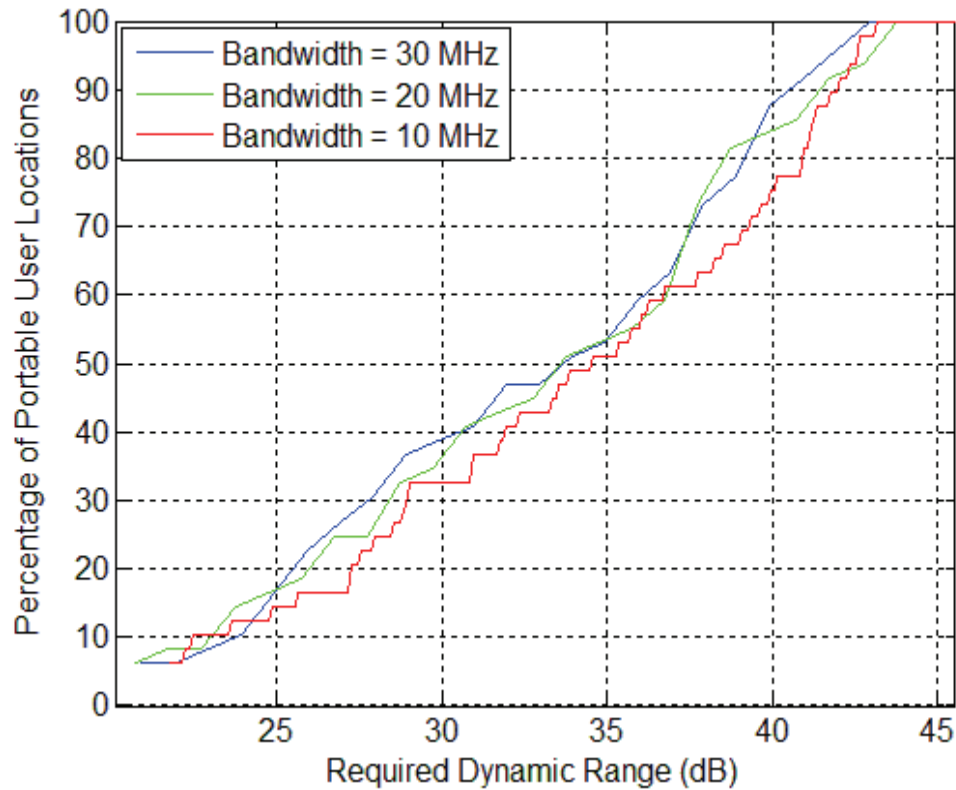


Figure 6.14: ADC Dynamic Range Requirements for oe_case4

The comparison of the results presented in table 6.5 clearly shows the effect of dimensions of an office environment on the systems ADC's dynamic range requirements. It shows that for an office environment with reduced dimensions the ADC dynamic range requirements are reduced and vice-versa. Additionally, it shows minor fluctuations in ADC's dynamic range requirements for different allocated user baseband bandwidths. The ADC dynamic range requirements computed using the relation presented in equation (3.46) are 41.47 dB for oe_case1 and 35.60 dB for oe_case4. Table 6.6 presents data recovered from Figures 6.13 and 6.14 in the tabulated form for the ADC dynamic range of 41.47 dB and 35.60 dB for oe_case1 and oe_case4 respectively.

Table 6.6: Percentage of Portable User Locations for oe_case1 and oe_case4

Allocated User Bandwidth	Percentage Portable User Locations for oe_case1	Percentage Portable User Locations for oe_case4
10 MHz	77.55 %	53.06 %
20 MHz	91.84 %	55.10 %
30 MHz	91.95 %	59.15 %

The data presented in table 6.6 shows that an ADC having dynamic range of 47.47 dB would result in satisfactory performance over majority of the portable user locations within an oe_case1. Similarly, an ADC having dynamic range of 35.60 dB would result in satisfactory performance over 60% of the portable user locations within an oe_case4. Additionally, the effect of allocated user baseband bandwidth on systems ADC dynamic range requirements is not very prominent however the collective trend is the reduction in ADC dynamic range requirement fluctuations with an increased allocated user bandwidth.

The measurement results presented in tables 6.3, 6.4 and 6.6 are in accordance with the theoretical analysis and presented simulation results. The carried out theoretical analysis predicted the 90-50 MMB values of 45 MHz and 90 MHz for office environments oe_case1 and oe_case4. The presented measurement results for oe_case1 shows satisfactory performance of MU-MIMO system for majority of the portable user locations for the allocated user baseband bandwidth of 30 MHz. The measurement results close to predicted value of 90 MHz for oe_case4 are not available due to spectrum limitations stated earlier. However, the presented results for oe_case4 shows that the system performance can further be improved by allocating higher bandwidths closer to the predicted value of 90 MHz. The results presented here in terms of specific values are

applicable to an office environment with present system setup under consideration. The importance of the presented research lies in indicating the generalized nature of results that are expected for different office environments with different system setups. The presented theoretical analysis, simulation results and measurement results follow the collective agreement which is stated as follows:

- An office environment with particular dimensions has an average user bandwidth and ADC dynamic range requirements which are required for satisfactory performance of system for majority of the portable user locations.
- The required user bandwidth is inversely proportional to office environment dimensions whereas ADC dynamic range requirements are directly proportional to office environment dimensions.
- For the case when allocated user baseband bandwidth and ADC dynamic range is too small the system performance is degraded due to reduction in user separability and decreased SQNR.
- System performance along with bandwidth utilization and ADC dynamic range utilization is improved by allocating user baseband bandwidth and ADC dynamic range in accordance with the 90-50 MMB.
- Allocating too high of user baseband bandwidth and ADC dynamic range would result in improved system performance however it results in inefficient usage of resources.

Chapter 7: Summary and Future Work

This chapter has been divided into two subsections where the first subsection summarizes the work that has been presented in this thesis. The second subsection presents future work. In addition, it also lists the hardware and software modifications that would be required for future work.

7.1 Summary

The presented work demonstrates the effect of allocated user baseband bandwidth and ADC dynamic range on the performance of a MU-MIMO system in an office environment. The theoretical and simulation results predict an improvement in the performance of a MU-MIMO system for larger allocated user baseband bandwidth. The measurements from the anechoic chamber and the office environment, with the help of the prototype 2×2 MU-MIMO system, attest the theoretical and simulation performance improvement predictions. The hypothesis is proposed that links the 90-50 MMB of an office environment to the physical dimensions of an office environment under consideration. The presented measurement results reveal the following:

- An office environment with particular dimensions has an average user bandwidth and ADC dynamic range requirements which are required for satisfactory performance of system for majority of the portable user locations.
- For the case when the allocated user baseband bandwidth and ADC dynamic range is too small, the system performance is degraded due to reduction in user separability and decreased SQNR.
- System performance along with bandwidth utilization and ADC dynamic range

utilization is improved by allocating user baseband bandwidth and ADC dynamic range in accordance with the 90-50 MMB.

- Allocating an excessive user baseband bandwidth and ADC dynamic range would result in improved system performance however it results in inefficient usage of resources.

7.2 Future Work

The presented theoretical analysis, simulation and measurement results suggested that allocating high user baseband bandwidth and high dynamic-range ADCs would result in improved system performance due to improved user separability and increased SQNR. The improvement in the system performance tends to saturate for excessive allocated user baseband bandwidth. This leads to inefficient usage of resources. It is suggested that the future work should be focused to analyze the efficient utilization of resources. The proposed future idea is based on the modified cellular system idea such that an indoor-office-environment is divided into physically overlapping cells with each cell allocated with a baseband bandwidth close to the predicted 90-50 MMB of a cell. It is proposed that the present 2×2 prototype MU-MIMO system should be upgraded to a 4×4 MU-MIMO system. The RF measurements and analysis could be carried out for the two different scenarios with first scenario being a 4×4 MU-MIMO system with an allocated user baseband bandwidth of 70 MHz. In the second scenario consider two individual 2×2 MU-MIMO systems with an allocated user baseband bandwidth of 35 MHz where the individual MU-MIMO systems do not overlap each other in the RF passband. This can be accomplished by allocating different carrier frequencies for individual 2×2 MU-MIMO systems such that both systems do not interfere with each

other in RF passband. The results could be presented by comparing the performance of both scenarios in terms of condition number and bandwidth utilization. It is expected that the scenario of two individual 2×2 MU-MIMO systems should outperform the single 4×4 MU-MIMO system scenario by resulting in better bandwidth utilization. The reason for this belief is that since for the scenario of individual 2×2 MU-MIMO systems the allocated user baseband bandwidth is closer to the 90-50 MMB therefore resulting in better bandwidth utilization.

The proposed system would require that the present RF passband bandwidth limit of 60 MHz be raised to 140 MHz. Industry Canada allows RF transmission in the amateur band of 2300 MHz – 2450 MHz therefore allowing for maximum RF passband bandwidth of up to 150 MHz. Since this allows for the maximum baseband bandwidth of 75 MHz therefore the measurements can be carried out by allocating higher baseband bandwidths of up to 75 MHz to portable users. This will require the design and construction of antennas with an ability to transmit over a passband bandwidth range of 150 MHz with suitable gain. In addition, the author would also recommend some hardware modifications to be carried out for future use of the prototype system. Following are some of the hardware modifications that are recommended to be incorporated into the system:

- The present system is a 2×2 MU-MIMO system consisting of two portable users and two receive antennas. To carry out the proposed future work two more portable users need to be designed and constructed. This would require the purchase of new hardware components required to construct additional portable users. Thorough market research would be needed as some of the

components used in the present portable users are no longer available and therefore compatibility of new portable users with existing portable users should be considered before purchase of new hardware components.

- In the present setup, the receiver consists of two separate tripods each employing a receive antenna, QAM demodulator board and required power supplies. It is recommended that the receiver should be modified such that it consists of all the receive antennas and the required circuitry installed on same tripod. This would greatly enhance the compatibility and movability of the receiver module. In addition, the receiver module should be designed such that it can be either used as a receiver consisting of two receive antennas or four receive antennas separated on a scale of a symbol wavelength.
- For a portable user MU-MIMO system the movability of the users plays a major role. Despite the fact that the present prototype system is a portable user MU-MIMO system setup, the individual users lack the ability to move, it is suggested that portable user tripods be replaced with tripods having wheels. This will ease the movability of the individual users. In addition, a small bulkhead can be designed and attached to tripod that can make cable connections more rigid therefore further enhancing the movability of the individual users.
- Presently the antennas being used as transmit and receive antennas are dipole antennas with a passband bandwidth of 60 MHz and capable of transmission in 1240 MHz –1300 MHz RF amateur band. The proposed system would require the design and development of wideband antennas to be capable of

transmission and reception in the RF amateur band of 2.3 GHz – 2.4 GHz.

Bibliography

- [1] A. F. Molisch, *Wireless Communications*, 2nd ed., West Sussex, UK: John Wiley & Sons Ltd., 2011.
- [2] A. Goldsmith, *Wireless Communications*, 1st ed., New York: Cambridge University Press, 2005.
- [3] F. Bøhagen, P. Orten and G. E. Øien, “Construction and capacity analysis of high-rank line-of-sight MIMO channels,” in *Proc. WCNC*, New Orleans, USA, Mar. 13 – 17 2005, pp. 432 – 437.
- [4] L. Liu, W. Hong, H. Wang, G. Yang, N. Zhang, H. Zhao, J. Chang, C. Yu, X. Yu, H. Tang, H. Zhu and L. Tian, “Characterization of line-of-sight MIMO channel for fixed wireless communications,” *IEEE Antennas Wireless Propag. Lett.*, vol. 6, pp. 36 – 39, Mar. 2007.
- [5] I. Sarris and A. R. Nix, “Maximum MIMO capacity in line-of-sight,” in *Proc. ICICS*, Bangkok, Japan, Dec. 6 – 9 2005, pp. 1236 – 1240.
- [6] J. Shen, Y. Oda, T. Furuno, T. Maruyama and T. Ohya, “A novel approach for capacity improvement for 2×2 MIMO in LOS channel using reflectarray,” in *Proc. IEEE VTC*, Yokohama, Japan, May 15 – 18 2011, pp. 1 – 5.
- [7] L. Liu, W. Hong, H. Wang, G. Yang, N. Zhang, H. Zhao, J. Chang, C. Yu, X. Yu, H. Tang, H. Zhu and L. Tian, “Characterization of line-of-sight MIMO channel for wireless communications,” *IEEE Antennas Wireless Propag. Lett.*, vol. 6, pp. 36 – 39, Mar. 2007.
- [8] J. Rasool, G.E. Øien, J. E. Håkegård and T. A. Myrvoll, “On multiuser MIMO

- capacity benefits in air-to-ground communication for air traffic management,” in *Proc. IEEE ISWCS*, Tuscany, Italy, Sept. 7 – 10 2009, pp. 458 – 462.
- [9] S. Yan and Z. Yerong, “Maximum MIMO capacity of rice channel,” in *Proc. WCSP*, Nanjing, China, Nov. 13 – 15 2009, pp. 1 – 5.
- [10] T. Haustein and U. Kruger, “Smart geometrical antenna design exploiting the LOS component to enhance a MIMO system based on Rayleigh-fading in indoor scenarios, in *Proc. IEEE PIMRC*, Beijing, China, Sept 7 – 10 2003, pp. 1144 – 1148.
- [11] G. Zhu, B. R. Petersen and B. G. Colpitts, “Signalling wavelength in an antenna array for space-time wireless over LOS channels,” in *Proc. CNSR*, Halifax, Canada, May 16 – 18 2005, pp. 69 – 73.
- [12] J. H. Winters, “On the capacity of radio communication systems with diversity in a Rayleigh fading environment,” *IEEE J. Select. Areas Commun.*, vol. 5, no. 5, pp. 871 – 878, Jun. 1987.
- [13] G. J. Foschini and M. J. Gans, “On limits of wireless communications in a fading environment when using multiple antennas,” *Wireless Personal Commun.*, vol. 6, pp. 311 – 335, Mar. 1998.
- [14] G. J. M. Janseen, P. A. Stigter and R. Prasad, “Wideband indoor channel measurements and BER analysis of frequency selective multipath channels at 2.4, 4.75 and 11.5 GHz,” *IEEE Trans. Commun.*, vol. 44, no. 10, pp. 1272 – 1288, Oct. 1996.
- [15] M. A. Jensen and J. W. Wallance, “A review of antennas and propagation for MIMO wireless communications,” *IEEE Trans. Antenna Propag.*, vol. 52, no. 11, pp. 2810 – 2824, Nov. 2004.

- [16] B. T. Walkenhorst, "Achieving near-optimal MIMO capacity in a rank-deficient LOS environment," Ph.D. Dissertation, Georgia Institute of Technology, Aug. 2009.
- [17] D. Tse and P. Viswanath, *Fundamentals of Wireless Communication*, 5th ed., New York: Cambridge University Press, 2011.
- [18] B. Vucetic and J. Yuan, *Space Time Coding*, 1st ed., West Sussex, U.K.: John Wiley & Sons Ltd., 2003.
- [19] T. S. Rappaport, *Wireless Communications: Principles and Practice*, 2nd ed., New Jersey: Prentice Hall PTR, 2001.
- [20] J. Hadamard, "Résolution d'une question relative aux déterminants," *Bulletin des Sciences Mathématiques* 17, pp 240 – 246, 1893.
- [21] J. A. Harriman, "A reconfigurable four-channel transceiver testbed with signalling-wavelength-spaced antennas," M.Sc.E dissertation, University of New Brunswick, Sept. 2006.
- [22] B. P. Lathi, *Modern Digital and Analog Communication Systems*, 3rd ed., New York: Oxford University Press, 1998.
- [23] J. D. Kraus, *Antennas*, 2nd ed., New York: McGraw-Hill, 1988.
- [24] J. G. Proakis, *Digital Communications*, 4th ed., New York: McGraw-Hill, 2001.
- [25] A. F. Molisch, M. Steinbauer, M. Toeltsch, E. Bonek and R. S. Thoma, "Capacity of MIMO systems based on measured wireless channels," *IEEE J. Select. Areas Commun.*, vol. 20, pp. 561 – 569, Apr. 2002.
- [26] P. F. Driessen and G. J. Foschini, "On the capacity formula for multi-input multi-output wireless channels: A geometric interpretation," *IEEE Trans. Commun.*, vol. 47, pp. 173 – 176, Feb. 1999.

- [27] P. Wilson, P. Papazian, M. Cotton and Y. Lo, "A comparison of 1920-MHz mobile channel diversity gain using horizontal and vertical arrays," *IEEE Trans. Commun.*, vol. 49, no. 12, pp. 2068 – 2070, Dec. 2001.
- [28] D. Gesbert, M. Shafi, D. Shiu, P. J. Smith and A. Naguib, "From theory to practice: An overview of MIMO space-time coded wireless systems," *IEEE J. Select. Areas Commun.*, vol. 21, no. 3, pp. 281 – 302, Apr. 2003.
- [29] W. Q. Malik, "MIMO capacity convergence in frequency selective channels," *IEEE Trans. Commun.*, vol. 57, no. 2, pp. 353 – 356, Feb. 2009.
- [30] W. Q. Malik, B. Allen and D. J. Edwards, "Fade depth scaling with channel bandwidth," *Electron. Lett.*, vol. 43, no. 24, pp. 1371 – 1372, Nov. 2007.
- [31] W. Q. Malik, B. Allen, D. J. Edwards, "Bandwidth dependent modelling of small scale fade depth in wireless channels," *IET Microw. Antennas Propag.*, vol. 2, no. 6, pp. 519 – 528, Sep. 2008.
- [32] D. N. C. Tse, P. Viswanath, L. Zheng, " Diversity-multiplexing tradeoff in multiple-access channels," *IEEE Trans. Inf. Theory*, vol. 50, no. 9, pp. 1859 – 1874, Sep. 2004.
- [33] G. Zhu, "On the Signalling Length in Digital Wireless Communication," M.Sc.E. dissertation, University of New Brunswick, Aug. 2005.
- [34] S. J. Howard and K. Pahlavan, "Measurement and analysis of the indoor radio channel in the frequency domain," *IEEE Trans. Instrum. Meas.*, vol. 39, no. 5, pp. 751 – 755, Oct. 1990.
- [35] D. P. McNamara, M. A. Beach, P. N. Fletcher and P. Karlsson, "Capacity variation of indoor multiple-input multiple-output channels," *Electron. Lett.*, vol. 36, pp. 2037 – 2038, Nov. 2000.

- [36] C. R. Anderson, D. J. Hibbard and R. M. Buehrer, "The impact of bandwidth on the performance of DSSS signals in indoor office environments," *IEEE Trans. Wireless Commun.*, vol. 10, no. 9, pp. 2792 – 2799, Sep. 2011.
- [37] A. M. Hayar, R. Knopp and R. Saadane, "Subspace analysis of indoor UWB channels," *Journal on Applied Signal Processing*, vol. 2005, pp. 287 – 295, Jan. 2005.
- [38] D. Chizhik, J. Ling, P. W. Wolniansky, R. A. Valenzuela, N. Costa and K. Huber, "Multiple-input-multiple-output measurements and modeling in Manhattan," *IEEE J. Select Areas Commun.*, vol. 21, pp. 321 – 331, Apr. 2003.
- [39] J. P. Kermoal, L. Schumacher, P. E. Mogensen and K. I. Pedersen, "Experimental investigation of correlation properties of MIMO radio channels for indoor picocell scenarios," in *Proc. IEEE VTC*, vol. 1, Boston, MA, Sept. 24 – 28, 2000, pp. 14 – 21.
- [40] P. Almers, F. Tufvesson and A. F. Molisch, "Measurement of keyhole effect in a wireless multiple-input multiple-output (MIMO) channel," *IEEE Commun. Lett.*, vol. 7, pp. 373 – 375, Aug. 2003.
- [41] H. Yanikomeroglu and E. S. Sousa, "Antenna gain against interference in CDMA macrodiversity systems," *IEEE Trans. Commun.*, vol. 50, no. 8, pp. 1356 – 1371, Aug. 2002.
- [42] S. Sandhu, R. U. Nabar, D. A. Gore and A. Paulraj, "Near-optimal selection of transmit antennas for a MIMO channel based on Shannon capacity," in *Proc. 34th Asilomar Conf. Signals, Systems and Computers*, vol. 1, Pacific Grove, CA, Oct.-Nov. 29 – 1, 2000, pp. 567 – 571.
- [43] J. B. Andersen, "Array gain and capacity for known random channels with multiple element arrays at both ends," *IEEE J. Select Areas Commun.*, vol. 18, no. 11, pp.

- 2172 – 2178, Nov. 2000.
- [44] S. Haykin, *Communication Systems*, 3rd ed., New York: John Wiley & Sons, 1994.
- [45] J. A. Wepman, “Analog-to-digital converters and their applications in radio receivers,” *IEEE Commun. Magazine.*, vol. 33, no. 5, pp. 39 – 45, May 1995.
- [46] A. K. Salkintzis, H. Nie and P. T. Mathiopoulos, “ADC and DSP challenges in the development of software radio base stations,” *IEEE Personal Commun.*, vol. 6, no. 4, pp. 47 – 55, Aug. 1999.
- [47] P. Wilson, P. Papazian, M. Cotton and Y. Lo, “A comparison of 1920-MHz mobile channel diversity gain using horizontal and vertical arrays,” *IEEE Trans. Commun.*, vol. 49, no. 12, pp. 2068 – 2070, Dec. 2001.
- [48] W. Q. Malik, “MIMO capacity convergence in frequency-selective channels,” *IEEE Trans. Commun.*, vol. 57, no. 2, pp. 353 – 356, Feb. 2009.
- [49] W. Q. Malik, B. Allen, D. J. Edwards, “Fade depth scaling with channel bandwidth,” *Electron. Lett.*, vol. 43, no. 24, pp. 1371 – 1372, Nov. 2007.
- [50] E. G. Larsson, O. Edfors, F. Tufvesson and T. L. Marzetta, “Massive MIMO for next generation wireless systems,” *IEEE Commun. Magazine*, vol. 52, no. 2, pp. 186 – 195, Feb. 2014.
- [51] A. Knopp, M. Chouayakh, R. Schwarz, and B. Lankl, “Measured MIMO capacity enhancement in correlated LOS indoor channels via optimized antenna setups,” in *Int. Conf. Wireless Information Networks and Systems*, Setubal, Portugal, Aug. 7 – 10 2006, pp. 187 – 193.
- [52] F. Bentosela, N. Marchetti and H. D. Cornean, “Influence of environment richness on the increase of MIMO capacity with number of antennas,” *IEEE Trans. Antennas.*

- and Prop.*, vol. 62, no. 7, pp. 3786 – 3796, July. 2014.
- [53] N. P. Le, L. C. Tran, F. Safaei, “Transmit antenna subset selection with power balancing for high data rate MIMO-OFDM UWB systems,” in *Proc. ICUWB*, Sydney, Australia, Sep. 15 – Sep. 18, 2013, pp. 159 – 164.
- [54] F. D. Cardoso and Luis M. Correia, “Fading depth dependence on system bandwidth in mobile communications-an analytical approximation,” *IEEE Trans. Veh. Tech.*, vol. 52, no. 3, pp. 587 – 594, May. 2003.
- [55] D. Debbarma, Q. Wang, A. Lo, S. M. H. de Groot, R. V. Prasad, V. S. Rao, “Multiuser – MIMO for capacity gain in Fi-Wi hybrid networks,” in *Proc. EUROCON*, Zagreb, Croatia, July 1 – 4, 2013, pp. 494 – 501.
- [56] E. Bjornson, L. Sanguinetti, J. Hoydis and M. Debbah, “Designing multi-user MIMO for energy efficiency: when is massive MIMO the answer?,” in *Proc. WCNC*, Istanbul, Turkey, Apr. 6 – 9, 2014.
- [57] C. Li, J. Zhang and K. B. Letaief, “Throughput and energy efficiency analysis of small cell networks with multi-antenna base stations,” *IEEE Trans. Wireless Commun.*, vol. 13, no. 5, pp. 2505 – 2517, May 2014.
- [58] L. W. Hanlen and T. D. Abhayapala, “Space-time-frequency degrees of freedom: fundamental limits for spatial information,” in *Proc. ISIT*, Nice, France, June 24 – 29, 2007, pp. 701 – 705.
- [59] J. Yuan, S. W. Fung, K. Y. Chan and R. Xu, “An interpolation-based calibration architecture for pipeline ADC with nonlinear error,” *IEEE Trans. Instrum. Meas.*, vol. 61, no. 1, pp. 17 – 25, Jan. 2012.
- [60] A. D. Ibukie and D. M. Hummels, “Background calibration of gain errors in $\pi\Delta\Sigma$ A/D

- converters,” *IEEE Trans. Instrum. Meas.*, vol. 59, no. 8, pp. 2005 – 2014, Aug. 2010.
- [61] R. Valenzuela, “A ray tracing approach to predicting indoor wireless transmission,” in *43rd IEEE Veh. Technol. Conf.*, Secaucus, New Jersey, May 18 – 20, 1993, pp. 214 – 218.
- [62] R. Kalbasi, D. D. Falconer and A. H. Banihashemi, “Optimum space-time processors with symbol rate sampling are bandlimited,” *IEEE Trans. Signal Processing*, vol. 54, no. 5, pp. 1936 – 1941, May 2006.
- [63] J. Joung, Y. K. Chia and S. Sun, “Energy-efficient, large scale distributed antenna system for multiple users,” *IEEE Journal Select. Signal. Proces.*, vol. 8, no. 5, pp. 954 – 965, Oct. 2014.
- [64] M. Karlsson and E. G. Larsson, “On the operation of massive MIMO with and without transmitter CSI,” in *Proc. SPAWC*, Ontario, Canada, June 22 – 25, 2014, pp. 1 – 5.
- [65] K. Kamohara, H. Iwai and H. Sasooka, “Evaluation of MIMO capacity improvement by active propagation control,” in *Proc. IWEM*, Sapporo, Japan, Aug. 4 – 6, 2014, pp. 28 – 29.
- [66] R. A. Kennedy, P. Sadeghi, T. D. Abhayapala and H. M. Jones, “Intrinsic limits of dimensionality and richness in random multipath fields,” *IEEE Trans. Signal Processing*, vol. 55, no. 6, pp. 2542 – 2556, June 2007.
- [67] D. Akerberg, “Properties of a TDMA cellular office communication system,” in *39th IEEE Veh. Technol. Conf.*, San Francisco, California, May 1 – 3, 1989, pp. 186 – 191.
- [68] M. Ashraphijuo, V. Aggarwal and X. Wang, “On the capacity and degrees of freedom regions of two-user MIMO interference channels with limited receiver cooperation,”

IEEE Trans. Inform. Theory, vol. 62, no. 7, pp. 4170 - 4196, July 2014.

- [69] S. Durrani and M. E. Bialkowski, "Effect of mutual coupling on the interference rejection capabilities of linear and circular arrays in CDMA systems," *IEEE Trans. Antennas and Prop.*, vol. 52, no. 4, pp. 1130 – 1134, Apr. 2004.
- [70] H. Suzuki, D. B. Hayman, J. Pathikulangara, I. B. Collings, Z. Chen and R. Kendall, "Design criteria of uniform circular arrays for multi-user MIMO in rural areas," in *Proc. ICWC*, Sydney, Australia, April 18 – 21, 2010, pp. 1 – 6.
- [71] Hittite Microwave Products, "SiGe Wideband Direct Modulator RFIC 100 – 4000 MHz," HMC497LP4 datasheet.
- [72] Hittite Microwave Products, "SiGe Wideband Direct Demodulator RFIC 100 – 4000 MHz", HMC597LP4 datasheet.

Appendix A: Alignment Angle for Spatial Signatures of a 2×2 MU-MIMO System

The alignment angle ϕ between the spatial signatures of a 2×2 MU-MIMO system is derived as follows:

The alignment angle ϕ between the two vectors can be modelled as [22]

$$\langle \vec{x}, \vec{y} \rangle = |\vec{x}| |\vec{y}| \cos(\phi), \quad \text{A.1}$$

where \vec{x} denotes a vector, \vec{y} denotes a vector, $|\cdot|$ denotes length of a given vector, $\langle \cdot \rangle$ denotes the inner product of the vectors and ϕ indicates angle between two given vectors.

The channel matrix \mathbf{H}_P for a 2×2 MU-MIMO can be modelled as

$$\mathbf{H}_P = \sqrt{2} \begin{bmatrix} \frac{e^{-j2\pi d_{11}}}{\lambda} & \frac{e^{-j2\pi d_{12}}}{\lambda} \\ \frac{e^{-j2\pi d_{11}}}{\lambda} e^{-j2\pi \Delta_r \cos(\alpha_{21})} & \frac{e^{-j2\pi d_{12}}}{\lambda} e^{-j2\pi \Delta_r \cos(\alpha_{22})} \end{bmatrix}; \quad \text{A.2}$$

therefore the alignment angle between the spatial signatures of individual users on different receive antennas for a 2×2 MU-MIMO system can be modelled as

$$|\cos(\phi)| = \left| \frac{1}{\sqrt{2}} \left[e^{\frac{j2\pi d_{11}}{\lambda}} \quad e^{\frac{j2\pi d_{11}}{\lambda}} e^{\frac{j2\pi \Delta_r \cos(\alpha_{21})}{\lambda}} \right] \frac{1}{\sqrt{2}} \left[\begin{array}{c} e^{-\frac{j2\pi d_{12}}{\lambda}} \\ e^{-\frac{j2\pi d_{12}}{\lambda}} e^{-\frac{j2\pi \Delta_r \cos(\alpha_{22})}{\lambda}} \end{array} \right] \right|, \quad \text{A.3}$$

$$|\cos(\phi)| = \frac{1}{2} \left| e^{\frac{j2\pi(d_{11}-d_{12})}{\lambda}} + e^{\frac{j2\pi(d_{11}-d_{12})}{\lambda}} e^{\frac{j2\pi \Delta_r (\cos(\alpha_{21}) - \cos(\alpha_{22}))}{\lambda}} \right|, \quad \text{A.4}$$

$$|\cos(\phi)| = \frac{1}{2} \left| e^{\frac{j2\pi(d_{11}-d_{12})}{\lambda}} \left[1 + e^{\frac{j2\pi \Delta_r (\cos(\alpha_{21}) - \cos(\alpha_{22}))}{\lambda}} \right] \right|, \quad \text{A.5}$$

$$|\cos(\phi)| = \frac{1}{2} \left| e^{\frac{j2\pi(d_{11}-d_{12})}{\lambda}} \left[1 + e^{\frac{j\pi \Delta_r (\cos(\alpha_{21}) - \cos(\alpha_{22}))}{\lambda}} e^{\frac{j\pi \Delta_r (\cos(\alpha_{21}) - \cos(\alpha_{22}))}{\lambda}} \right] \right|, \quad \text{A.6}$$

$$|\cos(\phi)| = \frac{1}{2} \left| \left[\cos\left(\frac{\pi \Delta_r (\cos(\alpha_{21}) - \cos(\alpha_{22}))}{\lambda}\right) \right] \right|, \quad \text{A.7}$$


```

rx_antenna_1 = [(mean(room_width) - 0.5*wavelength) mean(room_length)]; % Specify the location of
receive antenna 1
rx_antenna_2 = [(mean(room_width) + 0.5*wavelength) mean(room_length)]; % Specify the location of
receive antenna 2

% Start of determination of user locations
ratio_w = 1; % Set width ratio to zero
ratio_l = 1; % Set length ratio to zero
if room_width >= room_length % Check if room width is greater than room length
    ratio_w = max(room_width)/max(room_length); % Calculate the width ratio (room width > room
length)
else
    ratio_l = max(room_length)/max(room_width); % Calculate the length ratio (room length > room
width)
end

if (ratio_w > 1) % Check if width ratio is more than one (i.e. room width > room length)
    no_points_width = round(sqrt(no_locations*ratio_w));
    no_points_length = round(no_points_width/ratio_w);
elseif (ratio_l > 1) % Check if length ratio is more than one (i.e. room length > room width)
    no_points_length = round(sqrt(no_locations*ratio_l));
    no_points_width = round(no_points_length/ratio_l);
elseif (ratio_l == 1 && ratio_w == 1) % Check if width and length ratio equals one (i.e. room width =
room length)
    no_points_length = round(sqrt(no_locations));
    no_points_width = round(no_points_length);
end

points_width = min(room_width):(max(room_width)-min(room_width))/(no_points_width-
1):max(room_width);
points_length = min(room_length):(max(room_length)-min(room_length))/(no_points_length-
1):max(room_length);

i = 0; % Set the variable "i" to zero
pairs = zeros([no_points_width*no_points_length 2]); % Initilize an array "pairs" to be all zero
for val1 = points_length
    for val2 = points_width
        i = i + 1;
        pairs(i,1) = val1; % First column indicates length
        pairs(i,2) = val2; % Second column indicates width
    end
end

% End of determination of user locations

set_bandwidth = [10*10^6 20*10^6 30*10^6 60*10^6 90*10^6]; % Preset the allocated user bandwidths
count = 0; % Set the variable "count" to be zero
flag = 1; % Set the flag to value of one
while (flag == 1) % Set the "while" loop to repeat until flag == 1
    count = count+1; % Update the value of variable count
    for r = 1:length(pairs) % Set the loop to repeat for number of user locations
        user_1_w = pairs(r,2); % Select the location of user1 along the width of room
        user_1_l = pairs(r,1); % Select the location of user1 along the length of room
        user_2_w = (mean(room_width)); % Select the location of user2 along the width of room
        user_2_l = (min(room_length)+1*wavelength); % Select the location of user2 along the length of room
    end
end

```

```

    d11 = (sqrt(((user_1_w-rx_antenna_1(1))^2)+((user_1_l-rx_antenna_1(2))^2))); % Calculate the
propagation distance d11
    d12 = (sqrt(((user_2_w-rx_antenna_1(1))^2)+((user_2_l-rx_antenna_1(2))^2))); % calculate the
propagation distance d12
    d21 = (sqrt(((user_1_w-rx_antenna_2(1))^2)+((user_1_l-rx_antenna_2(2))^2))); % Calculate the
propagation distance d21
    d22 = (sqrt(((user_2_w-rx_antenna_2(1))^2)+((user_2_l-rx_antenna_2(2))^2))); % Calculate the
propagation distance d22

    tau11 = (sqrt(((user_1_w-rx_antenna_1(1))^2)+((user_1_l-rx_antenna_1(2))^2))/(3*10^8); %
Calculate the propagation delay tau11
    tau12 = (sqrt(((user_2_w-rx_antenna_1(1))^2)+((user_2_l-rx_antenna_1(2))^2))/(3*10^8); %
Calculate the propagation delay tau12
    tau21 = (sqrt(((user_1_w-rx_antenna_2(1))^2)+((user_1_l-rx_antenna_2(2))^2))/(3*10^8); %
Calculate the propagation delay tau21
    tau22 = (sqrt(((user_2_w-rx_antenna_2(1))^2)+((user_2_l-rx_antenna_2(2))^2))/(3*10^8); %
Calculate the propagation delay tau22

    if see_required_BW_effect == 1 % Check if the "see_required_BW_effect" flag is high
        bandwidth = abs(0.5/((-tau11-tau22+tau12+tau21))); % Calculate the bandwidth required to obtain
ideal channel matrix
        required_bandwidth(r) = bandwidth; % Update the required bandwidth array
        flag = 0; % Set the flag to zero such as to exit the "while" loop
    end

% Start of Large Scale Path Loss Calculation for ADC's
    LSPL_rx_power11 = tx_power_dbW + loss_factor_dbW - 10*LSPL_power_exponent*log10(d11);
    LSPL_rx_power12 = tx_power_dbW + loss_factor_dbW - 10*LSPL_power_exponent*log10(d12);
    LSPL_rx_power21 = tx_power_dbW + loss_factor_dbW - 10*LSPL_power_exponent*log10(d21);
    LSPL_rx_power22 = tx_power_dbW + loss_factor_dbW - 10*LSPL_power_exponent*log10(d22);

    LSPL_ADC1_resolution =
0.5*log2(3*((max(10^(LSPL_rx_power11/10),10^(LSPL_rx_power12/10)))/(min(10^(LSPL_rx_power11/
10),10^(LSPL_rx_power12/10))))*SQNR); % Calculate the required resolution for ADC1
    LSPL_ADC2_resolution =
0.5*log2(3*((max(10^(LSPL_rx_power21/10),10^(LSPL_rx_power22/10)))/(min(10^(LSPL_rx_power21/
10),10^(LSPL_rx_power22/10))))*SQNR); % Calculate the required resolution for ADC2

    LSPL_ADC1_dynamic_range(r) = 6*LSPL_ADC1_resolution; % Calculate the required dynamic
range for ADC1
    LSPL_ADC2_dynamic_range(r) = 6*LSPL_ADC2_resolution; % Calculate the required dynamic
range for ADC2

    LSPL_power_ratio1(r) =
max(10^(LSPL_rx_power11/10),10^(LSPL_rx_power12/10))/min(10^(LSPL_rx_power11/10),10^(LSPL_
rx_power12/10)); % Calculate the LSPL power ratio for receiver 1
    LSPL_power_ratio2(r) =
max(10^(LSPL_rx_power21/10),10^(LSPL_rx_power22/10))/min(10^(LSPL_rx_power21/10),10^(LSPL_
rx_power22/10)); % Calculate the LSPL power ratio for receiver 2
    LSPL_power_ratio1(r) = 10*log10(LSPL_power_ratio1(r)); % Convert the LSPL power ratio1 from
watts to dbW
    LSPL_power_ratio2(r) = 10*log10(LSPL_power_ratio2(r)); % Convert the LSPL power ratio2 from
watts to dbW

```

```

distance_ratio1(r) = max(d11,d12)/min(d11,d12); % Calculate the distance ratio for receiver 1
distance_ratio2(r) = max(d21,d22)/min(d21,d22); % Calculate the distance ratio for receiver 2

[distance_ratio_1,index1] = sort(distance_ratio1); % Sort distance_ratio1 in ascending order
[distance_ratio_2,index2] = sort(distance_ratio2); % Sort distance_ratio2 in ascending order

for g = 1:length(index1)
    LSPL_power_ratio_1(g) = LSPL_power_ratio1(index1(g)); % Sort LSPL_power_ratio1 as per
distance index1
    LSPL_power_ratio_2(g) = LSPL_power_ratio2(index2(g)); % Sort LSPL_power_ratio2 as per
distance index2
end
% End of Large Scale Path Loss Calculation for ADC's

% Start of Indoor Path Loss Calculation for ADC's
IPL_rx_power11 = tx_power_dbW + loss_factor_dbW - 10*indoor_power_exponent*log10(d11) +
normrnd(0,5.8);
IPL_rx_power12 = tx_power_dbW + loss_factor_dbW - 10*indoor_power_exponent*log10(d12) +
normrnd(0,5.8);
IPL_rx_power21 = tx_power_dbW + loss_factor_dbW - 10*indoor_power_exponent*log10(d21) +
normrnd(0,5.8);
IPL_rx_power22 = tx_power_dbW + loss_factor_dbW - 10*indoor_power_exponent*log10(d22) +
normrnd(0,5.8);

IPL_ADC1_resolution =
0.5*log2(3*((max(10^(IPL_rx_power11/10),10^(IPL_rx_power12/10)))/(min(10^(IPL_rx_power11/10),10
^(IPL_rx_power12/10))))*SQNR);
IPL_ADC2_resolution =
0.5*log2(3*((max(10^(IPL_rx_power21/10),10^(IPL_rx_power22/10)))/(min(10^(IPL_rx_power21/10),10
^(IPL_rx_power22/10))))*SQNR);

IPL_ADC1_dynamic_range(r) = 6*IPL_ADC1_resolution; % Calculate the required dynamic range
for ADC1
IPL_ADC2_dynamic_range(r) = 6*IPL_ADC2_resolution; % Calculate the required dynamic range
for ADC2

IPL_power_ratio1(r) =
max(10^(IPL_rx_power11/10),10^(IPL_rx_power12/10))/min(10^(IPL_rx_power11/10),10^(IPL_rx_powe
r12/10)); % Calculate the IPL power ratio for receiver 1
IPL_power_ratio2(r) =
max(10^(IPL_rx_power21/10),10^(IPL_rx_power22/10))/min(10^(IPL_rx_power21/10),10^(IPL_rx_powe
r22/10)); % Calculate the IPL power ratio for receiver 2
IPL_power_ratio1(r) = 10*log10(IPL_power_ratio1(r)); % Convert the IPL power ratio1 from watts to
dbW
IPL_power_ratio2(r) = 10*log10(IPL_power_ratio2(r)); % Convert the IPL power ratio2 from watts to
dbW

for g = 1:length(index1)
    IPL_power_ratio_1(g) = IPL_power_ratio1(index1(g)); % Sort IPL_power_ratio1 as per distance
index1
    IPL_power_ratio_2(g) = IPL_power_ratio2(index2(g)); % Sort IPL_power_ratio2 as per distance
index2
end
end

```

```

% End of Indoor Path Loss Calculation for ADC's

bandwidth = set_bandwidth(count); % Select the value of bandwidth depending upon value of
variable count
freq = 0:bandwidth/no_points:bandwidth; % Calculate the discrete frequency points on the bandwidth
range

H11 = cosd(2*180*tau11*(freq))-sqrt(-1)*sind(2*180*tau11*(freq)); % Calculate the phase response
of user 1 on receive antenna 1
H12 = cosd(2*180*tau12*(freq))-sqrt(-1)*sind(2*180*tau12*(freq)); % Calculate the phase response
of user 2 on receive antenna 1
H21 = cosd(2*180*tau21*(freq))-sqrt(-1)*sind(2*180*tau21*(freq)); % Calculate the phase response
of user 1 on receive antenna 2
H22 = cosd(2*180*tau22*(freq))-sqrt(-1)*sind(2*180*tau22*(freq)); % Calculate the phase response
of user 2 on receive antenna 2
% Calculate the channel matrix depending upon the bandwidth and
% propagation delays
for v = 2:length(freq)
    H = [H11(v) H12(v);H21(v) H22(v)];
    cond_H(v) = cond(H);
end
inst_condition_number(r) = mean(cond_H); % Calculate and store the condition number of channel
matrix H
end % End for "for loop" regarding number of iterations

if count == length(set_bandwidth)
    flag = 0;
end
condition_number(count,:) = inst_condition_number; % Update the variable condition number
end % End for "While" loop

% Plotting Section
if see_required_BW_effect == 1
    limit_bandwidth = 1000*10^6;%max(required_bandwidth); % Set the limit of bandwidth to be
maximum calculated bandwidth
    edges_bandwidth = 1:10^7:limit_bandwidth; % Define the edges to sort out the required
bandwidth
    sort_bandwidth = histc(required_bandwidth,edges_bandwidth); % Sort out the required bandwidth
according to the edges
    percent_bandwidth = (sort_bandwidth/(sum(sort_bandwidth)))*100; % Calculate the percentage of the
sorted bandwidth
    final_percent_ban = [];
    temp_ban = 0;
    for y = 1:length(percent_bandwidth) % Set the loop to repeat for the length of the
percent_bandwidth vector
        temp_ban = temp_ban + percent_bandwidth(y); % Update the temp_ban variable
        final_percent_ban = [final_percent_ban temp_ban];
    end
    figure(1)
    plot(edges_bandwidth,final_percent_ban,'b'); grid on
    set(gca,'fontsize',12)
    title('Percentage of Portable User Locations vs. Required User Bandwidth', 'FontSize',12)
    xlabel('Required Bandwidth (Hz)', 'FontSize',12)

```

```

ylabel('Percentage of Portable Locations','FontSize',12)

LSPL_edges_DR1 = min(LSPL_ADC1_dynamic_range):1:max(LSPL_ADC1_dynamic_range);
LSPL_sort_DR1 = histc(LSPL_ADC1_dynamic_range,LSPL_edges_DR1);
LSPL_percent_DR1 = (LSPL_sort_DR1/(sum(LSPL_sort_DR1)))*100;
LSPL_final_percent_DR1 = [];
LSPL_temp_DR1 = 0;
for s = 1:length(LSPL_percent_DR1);
    LSPL_temp_DR1 = LSPL_temp_DR1 + LSPL_percent_DR1(s);
    LSPL_final_percent_DR1 = [LSPL_final_percent_DR1 LSPL_temp_DR1];
end
figure(2)
plot(LSPL_edges_DR1,LSPL_final_percent_DR1,'b'); grid on
set(gca,'fontsize',12)
title('Percentage of Portable Locations vs. Required Dynamic Range for ADC1 for LSPL','FontSize',12)
xlabel('Required Dynamic Range (dB)','FontSize',12)
ylabel('Percentage of Portable User Locations','FontSize',12)

LSPL_edges_DR2 = min(LSPL_ADC2_dynamic_range):1:max(LSPL_ADC2_dynamic_range);
LSPL_sort_DR2 = histc(LSPL_ADC2_dynamic_range,LSPL_edges_DR2);
LSPL_percent_DR2 = (LSPL_sort_DR2/(sum(LSPL_sort_DR2)))*100;
LSPL_final_percent_DR2 = [];
LSPL_temp_DR2 = 0;
for s = 1:length(LSPL_percent_DR2);
    LSPL_temp_DR2 = LSPL_temp_DR2 + LSPL_percent_DR2(s);
    LSPL_final_percent_DR2 = [LSPL_final_percent_DR2 LSPL_temp_DR2];
end
figure(3)
plot(LSPL_edges_DR2,LSPL_final_percent_DR2,'b'); grid on
set(gca,'fontsize',12)
title('Percentage of Portable Locations vs. Required Dynamic Range for ADC2 for LSPL','FontSize',12)
xlabel('Required Dynamic Range (dB)','FontSize',12)
ylabel('Percentage of Portable User Locations','FontSize',12)

IPL_edges_DR1 = min(IPL_ADC1_dynamic_range):1:max(IPL_ADC1_dynamic_range);
IPL_sort_DR1 = histc(IPL_ADC1_dynamic_range,IPL_edges_DR1);
IPL_percent_DR1 = (IPL_sort_DR1/(sum(IPL_sort_DR1)))*100;
IPL_final_percent_DR1 = [];
IPL_temp_DR1 = 0;
for s = 1:length(IPL_percent_DR1);
    IPL_temp_DR1 = IPL_temp_DR1 + IPL_percent_DR1(s);
    IPL_final_percent_DR1 = [IPL_final_percent_DR1 IPL_temp_DR1];
end
figure(4)
plot(IPL_edges_DR1,IPL_final_percent_DR1,'b'); grid on
set(gca,'fontsize',12)
title('Percentage of Portable Locations vs. Required Dynamic Range for ADC1 for IPL','FontSize',12)
xlabel('Required Dynamic Range (dB)','FontSize',12)
ylabel('Percentage of Portable User Locations','FontSize',12)

IPL_edges_DR2 = min(IPL_ADC2_dynamic_range):1:max(IPL_ADC2_dynamic_range);

```

```

IPL_sort_DR2 = histc(IPL_ADC2_dynamic_range,IPL_edges_DR2);
IPL_percent_DR2 = (IPL_sort_DR2/(sum(IPL_sort_DR2)))*100;
IPL_final_percent_DR2 = [];
IPL_temp_DR2 = 0;
for s = 1:length(IPL_percent_DR2);
    IPL_temp_DR2 = IPL_temp_DR2 + IPL_percent_DR2(s);
    IPL_final_percent_DR2 = [IPL_final_percent_DR2 IPL_temp_DR2];
end
figure(5)
plot(IPL_edges_DR2,IPL_final_percent_DR2,'b'); grid on
set(gca,'fontsize',12)
title('Percentage of Portable Locations vs. Required Dynamic Range for ADC2 for IPL','FontSize',12)
xlabel('Required Dynamic Range (dB)','FontSize',12)
ylabel('Percentage of Portable User Locations','FontSize',12)

figure(6)
plot(distance_ratio_1/(max(distance_ratio_1)),LSPL_power_ratio_1);grid on
set(gca,'fontsize',12)
title('LSPL Power Ratio for ADC1 vs. Portable User Distance Ratio','FontSize',12)
xlabel('Normalised Distance Ratio')
ylabel('Power Ratio (dBW)');

figure(7)
plot(distance_ratio_2/(max(distance_ratio_2)),LSPL_power_ratio_2);grid on
set(gca,'fontsize',12)
title('LSPL Power Ratio for ADC2 vs. Portable User Distance Ratio','FontSize',12)
xlabel('Normalised Distance Ratio')
ylabel('Power Ratio (dBW)');

figure(8)
plot(distance_ratio_1/(max(distance_ratio_1)),IPL_power_ratio_1);grid on
set(gca,'fontsize',12)
title('IPL Power Ratio for ADC1 vs. Portable User Distance Ratio','FontSize',12)
xlabel('Normalised Distance Ratio')
ylabel('Power Ratio (dBW)');

figure(9)
plot(distance_ratio_2/(max(distance_ratio_2)),IPL_power_ratio_2);grid on
set(gca,'fontsize',12)
title('LSPL Power Ratio for ADC2 vs. Portable User Distance Ratio','FontSize',12)
xlabel('Normalised Distance Ratio')
ylabel('Power Ratio (dBW)');

else
    limit_condition = max(condition_number); % Set the limit of condition number to be maximum
calculated condition number
    edges_condition = 1:1:limit_condition; % Define the edges to sort out the condition number
    for u = 1:count
        con = condition_number(u,:); % Get the condition number for particular allocated user
bandwidth
        sort_condition = histc(con,edges_condition); % Sort out the condition number according to the edges
        percent_condition = (sort_condition/(sum(sort_condition)))*100; % Calculate the percentage of
sorted condition number

```



```

% Edit the above text to modify the response to help RS232_GUI

% Last Modified by GUIDE v2.5 01-Aug-2013 18:14:41

% Begin initialization code - DO NOT EDIT
gui_Singleton = 1;
gui_State = struct('gui_Name',    mfilename, ...
                  'gui_Singleton', gui_Singleton, ...
                  'gui_OpeningFcn', @RS232_GUI_OpeningFcn, ...
                  'gui_OutputFcn', @RS232_GUI_OutputFcn, ...
                  'gui_LayoutFcn', [], ...
                  'gui_Callback', []);
if nargin && ischar(varargin{1})
    gui_State.gui_Callback = str2func(varargin{1});
end

if nargout
    [varargout{1:nargout}] = gui_mainfcn(gui_State, varargin{:});
else
    gui_mainfcn(gui_State, varargin{:});
end
% End initialization code - DO NOT EDIT

% --- Executes just before RS232_GUI is made visible.

function RS232_GUI_OpeningFcn(hObject, eventdata, handles, varargin)
% This function has no output args, see OutputFcn.
% hObject    handle to figure
% eventdata  reserved - to be defined in a future version of MATLAB
% handles    structure with handles and user data (see GUIDATA)
% varargin   command line arguments to RS232_GUI (see VARARGIN)

% Choose default command line output for RS232_GUI
handles.output = hObject;

%%%%%%%%%%%%%%%%%%%%%%%%%%%%%%%%%%%%%%%%%%%%%%%%%%%%%%%%%%%%%%%%%%%%%%%%
handles.input1 = 0000.000; % Initialize input frequency for signal generator
handles.input2 = -000.0;   % Initialize input RF level for signal generator
handles.readings = 1;     % Initialize number of readings
handles.periods = 3;      % Initialize number of periods
handles.BW = 30;          % Initialize the value of bandwidth
%%%%%%%%%%%%%%%%%%%%%%%%%%%%%%%%%%%%%%%%%%%%%%%%%%%%%%%%%%%%%%%%%%%%%%%%

% Update handles structure
guidata(hObject, handles);

% UIWAIT makes RS232_GUI wait for user response (see UIRESUME)
% uiwait(handles.figure1);

% --- Outputs from this function are returned to the command line.

function varargout = RS232_GUI_OutputFcn(hObject, eventdata, handles)

```

```

% varargout cell array for returning output args (see VARARGOUT);
% hObject handle to figure
% eventdata reserved - to be defined in a future version of MATLAB
% handles structure with handles and user data (see GUIDATA)

% Get default command line output from handles structure
varargout{1} = handles.output;

%%%%%%%%%%%%%%%%%%%%%%%%%%%%%%%%%%%%%%%%%%%%%%%%%%%%%%%%%%%%%%%%%%%%%%%% Start of Signal Generator Section

%%%%%%%%%%%%%%%%%%%%%%%%%%%%%%%%%%%%%%%%%%%%%%%%%%%%%%%%%%%%%%%%%%%%%%%% Start of Signal Generator Reset
%%%%%%%%%%%%%%%%%%%%%%%%%%%%%%%%%%%%%%%%%%%%%%%%%%%%%%%%%%%%%%%%%%%%%%%%

% --- Executes on button press in signalgenerator_reset.

function signalgenerator_reset_Callback(hObject, eventdata, handles)
% hObject handle to signalgenerator_reset (see GCBO)
% eventdata reserved - to be defined in a future version of MATLAB
% handles structure with handles and user data (see GUIDATA)
s = serial('COM1');
fopen(s);
fprintf(s, '*RST');
fclose(s);
delete(s);

%%%%%%%%%%%%%%%%%%%%%%%%%%%%%%%%%%%%%%%%%%%%%%%%%%%%%%%%%%%%%%%%%%%%%%%% End of Signal Generator Reset
%%%%%%%%%%%%%%%%%%%%%%%%%%%%%%%%%%%%%%%%%%%%%%%%%%%%%%%%%%%%%%%%%%%%%%%%

%%%%%%%%%%%%%%%%%%%%%%%%%%%%%%%%%%%%%%%%%%%%%%%%%%%%%%%%%%%%%%%%%%%%%%%% Start of Set Signal Generator Frequency
%%%%%%%%%%%%%%%%%%%%%%%%%%%%%%%%%%%%%%%%%%%%%%%%%%%%%%%%%%%%%%%%%%%%%%%%

function signalgenerator_input_freq_Callback(hObject, eventdata, handles)
% hObject handle to signalgenerator_input_freq (see GCBO)
% eventdata reserved - to be defined in a future version of MATLAB
% handles structure with handles and user data (see GUIDATA)

% Hints: get(hObject,'String') returns contents of signalgenerator_input_freq as text
% str2double(get(hObject,'String')) returns contents of signalgenerator_input_freq as a double
handles.input1 = (get(hObject,'String'));
%checks to see if input is empty. if so, default input1_editText to zero
if (isempty(handles.input1))
    set(hObject,'String','0000.000')
end
guidata(hObject, handles);

% --- Executes during object creation, after setting all properties.

function signalgenerator_input_freq_CreateFcn(hObject, eventdata, handles)
% hObject handle to signalgenerator_input_freq (see GCBO)
% eventdata reserved - to be defined in a future version of MATLAB

```

```

% handles empty - handles not created until after all CreateFens called

% Hint: edit controls usually have a white background on Windows.
% See ISPC and COMPUTER.
if ispc && isequal(get(hObject,'BackgroundColor'), get(0,'defaultUicontrolBackgroundColor'))
    set(hObject,'BackgroundColor','white');
end

% --- Executes on button press in signalgenerator_freq_set.

function signalgenerator_freq_set_Callback(hObject, eventdata, handles)
% hObject handle to signalgenerator_freq_set (see GCBO)
% eventdata reserved - to be defined in a future version of MATLAB
% handles structure with handles and user data (see GUIDATA)
output1 = [blanks(1) handles.input1];
prefix = 'CFRQ:VALUE';
suffix = 'MHZ';
frequency = strcat(prefix,output1,suffix);
s = serial('COM1');
fopen(s);
fprintf(s,frequency);
fclose(s);
delete(s);

%%%%%%%%%%%%%%
%%%%%%%%%%%%%% End of Set Signal Generator Frequency %%%%%%%%%%%%%%%
%%%%%%%%%%%%%%
%%%%%%%%%%%%%% Start of Set Signal Generator Frequency Stepsize %%%%%%%%%%%%%%%
%%%%%%%%%%%%%%

% --- Executes on selection change in signalgenerator_freq_stepsize.

function signalgenerator_freq_stepsize_Callback(hObject, eventdata, handles)
% hObject handle to signalgenerator_freq_stepsize (see GCBO)
% eventdata reserved - to be defined in a future version of MATLAB
% handles structure with handles and user data (see GUIDATA)

% Hints: contents = cellstr(get(hObject,'String')) returns signalgenerator_freq_stepsize contents as cell
array
% contents{get(hObject,'Value')} returns selected item from signalgenerator_freq_stepsize
switch get(handles.signalgenerator_freq_stepsize,'Value')
case 1
    s = serial('COM1');
    fopen(s);
    fprintf(s, 'CFRQ:INC 1.0KHZ');
    fwrite(s,19);
    fclose(s);
    delete(s);
case 2
    s = serial('COM1');
    fopen(s);
    fprintf(s, 'CFRQ:INC 10.0KHZ');
    fclose(s);

```

```

delete(s);
case 3
s = serial('COM1');
fopen(s);
fprintf(s, 'CFRQ:INC 100.0KHZ');
fclose(s);
delete(s);
case 4
s = serial('COM1');
fopen(s);
fprintf(s, 'CFRQ:INC 1000.0KHZ');
fclose(s);
delete(s);
case 5
s = serial('COM1');
fopen(s);
fprintf(s, 'CFRQ:INC 10000.0KHZ');
fclose(s);
delete(s);
case 6
s = serial('COM1');
fopen(s);
fprintf(s, 'CFRQ:INC 100000.0KHZ');
fclose(s);
delete(s);
case 7
s = serial('COM1');
fopen(s);
fprintf(s, 'CFRQ:INC 1000000.0KHZ');
fclose(s);
delete(s);
end

```

% --- Executes during object creation, after setting all properties.

```

function signalgenerator_freq_stepsize_CreateFcn(hObject, eventdata, handles)
% hObject handle to signalgenerator_freq_stepsize (see GCBO)
% eventdata reserved - to be defined in a future version of MATLAB
% handles empty - handles not created until after all CreateFcns called

% Hint: popupmenu controls usually have a white background on Windows.
% See ISPC and COMPUTER.
if ispc && isequal(get(hObject,'BackgroundColor'), get(0,'defaultUicontrolBackgroundColor'))
set(hObject,'BackgroundColor','white');
end

```

```

%%%%%%%%%%
%%%%%%%%%% End of Set Signal Generator Frequency Stepsize %%%%%%%%%%
%%%%%%%%%%

```

```

%%%%%%%%%%
%%%%%%%%%% Start of Signal Generator Frequency Up/Down %%%%%%%%%%
%%%%%%%%%%

```

```

% --- Executes on button press in signalgenerator_freq_up.

function signalgenerator_freq_up_Callback(hObject, eventdata, handles)
% hObject handle to signalgenerator_freq_up (see GCBO)
% eventdata reserved - to be defined in a future version of MATLAB
% handles structure with handles and user data (see GUIDATA)
s = serial('COM1');
fopen(s);
fprintf(s, 'CFRQ:UP');
fclose(s);
delete(s);

% --- Executes on button press in signalgenerator_freq_down.

function signalgenerator_freq_down_Callback(hObject, eventdata, handles)
% hObject handle to signalgenerator_freq_down (see GCBO)
% eventdata reserved - to be defined in a future version of MATLAB
% handles structure with handles and user data (see GUIDATA)
s = serial('COM1');
fopen(s);
fprintf(s, 'CFRQ:DN');
fclose(s);
delete(s);
%%%%%%%%%%%%%%%%%%%%%%%%%%%%%%%%%%%%%%%%%%%%%%%%%%%%%%%%%%%%%%%%%%%%%%%%
%%%%%%%%%%%%%%%%%%%%%%%%%%%%%%%%%%%%%%%%%%%%%%%%%%%%%%%%%%%%%%%%%%%%%%%%
End of Signal Generator Frequency Up/Down
%%%%%%%%%%%%%%%%%%%%%%%%%%%%%%%%%%%%%%%%%%%%%%%%%%%%%%%%%%%%%%%%%%%%%%%%
%%%%%%%%%%%%%%%%%%%%%%%%%%%%%%%%%%%%%%%%%%%%%%%%%%%%%%%%%%%%%%%%%%%%%%%%

%%%%%%%%%%%%%%%%%%%%%%%%%%%%%%%%%%%%%%%%%%%%%%%%%%%%%%%%%%%%%%%%%%%%%%%%
%%%%%%%%%%%%%%%%%%%%%%%%%%%%%%%%%%%%%%%%%%%%%%%%%%%%%%%%%%%%%%%%%%%%%%%%
Start of Set Signal Generator RF Level
%%%%%%%%%%%%%%%%%%%%%%%%%%%%%%%%%%%%%%%%%%%%%%%%%%%%%%%%%%%%%%%%%%%%%%%%
%%%%%%%%%%%%%%%%%%%%%%%%%%%%%%%%%%%%%%%%%%%%%%%%%%%%%%%%%%%%%%%%%%%%%%%%

function signalgenerator_input_RF_level_Callback(hObject, eventdata, handles)
% hObject handle to signalgenerator_input_RF_level (see GCBO)
% eventdata reserved - to be defined in a future version of MATLAB
% handles structure with handles and user data (see GUIDATA)

% Hints: get(hObject,'String') returns contents of signalgenerator_input_RF_level as text
% str2double(get(hObject,'String')) returns contents of signalgenerator_input_RF_level as a double
handles.input2 = (get(hObject,'String'));
%checks to see if input is empty. if so, default input1_editText to zero
if (isempty(handles.input2))
    set(hObject,'String','-000.0')
end
guidata(hObject, handles);

% --- Executes during object creation, after setting all properties.

function signalgenerator_input_RF_level_CreateFcn(hObject, eventdata, handles)
% hObject handle to signalgenerator_input_RF_level (see GCBO)
% eventdata reserved - to be defined in a future version of MATLAB
% handles empty - handles not created until after all CreateFns called

```

```

% Hint: edit controls usually have a white background on Windows.
% See ISPC and COMPUTER.
if ispc && isequal(get(hObject,'BackgroundColor'), get(0,'defaultUicontrolBackgroundColor'))
    set(hObject,'BackgroundColor','white');
end

```

% --- Executes on button press in signalgenerator_RF_level_set.

```

function signalgenerator_RF_level_set_Callback(hObject, eventdata, handles)
% hObject handle to signalgenerator_RF_level_set (see GCBO)
% eventdata reserved - to be defined in a future version of MATLAB
% handles structure with handles and user data (see GUIDATA)
output2 = [blanks(1) handles.input2];
prefix = 'RFLV:VALUE';
rflvl = strcat(prefix,output2);
s = serial('COM1');
fopen(s);
fprintf(s,rflvl);
fclose(s);
delete(s);

```

```

%%%%%%%%%%
%%%%%%%%%% End of Set Signal Generator RF Level %%%%%%%%%%
%%%%%%%%%%

```

```

%%%%%%%%%%
%%%%%%%%%% Start of Set Signal Generator RF Level Step Size %%%%%%%%%%
%%%%%%%%%%

```

```

function signalgenerator_RF_stepsize_Callback(hObject, eventdata, handles)
% hObject handle to signalgenerator_RF_stepsize (see GCBO)
% eventdata reserved - to be defined in a future version of MATLAB
% handles structure with handles and user data (see GUIDATA)

```

```

% Hints: contents = cellstr(get(hObject,'String')) returns signalgenerator_RF_stepsize contents as cell array
% contents {get(hObject,'Value')} returns selected item from signalgenerator_RF_stepsize

```

```

switch get(handles.signalgenerator_RF_stepsize,'Value')

```

```

    case 1
        s = serial('COM1');
        fopen(s);
        fprintf(s, 'RFLV:INC 0.1');
        fclose(s);
        delete(s);

```

```

    case 2
        s = serial('COM1');
        fopen(s);
        fprintf(s, 'RFLV:INC 1.0');
        fclose(s);
        delete(s);

```

```

    case 3
        s = serial('COM1');
        fopen(s);

```

```

    fprintf(s, 'RFLV:INC 10.0');
    fclose(s);
    delete(s);
case 4
    s = serial('COM1');
    fopen(s);
    fprintf(s, 'RFLV:INC 100.0');
    fclose(s);
    delete(s);
end
% --- Executes during object creation, after setting all properties.

function signalgenerator_RF_stepsize_CreateFcn(hObject, eventdata, handles)
% hObject   handle to signalgenerator_RF_stepsize (see GCBO)
% eventdata reserved - to be defined in a future version of MATLAB
% handles   empty - handles not created until after all CreateFcns called

% Hint: popupmenu controls usually have a white background on Windows.
%       See ISPC and COMPUTER.
if ispc && isequal(get(hObject,'BackgroundColor'), get(0,'defaultUicontrolBackgroundColor'))
    set(hObject,'BackgroundColor','white');
end

%%%%%%%%%%%%%%%%%%%%%%%%%%%%%%%%%%%%%%%%%%%%%%%%%%%%%%%%%%%%%%%%%%%%%%%%
%%%%%%%%%%%%%%%%%%%%%%%% End of Set Signal Generator RF Level Step Size %%%%%%%%%
%%%%%%%%%%%%%%%%%%%%%%%%%%%%%%%%%%%%%%%%%%%%%%%%%%%%%%%%%%%%%%%%%%%%%%%%

%%%%%%%%%%%%%%%%%%%%%%%%%%%%%%%%%%%%%%%%%%%%%%%%%%%%%%%%%%%%%%%%%%%%%%%%
%%%%%%%%%%%%%%%%%%%%%%%% Start of Signal Generator RF Level Up/Down %%%%%%%%%
%%%%%%%%%%%%%%%%%%%%%%%%%%%%%%%%%%%%%%%%%%%%%%%%%%%%%%%%%%%%%%%%%%%%%%%%

function signalgenerator_RF_Level_Up_Callback(hObject, eventdata, handles)
% hObject   handle to signalgenerator_RF_Level_Up (see GCBO)
% eventdata reserved - to be defined in a future version of MATLAB
% handles   structure with handles and user data (see GUIDATA)
    s = serial('com1');
    fopen(s);
    fprintf(s, 'RFLV:UP');
    fclose(s);
    delete(s);

% --- Executes on button press in signalgenerator_RF_Level_Down.

function signalgenerator_RF_Level_Down_Callback(hObject, eventdata, handles)
% hObject   handle to signalgenerator_RF_Level_Down (see GCBO)
% eventdata reserved - to be defined in a future version of MATLAB
% handles   structure with handles and user data (see GUIDATA)
    s = serial('com1');
    fopen(s);
    fprintf(s, 'RFLV:DN');
    fclose(s);
    delete(s);

```



```

function data_collection_number_readings_CreateFcn(hObject, eventdata, handles)
% hObject handle to data_collection_number_readings (see GCBO)
% eventdata reserved - to be defined in a future version of MATLAB
% handles empty - handles not created until after all CreateFcns called

% Hint: popupmenu controls usually have a white background on Windows.
% See ISPC and COMPUTER.
if ispc && isequal(get(hObject,'BackgroundColor'), get(0,'defaultUicontrolBackgroundColor'))
    set(hObject,'BackgroundColor','white');
end

% --- Executes on selection change in data_collection_number_periods.

function data_collection_number_periods_Callback(hObject, eventdata, handles)
% hObject handle to data_collection_number_periods (see GCBO)
% eventdata reserved - to be defined in a future version of MATLAB
% handles structure with handles and user data (see GUIDATA)

% Hints: contents = get(hObject,'String') returns data_collection_number_periods contents as cell array
% contents {get(hObject,'Value')} returns selected item from data_collection_number_periods
switch get(handles.data_collection_number_periods,'Value')
    case 1
        handles.periods = 1;
        guidata(hObject, handles);
    case 2
        handles.periods = 2;
        guidata(hObject, handles);
    case 3
        handles.periods = 3;
        guidata(hObject, handles);
    case 4
        handles.periods = 4;
        guidata(hObject, handles);
end

% --- Executes during object creation, after setting all properties.

function data_collection_number_periods_CreateFcn(hObject, eventdata, handles)
% hObject handle to data_collection_number_periods (see GCBO)
% eventdata reserved - to be defined in a future version of MATLAB
% handles empty - handles not created until after all CreateFcns called

% Hint: popupmenu controls usually have a white background on Windows.
% See ISPC and COMPUTER.
if ispc && isequal(get(hObject,'BackgroundColor'), get(0,'defaultUicontrolBackgroundColor'))
    set(hObject,'BackgroundColor','white');
end

% --- Executes on selection change in data_collection_BW.

function data_collection_BW_Callback(hObject, eventdata, handles)
% hObject handle to data_collection_BW (see GCBO)

```



```
fopen(s);  
fprintf(s,'RFLV:VALUE 0.0');  
fclose(s);delete(s);  
pause(0.7);  
else  
s = serial('COM1');  
fopen(s);  
fprintf(s,'RFLV:VALUE -140');  
fclose(s);delete(s);  
pause(0.7);  
end  
end
```

B.3 Impulse Response and Condition Number Calculation

This section consists of a MATLAB code that is used to obtain data from the SignalTap Logic Analyzer module and compute the impulse response from each user to respective receive antennas. The calculated impulse response is then transferred into frequency domain transfer function and therefore calculate the performance of a MU-MIMO system with the help of condition number of the recovered channel transfer function matrix.

```
%%%%%%%%%%%%%%%%%%%%%%%%%%%%%%%%%%%%%%%%%%%%%%%%%%%%%%%%%%%%%%%%%%%%%%%%
%%%%%%%%%%%%%%%%%%%%%%%%%%%%%%%%%%%%%%%%%%%%%%%%%%%%%%%%%%%%%%%%%%%%%%%%
Author: Satinder Singh Gill
Last Modified: August01, 2013
All Copyrights of this Code are Reserved by Author
%%%%%%%%%%%%%%%%%%%%%%%%%%%%%%%%%%%%%%%%%%%%%%%%%%%%%%%%%%%%%%%%%%%%%%%%
%%%%%%%%%%%%%%%%%%%%%%%%%%%%%%%%%%%%%%%%%%%%%%%%%%%%%%%%%%%%%%%%%%%%%%%%
```

```
function [multiple_condition_number] = Impulse_Response(data_sent)
number_readings = data_sent(1); % Read the number of readings
number_periods = data_sent(2); % Read the number of periods
bandwidth = data_sent(3); % Read the user bandwidth

impulse_size = 2^8-1; % Set the size of impulse response
recovered_h11 = zeros(number_readings,impulse_size); % Define recovered impulse response h11 to be
% all zero
recovered_h12 = zeros(number_readings,impulse_size); % Define recovered impulse response h12 to be
% all zero
recovered_h21 = zeros(number_readings,impulse_size); % Define recovered impulse response h21 to be
% all zero
recovered_h22 = zeros(number_readings,impulse_size); % Define recovered impulse response h22 to be
% all zero
code = [1 0 0 0 0 0 0]; % Set the code to detect the presense of start of PN Sequence

for readings = 1:number_readings; % Set the loop to repeat for number of readings
% Start of Data Reading
addpath('C:\Altera\11.0\quartus\bin');
if bandwidth == 30
x = alt_sigaltap_run('C:\Users\A7t0r\Desktop\MIMO_30\Project\project.stp','signed');
downsample_rate = 120/30; % Set the downsample rate
elseif bandwidth == 20
x = alt_sigaltap_run('C:\Users\A7t0r\Desktop\MIMO_20\Project\project.stp','signed');
downsample_rate = 120/20; % Set the downsample rate
elseif bandwidth == 10
x = alt_sigaltap_run('C:\Users\A7t0r\Desktop\MIMO_10\Project\project.stp','signed');
downsample_rate = 120/10; % Set the downsample rate
end
alt_sigaltap_run('END_CONNECTION');
% End of Data reading

% Start of Data Read Section
read_data = double(x); % Convert signed decimal int32 data to signed decimal double data
read_data = downsample(read_data,downsample_rate); % Downsample the read data

% Find Start of PN Sequence
data = read_data(:,5);
```

```

flag = 0;
count = 1;
while flag == 0
    check = code == data(count:count+7);
    if (check(1) && check(2) && check(3) && check(4) && check(5) && check(6) && check(7) &&
check(8)) == 1
        flag = 1;
    else
        count = count + 1;
    end
end
% End Finding Start of PN sequence

read_data = read_data(count:count+254+(number_periods-1)*255,:); % Get number of periods of data

rx_I1 = read_data(:,1); % Get the received Inphase Component1
rx_Q1 = read_data(:,4); % Get the received Quadrature Component1
rx_I2 = read_data(:,2); % Get the received Inphase Component2
rx_Q2 = read_data(:,3); % Get the received Quadrature Component2
tx_I1 = 2*read_data(:,5)-1; % Get the transmitted Inphase Component1
tx_Q1 = 2*read_data(:,6)-1; % Get the transmitted Quadrature Component1
tx_I2 = 2*read_data(:,7)-1; % Get the transmitted Inphase Component2
tx_Q2 = 2*read_data(:,8)-1; % Get the transmitted Quadrature Component2
% End of Data Read Section

% Start of Real to Complex Conversion Section
tx1_signal = tx_I1 + 1i*tx_Q1; % Get the transmitted signal 1
tx2_signal = tx_I2 + 1i*tx_Q2; % Get the transmitted signal 2

rx1_signal = rx_I1 + 1i*rx_Q1; % Get the received complex signal1
rx2_signal = rx_I2 + 1i*rx_Q2; % Get the received complex signal2
% End of Real to Complex Conversion Section

% Start of Matched Filter Sliding Correlator Section
matched_filter1 = conj(tx1_signal(length(tx1_signal):-1:1)); % Get the matched filter1 from
% transmitted signal 1
matched_filter2 = conj(tx2_signal(length(tx2_signal):-1:1)); % Get the matched filter2 from
% transmitted signal 2

% End of Matched Filter Sliding Correlator Section

% Start of Impulse Response Determination Section
centre_point = number_periods*impulse_size; % Get the centre point for sliding correlator output
first_h11 = conv(matched_filter1,rx1_signal); % Matched Filter Correlator
h11 = [2*first_h11(centre_point); (first_h11(centre_point-impulse_size+1:centre_point-1) +
first_h11(centre_point+1:centre_point+impulse_size-1))];
first_h12 = conv(matched_filter2,rx1_signal); % Matched Filter Correlator
h12 = [2*first_h12(centre_point); (first_h12(centre_point-impulse_size+1:centre_point-1) +
first_h12(centre_point+1:centre_point+impulse_size-1))];
first_h21 = conv(matched_filter1,rx2_signal); % Matched Filter Correlator
h21 = [2*first_h21(centre_point); (first_h21(centre_point-impulse_size+1:centre_point-1) +
first_h21(centre_point+1:centre_point+impulse_size-1))];
first_h22 = conv(matched_filter2,rx2_signal); % Matched Filter Correlator
h22 = [2*first_h22(centre_point); (first_h22(centre_point-impulse_size+1:centre_point-1) +

```

```

    first_h22(centre_point+1:centre_point+impulse_size-1)];
% End of Impulse Response Determination Section

recovered_h11(readings,:) = h11; % Save the impulse response h11
recovered_h12(readings,:) = h12; % Save the impulse response h12
recovered_h21(readings,:) = h21; % Save the impulse response h21
recovered_h22(readings,:) = h22; % Save the impulse response h22

pause(0.1);
end % End for "readings" loop

% Start of Condition Number Calculation
[rows,coloumns] = size(recovered_h11);
for iterations = 1:rows % Set the loop to repeat for number of rows of recovered impulse response
    time_h11 = recovered_h11(iterations,:); % Load time domain impulse response h11
    time_h12 = recovered_h12(iterations,:); % Load time domain impulse response h12
    time_h21 = recovered_h21(iterations,:); % Load time domain impulse response h21
    time_h22 = recovered_h22(iterations,:); % Load time domain impulse response h22

    [peak1,index1] = max((time_h11)); % Detect the peak for impulse response h11
    [peak2,index2] = max((time_h12)); % Detect the peak for impulse response h12
    [peak3,index3] = max((time_h21)); % Detect the peak for impulse response h21
    [peak4,index4] = max((time_h22)); % Detect the peak for impulse response h22

    freq_h11 = angle(fft(time_h11(index1-6:index1+6))); % Convert time domain impulse response to
                                                    frequency domain impulse response
    freq_h12 = angle(fft(time_h12(index1-6:index1+6)));
    freq_h21 = angle(fft(time_h21(index1-6:index1+6)));
    freq_h22 = angle(fft(time_h22(index1-6:index1+6)));
    for j = 1:length(freq_h11)
        H = [freq_h11(j) freq_h12(j);freq_h21(j) freq_h22(j)];
        inst_condition_number(j) = cond(H);
    end
    condition_number = mean(inst_condition_number);
    multiple_condition_number(iterations,:) = condition_number;
end
% End of Condition Number Calculation
end % End for function

```



```

    ad2_5: in std_logic; ad2_6: in std_logic;
    ad2_7: in std_logic; ad2_8: in std_logic;
    ad2_9: in std_logic; ad2_10: in std_logic;
    ad2_11: in std_logic; ad2_12: in std_logic;
    ad2_13: in std_logic; ad2_14: in std_logic;
-----

    Q2: out std_logic; Q3: out std_logic;
    Q4: out std_logic; Q1: out std_logic;
    I2: out std_logic; I3: out std_logic;
    I4: out std_logic; I1: out std_logic;
-----

-----

    adc1clk: out std_logic;
    adc2clk: out std_logic;
    adc3clk: out std_logic;
    adc4clk: out std_logic;
-----

    lockdisplay: out std_logic:= '0');
end entity MIMO_Project;
-- End of Entity Declaration

-- Architecture Body
architecture project of MIMO_Project is
    signal reg1:std_logic_vector(7 downto 0):= seed1;
    signal reg2:std_logic_vector(7 downto 0):= seed2;
    signal reg3:std_logic_vector(7 downto 0):= seed3;
    signal reg4:std_logic_vector(7 downto 0):= seed4;
-- Start of PLL Section
    component mega_pll
    PORT
    (
        inclk0: IN STD_LOGIC:= '0';
        c0: OUT STD_LOGIC;
        c1: OUT STD_LOGIC;
        c2: OUT STD_LOGIC;
        c3: OUT STD_LOGIC;
        c4: OUT STD_LOGIC;
        locked: OUT STD_LOGIC
    );
end component;
    signal clock30: std_logic;
begin
    mega_pll_inst: mega_pll PORT MAP
    (
        inclk0 => clk,
        c0 => clock30,
        c1 => adc1clk,
        c2 => adc2clk,
        c3 => adc3clk,
        c4 => adc4clk,
        locked => lockdisplay
    );

```

```
-- End of PLL Section
```

```
a : process
variable modif1:std_logic;
variable modif2:std_logic;
variable modif3:std_logic;
variable modif4:std_logic;
begin
    I3<= reg1(0);
    Q3<= reg2(0);
    I4<= reg3(0);
    Q4<= reg4(0);

    -----
    modif1:= reg1(7) xor reg1(6) xor reg1(5) xor reg1(2) xor reg1(1) xor reg1(0);
    reg1(7 downto 0) <= modif1 & reg1(7 downto 1);

    -----
    modif2:= reg2(7) xor reg2(6) xor reg2(3) xor reg2(2) xor reg2(1) xor reg2(0);
    reg2(7 downto 0) <= modif2 & reg2(7 downto 1);

    -----
    modif3:= reg3(7) xor reg3(6) xor reg3(5) xor reg3(4) xor reg3(2) xor reg3(0);
    reg3(7 downto 0) <= modif3 & reg3(7 downto 1);

    -----
    modif4:= reg4(7) xor reg4(6) xor reg4(1) xor reg4(0);
    reg4(7 downto 0) <= modif4 & reg4(7 downto 1);

    wait until clock30 = '1';
end process a;
end architecture project;
```

Appendix D: Received Signal Power Level Ratios

Table below shows the received signal power level ratios in dBW for different allocated user baseband bandwidths for the oe_case1 GWD119 measurement results. The power level ratios are presented for fifty different portable user locations for three different values of allocated user bandwidths.

Allocated User Bandwidth = 10 MHz	Allocated User Bandwidth = 20 MHz	Allocated User Bandwidth = 30 MHz
3.23	1.62	0.64
1.01	2.11	0.90
4.45	6.70	4.71
5.93	1.59	1.87
14.02	8.47	7.56
2.61	2.71	1.28
5.59	5.62	5.55
4.19	6.99	6.02
8.99	7.65	6.04
4.78	2.80	3.21
8.14	7.06	4.81
5.27	8.73	6.09
6.7	8.04	7.02
12.81	8.52	9.27
12.46	14.31	12.57
12.07	10.42	11.25
8.86	11.94	8.56
11.39	10.19	8.41
16.37	15.91	14.52
14.62	16.03	15.63
13.35	11.35	13.62
12.59	12.89	13.52
14.27	13.80	12.26
17.34	20.29	15.68
12.72	17.11	15.02
12.62	16.90	15.44
15.48	14.75	14.57
12.89	11.68	10.50
13.44	14.55	12.11
13.30	16.00	15.39
15.10	21.04	17.21

23.29	19.72	20.56
20.32	20.05	19.62
19.09	19.94	18.87
23.64	18.07	20.01
21.52	23.96	22.12
21.65	21.49	20.38
21.89	21.49	20.38
21.89	21.18	20.06
20.92	20.48	18.29
20.31	23.58	21.02
20.98	21.47	19.27
26.50	20.30	20.01
16.23	19.19	18.26
19.06	18.73	17.20
22.72	21.29	22.18
20.58	20.64	21.24
23.89	24.91	24.56
28.10	27.22	26.11
33.63	31.68	28.00

Following table shows the received signal power level ratios in dBW for different allocated user baseband bandwidths for the oe_case4 GWD119 measurement results.

Allocated User Bandwidth = 10 MHz	Allocated User Bandwidth = 20 MHz	Allocated User Bandwidth = 30 MHz
1.08	0.93	0.21
1.56	1.15	0.33
1.12	0.02	0.54
1.04	0.5	2.99
4.22	4.66	5.13
1.8	3.4	4.41
5.00	3.43	4.97
8.42	6.95	6.2
3.03	3.59	3.53
6.62	5.24	5.63
7.33	6.18	7.01
8.34	8.43	5.92
6.65	8.72	6.97
7.87	7.00	7.29
12.91	8.10	7.98
11.37	11.34	9.08
8.17	12.72	10.04

11.10	10.52	8.87
6.91	8.27	8.76
11.70	10.81	11.69
12.70	13.25	12.13
13.26	10.22	11.52
10.32	9.51	11.12
15.11	13.50	14.04
18.48	16.38	14.95
10.35	14.40	14.17
13.94	16.46	16.10
18.77	18.07	16.39
14.72	15.66	15.31
15.60	13.97	15.68
19.36	18.78	17.52
21.46	17.73	17.02
15.40	17.87	18.01
16.13	17.33	17.95
17.96	17.30	18.12
19.02	18.96	19.02
19.55	18.13	19.34
17.62	17.48	18.25
21.80	17.14	19.37
17.15	18.19	18.97
20.61	19.17	20.21
22.07	20.96	20.10
20.33	21.76	19.58
20.57	23.37	21.82
20.80	22.13	20.56
20.37	22.02	21.01
22.59	24.60	23.79
25.42	23.84	22.72
22.10	21.40	22.50
21.12	23.52	22.50

Vitae

Candidate's full name: Satinder Singh Gill

Universities attended:

Punjab Technical University, B.Tech, 2002 – 2006

Saint Cloud State University, M.Sc.E, 2006 – 2009

University of New Brunswick, Ph.D, 2011 – 2015

Conference Publications:

S. S. Gill and B. R. Petersen, "Performance dependence of line-of-sight multiuser multi-input multi-output system on allocated user bandwidth in an office environment," in *Proc. ICACCI*, Delhi, India, Sept. 24 – 27 2014, pp. 1775 – 1780.

S. S. Gill and B. R. Petersen, "Line-of-sight multi –input multi-output capacity improvement using change of carrier frequency," in *Proc. ICACCI*, Mysore, India, Aug. 22 – 25 2013, pp. 321 – 326

S. S. Gill and B. R. Petersen, "Advanced adaptive call admission control for mobile cellular networks: Cell breathing, load shedding and bandwidth degradation," in *Proc. ICACCI*, Chennai, India, Aug. 3 – 5 2012, pp. 237 – 243

S. S. Gill and A. Batish, "Channel assignment in wireless mesh networks," in *Proc. ICWCOCN*, Punjab, India, Nov. 27 – 29 2010, pp. 40 – 44

S. S. Gill and M. Bharti, "Use of orthogonal frequency division multiplexing to overcome high data rate problems," in *Proc. ISCET*, Punjab, India, Mar. 19 – 20 2010, pp. 344 – 348

Presentations:

B. G. Colpitts, S. S. Gill, B. R. Petersen and C. D. Rouse, "The MIMO multiuser wireless bandwidth of this room," The University of Queensland St. Lucia Campus, Brisbane, Australia, Aug. 17 2012

B. G. Colpitts, S. S. Gill, B. R. Petersen and C. D. Rouse, "The MIMO multiuser wireless bandwidth of this room," The Australian National University, Canberra, Australia, Aug. 16 2012

B. G. Colpitts, S. S. Gill, B. R. Petersen and C. D. Rouse, "The MIMO multiuser wireless bandwidth of this room," The University of Canterbury, Christchurch, New Zealand, Aug. 3 2012

S. S. Gill, "Call admission control scheme for enhanced 3G cellular traffic," *NLT 2011 Symposium*, Guru Nanak Dev Engineering College, Punjab, India, Apr. 9 – 10 2010

S. S. Gill, "High peak to average power ratio problem in OFDM," *NLT 2011 Symposium*, Guru Nanak Dev Engineering College, Punjab, India, Apr. 9 – 10 2010

S. S. Gill, "Peak to average power ratio reduction of OFDM signals using adaptive digital filter," *SR 2009 Colloquium*, The Saint Cloud State University, Minnesota, USA, Apr. 21 2009

S. S. Gill, "PAPR reduction in OFDM," *SR 2008 Colloquium*, The Saint Cloud State University, Minnesota, USA, Apr. 22 2008

Thesis:

S. S. Gill, "Peak to average power ratio reduction in OFDM system", M.Sc.E. Dissertation, Saint Cloud State University, Jun. 2009